Time-Varying Identification of Human Look-Ahead Times in Preview Tracking Tasks

MSc Thesis Control and Operations

S.I.R. Piera

Delft University of Technology – Aerospace Engineering

TU Delft

Time-Varying Identification of Human Look-Ahead Times in Preview Tracking Tasks

by

S.I.R. Piera

to obtain the degree of Master of Science in Aerospace Engineering
at Delft University of Technology,

Course Code and Name:	AE5310: Thesis Control and Operations	
Student number:	4470370	
Graduation Committee:	Prof. dr. ir. M. Mulder	Chair
	Dr. ir. D. M. Pool	Daily supervisor
	Dr. ir. K. van der El	Supervisor (in absence)
	Dr. ir. M.M. van Paassen	Additional member
	Dr. ir. J.C.F. de Winter	External member

An electronic version of this thesis is available at `http://repository.tudelft.nl/`.

Cover Image: Top view of curved road, from *Wallpaper Flare*

TU Delft

Preface

The report you are reading concludes my thesis project at Delft University of Technology for obtaining the Master of Science degree in Aerospace Engineering. The document exists of three main parts: the Scientific Article (graded for the CO Thesis course), the Thesis Appendices, and the Preliminary Report (graded earlier for the AE Literature Study course).

Admittedly, my MSc thesis has been one of the most difficult projects I have ever completed in my life. After years of smooth sailing through my courses and working on all sorts of extra-curriculars, I have experienced quite some pressure from this final challenge. Nonetheless, I am happy that I have overcome this hurdle, that I have delivered a result of which I am proud, and that I can reflect on my studies in Delft as the best time of my life so far.

I hope that when MSc thesis students read this, they can find reassurance in my experience that it is completely fine to be temporarily slowed down sometimes. Let me elaborate on two important things I learned. First, research is not always about making things work, it is about understanding how they work. With systematic reflection and validation, the desired improvement is reached faster in the long run. If you feel like academic relevance is missing in your work because you are not building something that is directly applicable, know that your successors can still make substantiated improvements because of your findings. Second, research is all about synthesising a relevant solution to a manageable problem. Only many of these smaller solutions sum to the actual solving of the bigger picture. It is okay if the research initially sounds simpler than your ambition, because then you can spend more time on making your solution actually contribute.

"Instead of immediately aiming for the moon, start with the sky
Because before going to space, you have to know how to fly"

~ ***me*** **:)**

Let me start with sincerely thanking my daily supervisor Daan, who is one of the most approachable and involved TU Delft staff members I have ever met. Through our regular update meetings and additional problem solving sessions, my work's academic relevance and analysis quality has improved significantly. Furthermore, I would like to thank my chair Max, who regularly took a moment to talk about my well-being, or to zoom out and reflect on my progress in the bigger picture. Especially during the uncertain times in which my thesis took place, it was pleasant to have such a caring department chair. Last, my supervisor Kasper helped me with solving the most difficult coding-related problems throughout the project, for which I would like to thank him. Working with this great team stimulated me to finish the project successfully.

Of course, I would never have been able to receive this MSc degree without the unconditional support of the people around me. I have always felt appreciated by my parents and my two brothers, consistently celebrating my life's milestones and understanding my uncertainties. The incidental motivational speeches never felt really necessary before, but definitely helped me wrapping up my studies in the end. Furthermore, I would like to thank all the friends I made during high school and during my studies. Being able to go to university is already a blessing, but to share it with such wonderful people makes it truly unforgettable. I would like to conclude with a specific honourable mention to all the friends that proofread my scientific article. Although I am leaving TU Delft now to move on to the next exciting challenge, I feel very lucky to bring along all the amazing memories and friends I have made over the years!

S.I.R. Piera
Rotterdam, September 2022

Contents

Nomenclature

List of Abbreviations

CE controlled element
CL closed-loop
DEKF Dual Extended Kalman Filter
DI double integrator
FFT Fast Fourier Transform
FRF frequency response function
HMI(Lab) Human-Machine Interaction (Laboratory)
HO human operator
IQR inter-quartile range
KF Linear Kalman Filter
LTI linear time-invariant
MIMO multiple input multiple output
MLE maximum likelihood estimation
OL open-loop
SI single integrator
SS state-space
TF transfer function
TI time-invariant
TU Delft Delft University of Technology
TV time-varying
UKF Unscented Kalman Filter
VAF variance accounted for

List of Symbols

$\boldsymbol{\theta}$ DEKF parameter vector
$\boldsymbol{x_s}$ DEKF state vector
$\boldsymbol{x_y}$ canonical state vector state response
$\boldsymbol{x_{f_t}}$ canonical state vector target response
$\Delta\tau_f$ look-ahead time step taken
ϵ_{τ_f} look-ahead time estimation absolute error
Γ discrete input identitiy matrix
$\hat{\tilde{u}}$ DEKF re-simulated input value
μ_{τ_f} mean value DEKF look-ahead time estimations
μ_{τ_p} mean value of sine variation in experiment
ω sine frequency
$\omega_{b,f}$ preview break frequency
ω_{nms} neuromuscular break frequency
Φ discrete state transition matrix
ϕ sine phase
σ standard deviation
$_{l,f}$ preview smoothing time-constant
τ_f^* apparent delay
τ_f look-ahead time
τ_p display preview time
τ_s suspension time
τ_v response delay time
$\tau_{f,0}$ look-ahead time initialization
$\tau_{f,crit}$ critical preview time
$\tau_{f,est}$ DEKF estimated look-ahead time
$\tau_{f,ref}$ reference look-ahead time value (simulated/LTI)
$\tau_{f,reg}$ sine-fitted look-ahead time estimation, same subscript for the fitted sine parameters
VAF_w windowed variance accounted for
$\tilde{u}$ open-loop simulated input value
ζnms neuromuscular damping ratio
A sine amplitude
A_{τ_p} amplitude value of sine variation in experiment
D & d estimate projection matrices
$e(t)$ / $E(j\omega)$ / $E(s)$ tracking error
$e^*(t)$ / $E^*(j\omega)$ / $E^*(s)$ internal tracking error
$f_t^*(t)$ / $F_t^*(j\omega)$ / $F_t^*(s)$ internal tracking target
$f_d(t)$ / $F_d(j\omega)$ / $F_d(s)$ tracking disturbance
$f_t(t)$ / $F_t(j\omega)$ / $F_t(s)$ tracking target
f_{sp} sampling frequency
G Jacobian of output equation
G^{tot} total derivative
H observation matrix
$H_{O_t}^{mod}$ preview model target response function
$H_{O_y}^{mod}$ preview model state response function
H_n low-pass filter transfer function to create remnant
H_{CE} controlled element response function

H_{nms}	neuromuscular response function
H_{O_f}	human preview target response function
H_{O_t}	human target response function
H_{O_y}	human state response function
$H_{O_{e^*}}$	human error response function
I	identity matrix
K	Kalman gain
k	discrete time step
K_f	target response gain
K_n	remnant gain
K_p	error response gain, equal to K_{e^*}
K_v	lead equalization gain, equal to $K_{e^*} T_{L,e^*}$
k_{CT}	convergence time index
K_{e^*}	error response gain, equal to K_p
N	number of time steps
$n(t)$	human operator remnant
N_{retro}	number of steps for variance calculation
P	prediction error covariance matrix
P_n	remnant power ratio
P_{τ_p}	period value of sine variation in experiment
Q	process noise covariance matrix
$q^2_{(f)}$	process noise covariance matrix sensitivity
R	measurement noise covariance value
r^2	measurement noise covariance matrix sensitivity
r_k	Kalman Filter innovation
T_{conv}	convergence time
T_{L,e^*}	lead time-constant
$u(t)$ / $U(j\omega)$ / $U(s)$	human operator input
v	noise on output
$w_{s/p}$	random walk on state / parameter dynamics
$x_{s,...}$	a canonical state
$y(t)$ / $Y(j\omega)$ / $Y(s)$	controlled element state

List of Figures

List of Tables

I

Scientific Article

Time-Varying Identification of Human Look-Ahead Time in Preview Tracking Tasks

S.I.R. Piera, *Author*
M. Mulder, D.M. Pool, and K. van der El, *Supervisors*

***Abstract*—Future human-machine control tasks with preview (e.g., car driving) are expected to include automation for safety, but keep operators in charge for liability. Such shared control applications require time-varying human identification because the control feedback should be compatible with the operator's variable behavior. A promising time-domain identification algorithm is the *Dual Extended Kalman Filter* (DEKF), estimating human operator parameters from Van der El's preview model. In this article, the DEKF's time-varying identification performance is studied with realistic simulations, followed by human operator experiments in a fixed-base simulator. The investigation focuses on look-ahead time, indicating how much future information the operator uses for control. Compared to other parameters, look-ahead time is adapted most considerably with preview. The results suggest that this parameter should be initialized in a 0.25 s proximity of its actual value to make the DEKF converge within 30 s. Although only estimating look-ahead time while fixing the other parameters, the DEKF is capable of identifying time variations in preview. Based on the sigmoid results, the estimation bias increases linearly to 0.35 s at the largest 0.75 s steps in look-ahead time. For sine variations, the DEKF estimations are in phase with the look-ahead time until 0.03 rad/s. Between 0.03 rad/s and 0.4 rad/s the DEKF behaves as a lag function, and for higher frequencies the estimation response is decayed. For the first time, it is quantified how well the DEKF can identify variations in look-ahead time during preview tracking tasks. With further research, the DEKF might become capable of real-time identification, bringing the cybernetics community one step closer to intuitive shared control applications.**

***Index Terms*—Manual control, cybernetics, preview display, time-varying identification, Dual Extended Kalman Filter (DEKF), human-machine interaction (HMI) experiments.**

I. INTRODUCTION

OVER the past century, automation has been introduced in manual control tasks with preview (e.g., car driving), with the aim to enhance safety, efficiency, and comfort [1]–[3]. Completely autonomous vehicles are not considered a near-future solution, because it is difficult to establish legislation around liability. Furthermore, the nature of vehicle operations is usually highly decentralized and prone to unexpected events, requiring an adaptive and creative operator (i.e., human) [4]. A promising compromise between autonomous and manual control is shared control. For effective shared control, the control system is required to constantly understand the human control strategy and adapt the tracking feedback in line with the task [5]–[7]. Currently, many vehicle operators choose to disable such assisting functionalities, because the automation's control inputs can feel counter-intuitive [5], [8]. For acceptance, humans should stay well-informed and be able to adapt their control behavior to task variations [9]–[11]. A requirement for adaptive shared control is time-varying human identification, described as a key area of improvement in cybernetics [4]. Van der El developed a *preview model* [12], which can serve as a basis for describing human operator behavior using a range of parameters. Ultimately, it is desired to determine the preview model parameters in real-time. For preview tasks, the *look-ahead time* parameter describes the amount of future information processed by the operator. A promising algorithm for identifying variations in look-ahead time is the *Dual Extended Kalman Filter* (DEKF) [13], [14].

All authors are with the Section Control & Simulation, Department of Control & Operations, Faculty of Aerospace Engineering, Delft University of Technology, 2629 HS Delft, The Netherlands.

The DEKF is a simultaneous state-parameter estimation tool, capable of real-time identification of human operator behaviour in the time-domain. As alternatives, maximum likelihood estimations [15], wavelets [16], recursive auto-regressive exogenous models [17], and Unscented Kalman Filters [18] have been studied. The DEKF is selected for preview applications, because it can estimate all the preview model's parameters simultaneously and the estimation traces are not dependent on a pre-defined time progression function. Furthermore, it can sustain estimation performance when exposed to human remnant and it is a compromise between computational power and expense [14]. The DEKF has already been verified and validated for compensatory tracking tasks [13]. Following this research, Vertregt developed an algorithm [14] to perform preview task identification.

Until now, research into the DEKF during time-varying preview tracking tasks focused on developing the algorithm and on finding workable settings to show its potential [14]. Vertregt's study implies that the DEKF can estimate look-ahead time variations and that fixing other human parameters improves the estimation speed and stability. A couple of cases have been analyzed thus far, and performance has been shown for averages of large batches, rather than for individual runs. A quantitative analysis, stress-testing the DEKF's behavior and reporting the performance with statistically substantiated results, is still missing. Such a validation study requires a tuning strategy, research into the effect of modeling assumptions, and an investigation of human parameter time variations. This will enable the research community to improve and implement the DEKF for real-life tracking applications.

The aim of this research is to validate the implementation of a DEKF for the time-varying identification of look-ahead time in preview tracking tasks. Furthermore, the goal is to quantify the limits of the domain in which the DEKF performs consistently, and to show the expected trends within the feasible domain. For the first time, a sensitivity analysis of the algorithm settings is performed for simulation data and for human experiment data. After that, the identification performance is studied for sigmoid and sine time variations in the preview. Such realistic time-varying simulations and experimental validation runs have never been analyzed before. All experimentally acquired data are designed to be complementary to Van der El's established preview tracking research [12]. This study can serve as a starting point for the improvement of the DEKF, aiming for accurate time-varying identification of human behavior. With such an estimation algorithm at hand, a first step is made towards intuitive shared control vehicles, increasing safety, efficiency, and comfort.

This article is structured as follows. In Section II, fundamental theory is explained to facilitate the reader's understanding. First, the preview model is elaborated on, after which the time-varying model representation is explained, to conclude with an overview of the DEKF algorithm. Section III describes the methodology, and Section IV outlines the three main research steps: (1) the DEKF's initialization, (2) implementing the DEKF to only estimate look-ahead time, and (3) DEKF parameter identification with time-varying preview, both sigmoidal and sinusoidal. Results are presented in Section V, followed by a discussion and recommendations in Section VI. Section VII presents the research conclusion.

II. Background

A. Preview Model in Manual Control

In the early stages of cybernetics research, *preview displays* have been developed for human-machine experiments [19]. As shown in Fig. 1c, experimental preview tasks are abstracted representations of real-life tracking tasks, with the objective to anticipate on a target signal ahead, while rejecting the error on the current state. From a signal processing perspective, a pursuit display (Fig. 1b) corresponds to a preview display where the amount of preview time (τ_p) is reduced to zero. The conceptually simplest, and best-understood human tracking tasks include a compensatory display (Fig. 1a), where merely the state error should be rejected. However, many real-life manual control tasks are of preview nature, including a current state (position $y(t)$), a desired state (target $f_t(t)$), and the distance between the two (error $e(t)$). Furthermore, future information up to a certain point (e.g., a road) is normally available, described by the display preview time ($\tau_p(t)$). The observable preview time is variable with external factors (e.g., rain and obstructions [20]) and is a function of other states (e.g., velocity and heading [21]). How much preview is used by human operators (HOs) to support their behavior is parameterized as the *look-ahead time* ($\tau_f(t)$, Fig. 1c). Understanding how an HO processes its position, target and error, and what the effect is of look-ahead time is essential for creating a cybernetic model for preview tracking tasks.

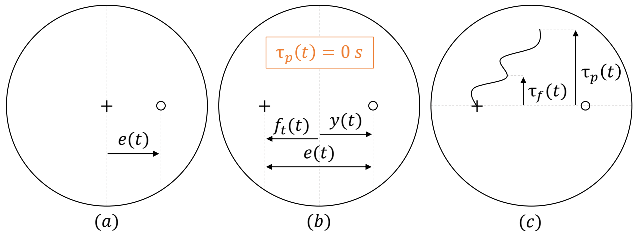

Fig. 1: Overview of McRuer's experimental displays for compensatory (a), pursuit (b) and preview (c) tracking tasks [19].

Van der El's proposed *preview model* [12] can predict how humans behave in preview tasks for a range of forcing function bandwidths and controlled element (CE) dynamics. Looking at a preview display (Fig. 1b-c), three visible signals have to be processed by the HO. The model identification procedure requires frequency response function (FRF) reconstruction of $U(j\omega)/F(j\omega)$ (feed-forward), $U(j\omega)/Y(j\omega)$ and $U(j\omega)/E(j\omega)$ (feed-back). For solving these three unknowns, three uniquely identifiable forcing functions must be included in the preview tracking task. From an experimental perspective, this is infeasible, because only one forcing function can be introduced in the target signal (processed as feed-forward) and one disturbance signal in the position signal (processed as feed-back) [12]. As direct consequence, a maximum of two FRFs can be reconstructed from experimental data. The three visible preview display signals from Fig. 1b-c are mathematically related ($e(t) = f_t(t) - y(t)$), making it still possible to completely model the HO behavioral response ($u(t)$) with merely two FRFs. As can be seen in Fig. 2, Van der El concluded H_{O_t} and H_{O_y} to be the most suitable for modeling. The superscript TY indicates that the response to the error signal is omitted and divided over the other two FRFs, as shown in the equations of Fig. 2.

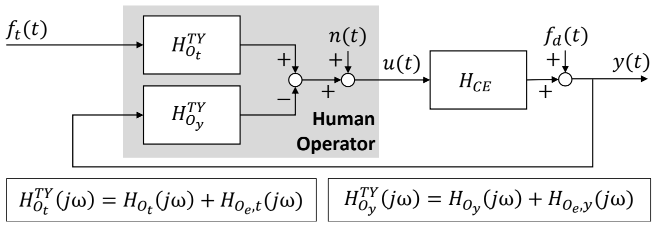

Fig. 2: Equivalent two-channel control diagram for preview tracking including FRF assumptions [12].

Using similar parameterization to McRuer's Crossover model [22], the preview model includes a feed-back loop intended to minimize an error. The error signal is a direct input ($e(t)$) to the HO in the Crossover model, but it is an internally processed signal in Van der El's preview model ($e^*(t)$). This internal error is created by subtracting the CE position ($y(t)$) from the processed preview target signal ($f_t^*(t)$). In the preview model, the HO feed-forward processes the original target signal ($f_t(t)$) using the look-ahead time (τ_f) and the low-pass FRF $H_{O_f}(j\omega)$. The control diagram shown in Fig. 3 includes eight uniquely identifiable parameters that describe the preview model HO control response.

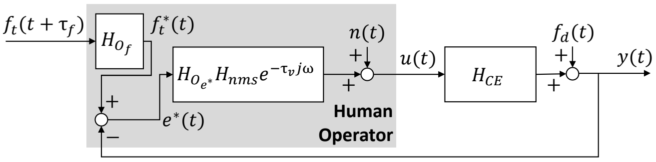

Fig. 3: Van der El's derived preview model [12].

The HO control output is weighted with the target response gain K_f and smoothed with the preview lag time constant $T_{l,f} = 1/\omega_{b,f}$. After the signal is processed to an internal error, equalization takes place with the error response gain $K_{e^*} = K_p$ for single integrator (SI) CE dynamics. For double integrator (DI) tasks, a lead time-constant $K_{e^*}T_{L,e^*} = K_v$ can be added (zero for SI tasks). The neuromuscular activation is described by a break frequency ω_{nms} and a damping ratio ζ_{nms}, differing per HO. A response time delay τ_v is included, describing the average time that passes between signal presentation and physical reaction of the operator. Because humans show non-linear and variable control behavior, the preview model is considered to be quasi-linear. All unexplained behavior is assigned to the HO *remnant* ($n(t)$). The FRF blocks are mathematically elaborated on in Eq. (1)–(3):

$$H_{O_f}(j\omega) = \frac{K_f}{1 + T_{l,f}j\omega} = K_f\frac{\omega_{b,f}}{\omega_{b,f} + j\omega} \tag{1}$$

$$H_{O_{e^*}}(j\omega) = K_{e^*}(1 + T_{L,e^*}j\omega) = K_p + K_v j\omega \tag{2}$$

$$H_{nms}(j\omega) = \frac{\omega_{nms}^2}{(j\omega)^2 + 2\zeta_{nms}\omega_{nms}j\omega + \omega_{nms}^2} \tag{3}$$

B. Time-Varying Model Representation

In previous human preview tracking studies, the preview model is parameterized using a linear time-invariant (LTI) methodology [12], [23]–[26]. The first LTI estimation step is to Fast Fourier Transform (FFT) the measurable signals ($f_t(t)$, $u(t)$, $y(t)$) to form $F_t(j\omega)$, $U(j\omega)$ and $Y(j\omega)$. Simultaneously, two model FRFs ($H^{mod}_{O_t}(j\omega)$ and $H^{mod}_{O_y}(j\omega)$) are created in line with Fig. 2. These FRFs can recreate the relation between the inputs ($f_t(t)$, $y(t)$) and outputs ($u(t)$) of the HO control system, resulting in a modeled output ($u^{mod}(t)$) for every run. The second step is an iterative gradient search optimization, minimizing the difference in *variance accounted for* (VAF, Eq. (21)) between $u^{mod}(t)$ and $u(t)$. Here, the preview model parameters from Eq. (1)-(3) are altered, after being initialized at an expected. The LTI estimation's drawback is that the full experiment data trace is required to calculate a single parameterization. With the ambition of capturing HO adaptation to time-varying (TV) preview, the model control scheme (Fig. 3) should be transformed into a TV format.

Preceding this study, a DEKF was developed that can perform simultaneous state-parameter estimations [14]. Comparable to the work of Popovici et al. [13], where the DEKF was applied to compensatory tracking tasks, the FRFs are transformed into state-space (SS) format. Transforming a control diagram to a SS system requires all FRFs to be converted to polynomial transfer functions (TFs). Time-delays have no direct transition into polynomial fractions and require a Padé approximation [27], as shown in Eq. (4):

$$H_{delay}(j\omega) = e^{-\tau j\omega} \approx \frac{\sum_{i=0}^{m}\frac{(2r-i)!}{i!(r-i)!}(-\tau j\omega)^i}{\sum_{k=0}^{m}\frac{(2r-k)!}{k!(r-k)!}(\tau j\omega)^k} \tag{4}$$

A higher order (i and k) increases the delay Padé approximation's fidelity, but leads to more poles and zeros in the SS system. This increases the system's states to be estimated by the DEKF significantly, impeding DEKF's capability to focus on HO parameter estimation. A third order delay was determined an optimum between signal quality and estimation capability [14]. Look-ahead time τ_f is effectively a negative time-delay, but for the Padé approximation equation to hold, delays should be positive [14], [27]. Furthermore, only positive delays can be included in a TV model description, because only signals that are already present in the control loop can affect the current states. This is solved by transforming look-ahead time into apparent time-delay ($\tau_f^* = \tau_s - \tau_f$), as shown in Fig. 4. This means that the time reference is shifted to the future, which must be further away than τ_f. The target signal can then be described as the original signal ($f_t(t)$) suspended into the future ($f_t(t+\tau_s)$). Based on research from Vertregt [14] and Van der El [23], a τ_s value of 0.9 s and 1.5 s is selected for SI and DI dynamics, respectively. A limitation of this procedure is that the algorithm can estimate no values larger than the suspension time. Furthermore, Padé approximations are more accurate for lower delay values, meaning that low look-ahead time estimations are less accurate. A time delay block with τ_f^* is added to the control diagram and it is Padé approximated, just as τ_v's delay block.

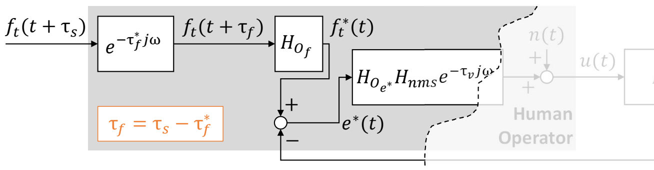

Fig. 4: Preview model, with apparent delay addition [14].

To transform the control diagram (Fig. 3) into a SS system, the FRFs have to be redefined as polynomial TFs. Three requirements for the SS system are set. First, the system should be constructed in controllable canonical form, because this enables future researchers to repeat the analyses and this form lends itself well for multiple input multiple output (MIMO) systems. Simultaneously, the number of canonical states has to be kept as low as possible for better HO look-ahead time estimation performance. Last, the polynomial TFs $\hat{U}(s)/F_t^*(s)$ and $\hat{U}(s)/Y(s)$ should be identical in the simulations of measurable signals and the estimations of HO parameters for transparency of performance. This way, if estimations differ from the expected values, it can be analyzed at which state or parameter exactly the anomaly occurred. The complete TF-SS relation for the HO behaviour ($\hat{U}$) can be found in Vertregt's work [14], and is schematically presented in Eq. (5):

$$\begin{bmatrix} \dot{\boldsymbol{x}}_{\boldsymbol{y}} \\ \dot{\boldsymbol{x}}_{\boldsymbol{f_t}} \end{bmatrix} = \left[\begin{array}{c:c} \boldsymbol{A}_{\boldsymbol{y}}^{(5\times5)} & \begin{matrix}\mathbf{0}^{(4\times4)} \\ \boldsymbol{C}_{\boldsymbol{f_t}}^{(1\times4)}\end{matrix} \\ \hdashline \mathbf{0}^{(4\times5)} & \boldsymbol{A}_{\boldsymbol{f_t}}^{(4\times4)} \end{array}\right] \begin{bmatrix} \boldsymbol{x}_{\boldsymbol{y}} \\ \boldsymbol{x}_{\boldsymbol{f_t}} \end{bmatrix} + \left[\begin{array}{c:c} \begin{matrix}\mathbf{0}^{(4\times1)} \\ \boldsymbol{D}_{\boldsymbol{f_t}}^{(1\times1)}\end{matrix} & \boldsymbol{B}_{\boldsymbol{y}}^{(5\times1)} \\ \hdashline \boldsymbol{B}_{\boldsymbol{f_t}}^{(4\times1)} & \mathbf{0}^{(4\times1)} \end{array}\right] \begin{bmatrix} f_t \\ y \end{bmatrix}$$

$$\hat{u} = \left[\begin{array}{c:c} \boldsymbol{C}_{\boldsymbol{y}}^{(1\times5)} & \mathbf{0}^{(1\times4)} \end{array}\right] \begin{bmatrix} \boldsymbol{x}_{\boldsymbol{y}} \\ \boldsymbol{x}_{\boldsymbol{f_t}} \end{bmatrix} + \left[\begin{array}{c:c} \mathbf{0}^{(1\times1)} & \boldsymbol{D}_{\boldsymbol{y}}^{(1\times1)} \end{array}\right] \begin{bmatrix} f_t \\ y \end{bmatrix} \quad (5)$$

As shown in Fig. 2, the two governing TFs for the open-loop (OL) human response are $\hat{U}(s)/F_t(s)$ and $\hat{U}(s)/Y(s)$. A large part of the signal dynamics is shared in the feed-back loop. Recognizing this shared dynamics, the number of canonical states can be significantly reduced by specifically designing the SS system (Appendix A, Part II). The output of the feed-forward part $F_t^*(s)/F_t(s)$ is direct input to the same dynamics as the feed-back loop. This internal transmission $\hat{U}(s)/F_t^*(s)$ should carry a positive sign, as opposed to the TF describing the response to the CE state $\hat{U}(s)/Y(s)$. The sub-matrices ($\boldsymbol{A}_{\boldsymbol{f_t/y}}$, $\boldsymbol{B}_{\boldsymbol{f_t/y}}$, $\boldsymbol{C}_{\boldsymbol{f_t/y}}$, $\boldsymbol{D}_{\boldsymbol{f_t/y}}$) are all conform to the controllable canonical format, and their matrix values are described by the HO parameters. The canonical state vector $[\boldsymbol{x}_{\boldsymbol{y}}, \boldsymbol{x}_{\boldsymbol{f_t}}]^T$ includes all canonical states $[x_{s,1}, ..., x_{s,9}]^T$. These parameterized matrices and state vectors do not necessarily coincide with the DEKF's parameter and state vectors, which can be arbitrarily selected, as explained in Subsec. II-C.

C. Dual Extended Kalman Filter (DEKF)

The ideal TV identification method should be able to (1) estimate time-delays because the preview model includes two [28], (2) converge even when exposed to remnant due to the HO tracking application [14], (3) allow for parameter estimations that have no pre-defined trace shape in order to function for a wide range of TV conditions [29], and (4) directly identify HO preview model parameters to explain behavior changes in terms of physiological variations [30]. The DEKF is most suitable for the combined state-parameter estimation problem compared to other time-domain tools. Maximum likelihood estimations (MLE) [15] can only express the parameter variations in terms of pre-defined progressions, which have to be designed beforehand. Wavelets [16] are too sensitive to HO remnant and the HO model parameters cannot be directly estimated during the procedure, but have to be acquired with frequency response analyses. Recursive auto-regressive exogenous models [17] have their own representation of parameters and time delays cannot be estimated, which impedes the desired HO parameterization for preview tracking tasks. Unscented Kalman Filters (UKFs) [18] are relatively costly with regard to computational expense, which can possibly introduce difficulties for real-time applications.

DEKFs [13] are a good compromise between power and expense, although their initialization and tuning should be monitored for consistent performance [14]. In car driving experiments, non-linear parameter estimations have been performed with a DEKF to study advanced driver-assist systems [31]. Additionally, recent research into parameter identification for permanent magnet synchronous machines has shown that the DEKF is promising for online identification [32].

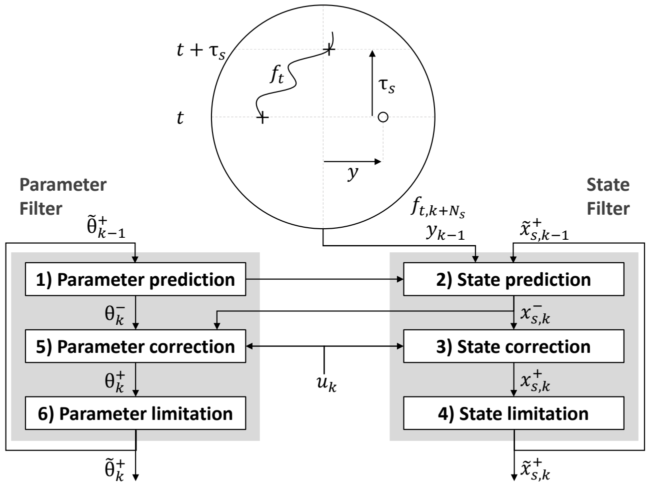

Fig. 5: Schematic overview of Vertregt's DEKF algorithm [14].

In preceding research by Vertregt [14], the DEKF was constructed as a six-step procedure, which is graphically presented in Fig. 5. A description of the governing differential equation to be solved is shown in Eq. (6)–(8). The estimation problem consists of a canonical state update equation ($\dot{\boldsymbol{x}}_{\boldsymbol{s}}(t)$), a parameter update equation ($\dot{\boldsymbol{\theta}}(t)$), and one shared output equation ($u(t)$). The *state filter*, is responsible for solving the state equation, and the *parameter filter* solves the parameter equation. Mathematically, it is a design choice which canonical states and parameters are assigned to which filter [13]. Based on the preview state-parameter estimation problem, preceding researchers [14] used $\boldsymbol{x}_{\boldsymbol{s}}(t) = [x_{s,1}, ..., x_{s,9}, K_p, K_v]^T$ and $\boldsymbol{\theta}(t) = [\omega_{nms}, \zeta_{nms}, \tau_v, K_f, \omega_{b,f}, \tau_f^*]^T$. They decided to place the equalization gains K_p and K_v in the state filter because these are only active in the output equation (lower part of Eq. (5)). The number of canonical states depends on the Padé approximation order and the manner in which the SS system is constructed. The nine canonical states in the DEKF model are the result of performing third order Padé approximations for $e^{-\tau_f^* j\omega}$ and $e^{-\tau_f j\omega}$ and of using the minimal SS realization.

$$\dot{\boldsymbol{x}}_{\boldsymbol{s}}(t) = f(\boldsymbol{x}_{\boldsymbol{s}}(t), \boldsymbol{\theta}(t), f_t(t+\tau_s), y(t)) + \boldsymbol{w}_{\boldsymbol{s}}(t) \quad (6)$$

$$\dot{\boldsymbol{\theta}}(t) = \boldsymbol{w}_{\boldsymbol{p}}(t) \quad (7)$$

$$u(t) = g(\boldsymbol{x}_{\boldsymbol{s}}(t), \boldsymbol{\theta}(t)) + v(t) \quad (8)$$

The original Linear Kalman Filter (KF) [33] algorithm consists of five governing equations, repeated for every time step. The one-step ahead prediction ($x^-_{s,k}$, Eq. (9)) is the model-based update, after which the covariance matrix of the state prediction error ($P^-_{s,k}$, Eq. (10)) can be calculated using the system noise. The prediction error in combination with the measurement noise can be used to calculate a value between 0 and 1 for the Kalman gain ($K_{s,k}$, Eq. (11)), which determines how confident the KF is in its prediction. A measurement update ($x^+_{s,k}$, Eq. (12)) is performed, where the one-step ahead prediction is altered using the Kalman gain and the measurement. Again, a covariance matrix ($P^+_{s,k}$, Eq. (13)) is calculated to serve the basis for the next iteration.

$$x^-_{s,k} = \Phi_{s,k-1} x^+_{s,k-1} + \Psi_{s,k-1} \underline{u}_k \tag{9}$$

$$P^-_{s,k} = \Phi_{s,k-1} P^+_{s,k-1} \Phi^T_{s,k-1} + \Gamma_{s,k-1} Q_{s,k} \Gamma^T_{s,k-1} \tag{10}$$

$$K_{s,k} = P^-_{s,k} H^T_{s,k} (H_{s,k} P^-_{s,k} H^T_{s,k} + R_k)^{-1} \tag{11}$$

$$x^+_{s,k} = x^-_{s,k} + K_{s,k}(\underline{z}_k - H_{s,k} x^-_{s,k}) \tag{12}$$

$$P^+_{s,k} = (I - K_{s,k} H_{s,k}) P^-_{s,k} \tag{13}$$

To cope with non-linear behavior in human experiments, the EKF is applied, which linearlizes the system around the operating point at every time step and tries to estimate the increment to provide a prediction on the next step. This results in the filter needing to *converge* before it can rely on its predictions. Knowledge-based initialization is beneficial for the EKF performance [13], [14], because it can easier find a global optimum. Another challenge for HO parameter estimation is that the identification tool should be capable of simultaneous state-parameter estimations, leading to large vectors that are computationally expensive to solve. Therefore, the vector with states and parameters to be estimated is split over two EKFs, resulting in a DEKF (Appendix B, Part II).

The parameter and state prediction steps of the DEKF (Fig. 5) are used to find an initial prediction ($x^-_{s,k}$), as a function of the previous best estimate ($x^+_{s,k-1}$). In the differential model, the parameter progression only depends on random walk, because they are generally assumed to be constant [13] (Eq. (7)), thus the prediction (θ^-_k) is equal to the previous corrected value (θ^+_{k-1}. This is followed by a parameter covariance matrix ($P^-_{p,k}$) calculation. The state progression is a function of the states, parameters, suspended target, CE position and random walk (Eq. (6)), meaning that the DEKF prediction ($x^-_{s,k}$) is as well. Also for the states covariance matrix ($P^-_{s,k}$) is calculated. The state correction steps are introduced to make a better estimation of the new state ($x^+_{s,k}$) using the Kalman gain ($K_{s,k}$). With the new state estimation comes a new state covariance matrix ($P^+_{s,k}$). The state limitation step introduces a ceiling and floor to the estimated values, resulting in a bounded a posteriori state estimation ($\tilde{x}^+_{s,k}$). The parameter correction step and the parameter limitation step work similarly.

As explained by Popovici et al. [13] and Vertregt [14], the *total derivative* $G^{tot}_{p,k}$ is applied for the parameter correction step (Fig. 5). For both filters, this should be a step where the Jacobian is calculated for the output equation $g(x_s, \theta)$ with respect to either the states or the parameters. However, in Subsec. II-B it was shown that the preview processing parameters (τ_f, K_f, $\omega_{b,f}$) are not explicitly represented in the output equation (Eq. (5)). To still provide sensible values for this variable, it is chosen to calculate the total derivative $\frac{d\bullet}{d\theta}$, rather than the Jacobian. The Jacobian calculation is possible for the canonical states using $\frac{\delta\bullet}{\delta x_s}$. The state Jacobian and the parameter total derivative are used to calculate a Kalman gain, serving to correct the linearized step that was estimated based on the DEKF model. The complete DEKF algorithm is elaborated upon in Vertregt's work [14].

III. Methods

A. Research Settings

Preliminary analyses of the DEKF have shown that tuning and performance are condition-specific [13], [14]. It is difficult to perform one generalized validation, spanning the complete range of forcing function bandwidths and CE dynamics. For that reason, a range of research settings are fixed, in line with the results of Vertregt's DEKF study [14]. These design choices are discussed below.

1) ***Pure Integrator Dynamics:*** Only SI tracking experiments ($H_{CE}(j\omega) = 1.5/(j\omega)$) are investigated, meaning that conclusions only hold for this CE sub-domain. It has been shown by Vertregt [14] that for SI dynamics, the DEKF can well estimate the HO look-ahead time based on TV simulations and time-invariant (TI) experiments. Studying and improving the identification performance for SI tracking tasks in TV conditions is considered the most valuable next step, because it can possibly show TV DEKF behaviour for the first time ever. Vertregt's DI dynamics study [14] showed less promising results with the current DEKF design, because of the more pronounced low-pass filtering characteristics of the HO remnant. Also, for DI tasks, the preview lag time constant $T_{l,f}$ $(= 1/\omega_{b,f})$ increases with increasing display preview time, causing the HO to low-pass filter a higher bandwidth of the target signal.

2) ***Fixation of Non-τ_f Parameters:*** Only τ_f is free to vary during estimations, while all other HO parameter are fixed at a pre-determined value. Limiting the estimations to τ_f ensures that the DEKF converges to feasible solutions. It also prevents that the algorithm constantly interchanges weights of HO parameters that have similar effect on HO model output, while on tracking input level nothing changes. For example, delay time τ_v and look-ahead time τ_f have fairly similar but opposite effects on the HO model's output, so the DEKF may estimate the parameters as constantly varying, where they should be stationary. This HO parameter fixation is in line with the observation that look-ahead time is the most variable parameter as function of display preview time [23]. However, this assumption can cause artefacts in the results, since all behavioral changes of the HO have to be attributed to variations in the HO model's τ_f parameter, whereas they might have been better explained by other parameters. If the DEKF can still identify look-ahead time with this assumption, that would be a revolutionary development in time-varying cybernetics research.

3) ***Baseline HO Parameter Settings:*** Central in this research is the effect of time variations in the display preview time τ_p on HO look-ahead time τ_f. The sensitivity study of Van der El and Padmos [23] serves as starting point. They showed with TI experiments that an HO processes all available preview information ($\tau_f = \tau_p$), up until a critical point: $\tau_{f,crit} = 0.6$-0.8 s for SI tracking tasks. The four research conditions spanning this critical region for SI tracking tasks [23] are $\tau_p = 0.00$ s, $\tau_p = 0.25$ s, $\tau_p = 0.50$ s, and $\tau_p = 0.75$ s. At these display settings, the preview model parameters have been determined by Van der El [23] for eight participants using a frequency-domain LTI identification method. Looking at these

LTI identification results, four baseline parameter settings are determined for further research into the DEKF, as described in Table I. These parameter settings serve as the basis for both TI and TV simulations in this article, performed for testing the DEKF. The gain K_v describing the combined lead time constant and error rejection gain is excluded because only SI dynamics are considered.

TABLE I: Four baseline HO parameter settings.

τ_p	K_f	$\omega_{b,f}$	τ_f	K_p	ω_{nms}	ζ_{nms}	τ_v
[s]	[-]	[rad/s]	[s]	[-]	[rad/s]	[-]	[s]
0.00	1.0	**80**	**0.00**	1.3	**18**	0.2	**0.31**
0.25	1.0	**40**	**0.25**	1.3	**15**	0.2	**0.27**
0.50	1.0	**20**	**0.45**	1.3	**12**	0.2	**0.21**
0.75	1.0	**15**	**0.55**	1.3	**10.5**	0.2	**0.18**

*4) **Construction of Forcing Functions**:* The forcing functions for the target signal ($f_t(t)$) and disturbance signal ($f_d(t)$) are generated by summing a range of sine waves (Eq. (14)-(15)). The signals are composed of a selection of frequencies using a 4 rad/s bandwidth, comparable to the high-bandwidth conditions from McRuer's research [19], later also applied by Van der El [12], [23]. The disturbance frequencies are neighboring the target frequencies, but have no direct overlap to ensure that the power spectra are uniquely identifiable. To mitigate confounding factors of the signal sequence during human experiments, five different realizations of the forcing functions are introduced by shifting the phases of the sines. In simulations, the same five target functions are used, in order to create expectations for the experiment results. For HOs, the target and disturbance signals will appear to be completely random for every experiment run.

$$f_t(t) = \sum\nolimits_{i=1}^{n} A_i \sin(\omega_i t + \phi_i) \tag{14}$$

$$f_d(t) = \sum\nolimits_{j=1}^{m} A_j \sin(\omega_j t + \phi_j) \tag{15}$$

*5) **Time Trace and Sampling**:* In line with earlier preview research [14], [34], the sampling frequency f_{sp} of data points is 100 Hz. For the simulations, a complete run consists of 60 s of run-in time and 120 s of performance assessment time, summing to a total of 18,000 time steps. This relatively long run-in time is selected to ensure that the DEKF is converged during the measurement period for as many settings and conditions as possible. The validation tracking experiments entail a run-in time of 30 s, followed by a performance assessment time of 120 s. This shorter run-in time is a trade-off between HO focus and DEKF convergence. Both for the TV simulation of tracking data and for the DEKF estimation of HO parameters, the time delays are third order Padé approximated.

*6) **Remnant Model**:* As described by Levison [35], the remnant is modeled by passing white noise through a low-pass filter (Eq. (16)). In this SI research, the remnant break frequency is fixed at $\omega_{b,n} = 10$ rad/s [14]. The remnant gain K_n is a function of the remnant to tracking input power ratio ($P_n = \sigma^2_{u,n}/\sigma^2_u$) [25]. Literature shows that a realistic remnant power ratio for individual HO trials can be set at $P_n = 0.35$ [25]. Before simulating human behaviour, K_n is tuned to ensure this power ratio. Varying human remnant is impossible to capture with the current DEKF design, because it is not explicitly modeled in Van der El's preview model [12]. To take away the possibility that the DEKF performs only under specific remnant conditions and avoid artefacts in the results, different remnant realizations are used, created with randomly generated white noise signals.

$$H_n(j\omega) = \frac{K_n}{\omega_{b,n} + j\omega} \tag{16}$$

B. Data Acquisition and Processing

*1) **Simulations**:* Continuing the work of Vertregt [14], in the TV simulation environment, three main operations are executed. To create signals for $y(t)$ and $u(t)$, a CL simulation is performed for the entire human-machine system. Simultaneous to the CL simulation, an OL run is calculated to find how the remnant-free $\tilde{u}(t)$ would look when just $f_t(t)$ and $y(t)$ are used as input. The second operation is a parameter estimation by the DEKF, applying the same OL structure. The third step serves as verification, where $\hat{\tilde{u}}(t)$ is re-simulated using the estimated HO parameters. If the parameter estimations are exactly the same as the simulations, the re-simulated $\hat{\tilde{u}}(t)$ signals exactly coincide with the original OL $\tilde{u}(t)$ signals.

Every condition is simulated with five realizations of the forcing functions and with 20 differently seeded remnant signals. This reduces the possibility that the results only hold for limited and very specific combinations of research settings. All combinations of the above variations sum up to a total of 100 CL and 100 OL simulation runs. In real-life, a remnant realization can never repeat itself, even if the same person performs an identical task. Still, the same range of remnant realizations is used for every condition, to facilitate reproduction of the results. The compilation of these 100 simulations is saved to a batch, which can be unpacked in the estimation environment.

*2) **Experiments**:* The difference for experiments is that only tracking task variables (i.e., τ_p) can be varied, instead of actual HO parameters (i.e., τ_f). In previous research by Van der El [23], for TI task variable analyses, the DEKF's time-domain estimations can be compared to a frequency-domain LTI parameter estimation method. Unfortunately, in TV experimental analyses, a direct link is missing between τ_p and τ_f. This means that it is impossible to reconstruct the actual HO parameter values. For experimental data, a different procedure is applied. The HO tracking input can be re-simulated to form $\hat{\tilde{u}}(t)$, which can be compared to the experimentally acquired – thus CL, remnant-including – signal $u(t)$. Collecting tracking data from TV preview experiments is valuable, because it shows how the DEKF reacts when humans are exposed to such tasks and whether the simulated parameter variations are representative. Furthermore, the data acquired can be stored and used for future TV identification studies.

Humans show an identifiable response to isolated task variations, but simultaneously, other factors uncontrollably reverberate in their behavior. This can be on a cognitive level (e.g., fatigue), and on a motor-sensory level (e.g., tremors).

Some of this stochastic variability can show overlap with how the HO remnant is modeled in simulations, but chances are that a large part is not modeled. Therefore, one should at all times be cautious with drawing conclusions regarding an HO's response to TV task variables. The order in which different conditions are presented matters due to HO variability. To mitigate the possible confounding effect of condition order, a balanced Latin Square (Table II) is introduced, facilitating a within-subject analysis. The experiment counts eight participants, which is the minimum required to fully balance the eight conditions.

TABLE II: Balanced within-subject experiment design.

Condition	**C1**	**C2**	**C3**	**C4**	**C5**	**C6**	**C7**	**C8**
Subject 1	A	B	H	C	G	D	F	E
Subject 2	B	C	A	D	H	E	G	F
Subject 3	C	D	B	E	A	F	H	G
Subject 4	D	E	C	F	B	G	A	H
Subject 5	E	F	D	G	C	H	B	A
Subject 6	F	G	E	H	D	A	C	B
Subject 7	G	H	F	A	E	B	D	C
Subject 8	H	A	G	B	F	C	E	D

Available data collection time was the constraining factor. The data measurements take 150 s per run (Subsec. III-A), and at least five forcing function realizations are collected per condition. Not taking into account briefing (Appendix C, Part II), training, and breaks, this results in approximately 15 minutes of active measurement time per condition. As design choice, it was decided that volunteers should be able to finish the experiment within three hours, which was considered the maximum mental strain for this research. Within the scope of eight available experiment conditions (approximately three hours), a selection was made that can show DEKF performance for different TV conditions.

It was chosen to include **three TI baseline conditions (A-C)**, which serve as a starting point for the time variations. For these TI experiments, an LTI-estimated validation of the DEKF results is possible. Furthermore, **two sigmoid conditions were applied (D-E)**, investigating how well the DEKF can identify look-ahead time changes for both a large and a small step in display preview time during an experiment. In the preliminary phase of this research (Part III), it was shown that steps up in preview time are easier to detect for the DEKF. Therefore, both sigmoid experiments make a step up. Lastly, **three sine conditions were studied (F-H)**, that can help understanding what the DEKF performance is at different frequencies of preview variation in tracking tasks. Based on the preliminary study (Part III), one sine wave is selected with a large amplitude and a relatively low frequency, to verify that the DEKF can identify a look-ahead time variation pattern that is comparable to the preview time variations. A sine with the same amplitude and a higher frequency is selected to verify that the amplitude gain and phase delay decrease, comparing the preview time variation and the look-ahead time estimations. Another sine experiment with a high frequency and a lower amplitude is performed to verify whether the DEKF can identify consistent small HO behavioral changes, when the preview time variation is small. Even higher frequencies were undesirable to study, due to the experiment volunteer losing its focus in such an uncomfortable experiment.

A. TI: $\tau_p = 0.75$ s
B. TI: $\tau_p = 0.50$ s
C. TI: $\tau_p = 0.25$ s
D. TV (sigmoid): $\tau_{p,1} = 0.25$ s, $\tau_{p,2} = 0.75$ s
E. TV (sigmoid): $\tau_{p,1} = 0.50$ s, $\tau_{p,2} = 0.75$ s
F. TV (sine): $\mu_{\tau_p} = 0.50$ s, $A_{\tau_p} = 0.25$ s, $P_{\tau_p} = 60$ s
G. TV (sine): $\mu_{\tau_p} = 0.625$ s, $A_{\tau_p} = 0.125$ s, $P_{\tau_p} = 20$ s
H. TV (sine): $\mu_{\tau_p} = 0.50$ s, $A_{\tau_p} = 0.25$ s, $P_{\tau_p} = 20$ s

Experimental data are acquired in TU Delft's Human-Machine Interaction Laboratory (HMILab), a fixed-base simulator (Fig. 6). The apparatus set-up is to a large extent identical to Van der El's TI preview time experiment [23]. The participants are seated in front of the screen (1280x1024 px, 100 Hz), where the display of Fig. 1c is shown with green indicators and lines on a black background. The side-stick used to provide control input to the CE was located on the participant's right-hand side. The stick is electro-hydraulic and servo-controlled, it has a 9 cm moment arm and it is limited to only rotate around the roll axis. The seat is adjustable to ensure a comfortable distance to the screen.

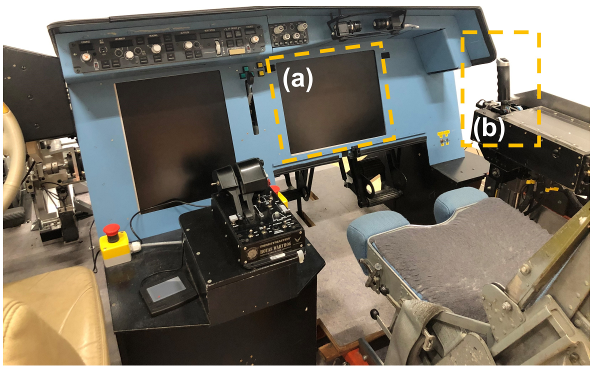

Fig. 6: TU Delft's Human-Machine Interaction Laboratory with LCD screen (a) and servo-controlled side-stick (b).

*3) **DEKF Estimation:*** Data sets of tracking input $u(t)$ and target $f_t(t)$ for different conditions are compiled to batches of 100 (simulations) or 40 (experiments) realizations. Based on the OL SS system, the DEKF reconstructs the HO look-ahead time τ_f from $u(t)$ and $f(t)$ for every realization. For simulated data, the fixed HO parameters are based on their set simulated values. For experimentally acquired data, the non-τ_f parameters are kept constant at values that have been LTI identified during a TI run for a specific condition and participant. This means that for TV simulations, the DEKF can be verified at every time step by comparing the scheduled τ_f values in the closed-loop simulation to the estimated τ_f values. Experiment data cannot serve as a validation on parameter level, because the exact HO parameter values and their time variations are unknown. Nonetheless, an OL re-simulation can be performed to compare the original tracking data $u(t)$ to the reconstruction $\hat{\hat{u}}(t)$.

C. *Performance Analysis*

Due to the time-domain research, large data sets have to be analyzed for performance assessment. This performance can be studied on a DEKF variable level (P, Q, R), on a parameter estimation level (τ_f) and a behavior reconstruction level ($\hat{\tilde{u}}(t)$). Time traces need to be abstracted to comprehensible performance indicators to compare conditions. The most important indicators are convergence time (k_{CT}), estimation bias, estimation standard deviation (σ), and *variance accounted for* (VAF) between the original an reconstructed behavior trace.

*1) **Convergence Time**:* DEKF convergence can be determined by the P-matrix or the filter innovation reaching constant minimal values. This method cannot directly explain how well the DEKF estimates τ_f and the innovation constantly changes due to the adaptive nature of the DEKF. It is chosen to investigate convergence time on a parameter estimation level (Eq. (17)) and on a behavioral level (Eq. (23)). The τ_f-level method directly supports the main goal of time-varying HO parameter identification. The u-level method can help explaining unexpected τ_f estimation results, because the DEKF only observes measurable signals, including tracking behavior. Convergence time has to be kept as low as possible in the performance optimization process. In Eq. (17) (Fig. 7), the τ_f-based convergence time calculation is shown. The estimated look-ahead time $\tau_{f,est}$ is compared to a reference value $\tau_{f,ref}$ at every time step. For simulations, this reference is known, and for experiments, it can be LTI-determined. In the preliminary phase of this research (Part III), it was found that 0.05 s variations in τ_f have little effect on HO model's output behavior. Therefore, convergence is determined to be reached (k_{CT}) when $\tau_{f,est}$ stays within a 0.5 s boundary around $\tau_{f,ref}$.

$$k_{CT,par} = k(|\tau_{f,est} - \tau_{f,ref}| < 0.025 \mid k_{CT} < k < k_{end}) \tag{17}$$

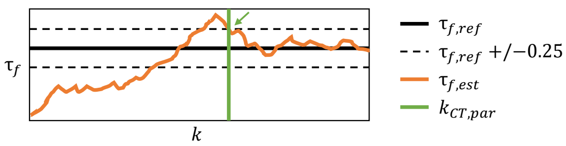

Fig. 7: Schematic representation of how parameter-based convergence time is calculated.

*2) **Bias**:* In this research, the bias is expressed on a τ_f-estimation level. For a specific range, the τ_f estimations are summed and divided by the number of samples considered. The starting point k_{start} can be set arbitrarily, or can be based on the convergence time k_{CT} found before, to prevent the artefact that non-converged estimations influence the mean estimated values. From this mean value μ_{τ_f}, the original look-ahead time is subtracted. This is a known value in the simulated environment and an LTI-identified value for the experimentally acquired data. The absolute bias should be low for optimal DEKF performance.

$$\mu_{\tau_f} = \frac{\sum_{k=k_{start}}^{k_{end}} \tau_{f,est}(k)}{k_{end} - k_{start}} \tag{18}$$

$$\text{bias}(\tau_{f,est}) = \mu_{\tau_f} - \tau_{f,ref} \tag{19}$$

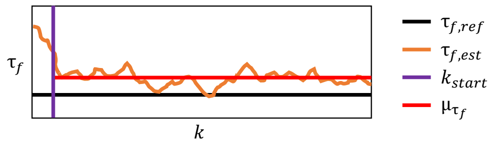

Fig. 8: Schematic representation of how look-ahead time estimation bias is calculated.

*3) **Standard deviation**:* The standard deviation of the estimations σ_{τ_f} can be calculated by taking the square root of the equation for discrete variance. The calculation presented in Eq. (20) is based on Matlab's built-in `std.m` function. Again, a value needs to be specified for k_{start}. Low values of the standard deviation correspond to more consistent DEKF performance, making it desirable.

$$\sigma_{\tau_f} = \sqrt{\frac{1}{N-1}\sum_{k=k_{start}}^{k_{end}} (\tau_{f,est}(k) - \mu_{\tau_f})^2)} \tag{20}$$

*4) **Variance Accounted For (VAF)**:* The VAF represents how well the original behavior is re-simulated using the HO parameter estimations. It is a measure for similarity expressed in percentages between two time traces based on their variance. The best attainable value is 100%. The VAF can be presented as a single value (Eq. (21), [34]), or as a windowed value, calculated at every time step (Eq. (22), [14]). Specifically for experimental data, where actual HO parameter values are unknown, this windowed VAF can be used to indicate convergence time (Eq. (23)). The general description of the VAF is shown in Eq. (21) comparing the tracking input reconstructed from estimated parameters u_{est}, with the original tracking input u_{ref} in a selected time domain $[k_{start}, k_{end}]$. The windowed VAF (Eq. (22)), performs the same operation over a smaller domain $[k - N_w, k]$ at every time step. In this research, the window size N_w is fixed at 1,000 (10 s) as a compromise between transition smoothness and variation detail. This performance indicator can be used to calculate behavior-level convergence time for the DEKF (Eq. (23)). The windowed VAF values for the estimation and reference trace are determined ($\text{VAF}_{w,est}$,$\text{VAF}_{w,ref}$), and when the fraction between the two stays above a certain threshold TH_{VAF}, the DEKF is considered converged. The threshold value for behavior-level convergence is set at $\text{TH}_{\text{VAF}} = 95\%$ in simulations, meaning that the re-simulated and reference behavior is nearly equal. An artefact of this methodology is that the entire sub-domain of 10 s is included in the VAF calculations, causing a delay between actual convergence and the detection moment when the convergence threshold is surpassed. In general, the VAF is aimed to be as high as possible in the algorithm optimization, meaning that the original tracking signal is well-reconstructed.

$$\text{VAF} = \left(1 - \frac{\sum_{k=k_{start}}^{k_{end}} |u_{ref}(k) - u_{est}(k)|^2}{\sum_{k=k_{start}}^{k_{end}} u_{ref}^2(k)}\right) \cdot 100\% \tag{21}$$

$$\text{VAF}_w(k) = \left(1 - \frac{\sum_{l=k-N_w}^{k} |u_{ref}(l) - u_{est}(l)|^2}{\sum_{l=k-N_w}^{k} u_{ref}^2(l)}\right) \cdot 100\% \tag{22}$$

$$k_{CT,\text{VAF}} = k\left(\frac{\text{VAF}_{w,est}}{\text{VAF}_{w,ref}} > \text{TH}_{\text{VAF}} \mid k_{CT} < k < k_{end}\right) \tag{23}$$

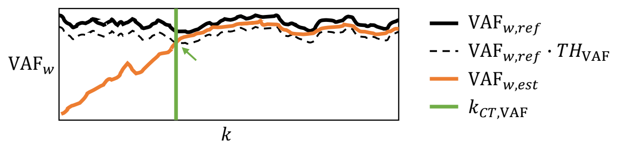

Fig. 9: Schematic representation of how VAF-based convergence time is calculated.

To understand how look-ahead time variations relate to HO behavior, Fig. 10 and Fig. 11 show the effect of changing the τ_f values on the HO model's tracking output. In Fig. 10, the solid line corresponds to the condition in Table I, where $\tau_p = 0.25$ s and $\tau_f = 0.25$ s. For the dashed and the dotted lines, only the value of τ_f is changed to 0.00 s and 0.50 s, respectively. Lowering the look-ahead time delays the HO tracking response and causes the input to increase at the ultimate values. Increasing look-ahead time effectively results in a negative delay (preview), while smoothing the tracking input with lower ultimate values. In Fig. 11, the colored lines show what happens to the VAF when only the look-ahead time is varied for three different scenarios. The peaks of the plots coincide with $\tau_p = \{0.25$ (magenta), 0.50 (blue), 0.75 (red)$\}$ s from Table I. The black markers correspond to the traces in Fig. 10. At every condition, a similar parabolic relation is visible between offsetting τ_f and the VAF. For these case studies, all τ_f values in the neighbourhood of the original values result in comparable HO model tracking input. For all conditions, a τ_f mismatch smaller than 0.05 s still reaches a VAF higher than 95%, comparing the reconstructed signals. This supports convergence threshold decisions earlier.

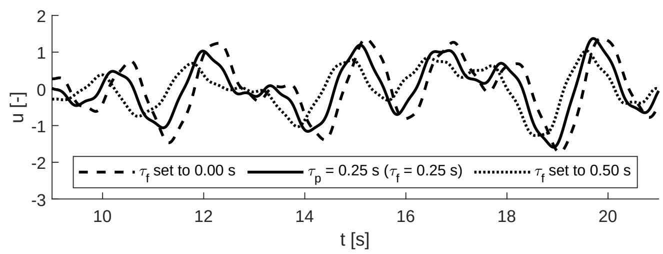

Fig. 10: Snippet of simulated tracking input $u(t)$ with $\tau_f = 0.25$ s (solid), $\tau_f = 0.00$ s (dashed) and $\tau_f = 0.50$ s (dotted).

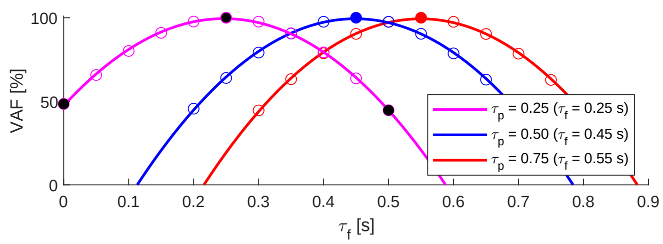

Fig. 11: Simulated VAF sensitivity study for $\tau_f = 0.25$ s (magenta), $\tau_f = 0.45$ s (blue) and $\tau_f = 0.55$ s (red). The black markers correspond to the τ_f offsets in Fig. 10.

IV. Research Steps

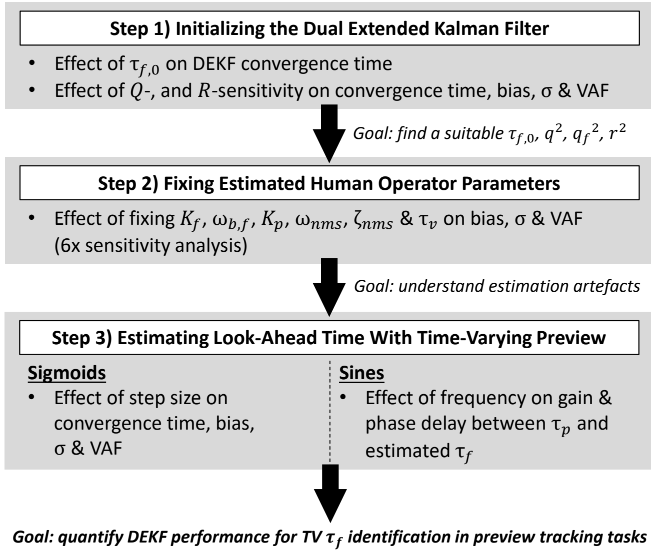

Fig. 12: Overview of the research steps to be taken in consecutive order.

A. Initializing the DEKF (Step 1)

The DEKF's initial look-ahead time estimate ($\tau_{f,0}$) and the initial noise covariance matrices (Q, R) are evaluated. Based on the preliminary research phase (Part III), the convergence speed is expected to depend on $\tau_{f,0}$, Q and R. Bias and standard deviation after convergence seem to be mostly dependent on Q and R. An example of the effect of $\tau_{f,0}$ on convergence speed is shown in Fig. 13. On the y-axis, the difference between the initial and actual look-ahead time value is presented $\Delta\tau_f = \tau_{f,0} - \tau_{f,ref}$. For $\tau_f = \{0.25, 0.45, 0.55\}$ s (Table I, opaque lines), as well as for their averaged values (solid lines), it is simulated how the DEKF's τ_f estimations progress in time towards their actual value. The $\Delta\tau_f$ values are thus relative to the three baseline conditions. It can be seen that the DEKF converges approximately twice as fast when $\tau_{f,0} < \tau_f$ and that after convergence, the algorithm shows consistent behavior. The significance of $\tau_{f,0}$ for DEKF performance motivates for a further investigation of the look-ahead time initialization.

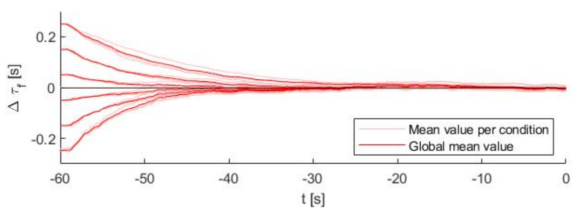

Fig. 13: Simulated $\tau_{f,0}$-sensitivity study, averaged for individual conditions (opaque) and for all estimations (solid).

The DEKF's convergence time k_{CT} can be determined on both a τ_f-level (Fig. 13) and on a VAF-level. For the τ_f-level calculations, a reference estimation can be performed, where $\tau_{f,0} = \tau_f$. Where the investigated estimation stays within a selected margin from the reference estimation, is the convergence point. For the VAF-level calculations, the 10 s windowed VAF between the original tracking signal $u(t)$ and the re-simulated tracking signal $\hat{\tilde{u}}(t)$ is used, which shows how well the DEKF was able to capture the measured behavior change with a τ_f variation. If the VAF value reaches a new equilibrium value after the HO variation, the filter is considered to be converged. Fig. 14 shows an example of such a VAF plot in a simulated environment. The black dotted line serves as reference, representing the original CL simulation data of $u(t)$. The blue line represents the OL simulation ($\tilde{u}(t)$) VAF and the red line shows the VAF of the re-simulated tracking signal ($\hat{\tilde{u}}(t)$). The OL simulation is described as *ideal*, because it corresponds to the theoretically best values the DEKF re-simulation can reach (Subsec. III-B). Where the red line coincides for the first time with the blue line indicates the convergence time.

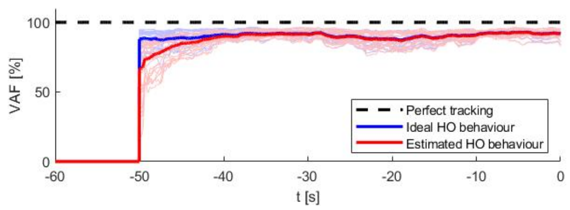

Fig. 14: Simulated VAF$_w$ for a $\tau_{f,0}$-τ_f couple, with reference u (dashed), theoretical $\tilde{u}$ (blue) and estimated $\hat{\tilde{u}}$ (red).

Another influential setting is the sensitivity of the adaptive Q-matrix and R-value. As presented in Eq. (24)–(26), these DEKF variables are designed to be a function of variances for the error $e(t)$, target $f_t(t)$, and input $u(t)$. How many time steps are included in the variance calculation window is described by N_{retro}. The value of N_{retro} is set to 500 [14], corresponding to five seconds of tracking data. The adaptability of $Q_{s,k}$ and R_k enables the algorithm to scale its prediction confidence with the variations in the system. This way, it can easily respond and re-converge when sudden changes in the estimated HO dynamics occur [13]. The design settings of q^2, q_f^2 and r^2 determine how sensitive the DEKF becomes to such variations. The process noise covariance matrix for the canonical states is only defined for the fifth and ninth state. This is because in the controllable canonical SS equation (Eq. (5)), the characteristic polynomials of the system are located at the fifth and ninth row.

$$Q_{s,k}(\dot{x}_{s,5}) = q^2\sigma^2_{e(k-N_{retro}:k)} \tag{24}$$

$$Q_{s,k}(\dot{x}_{s,9}) = q_f^2\sigma^2_{f_t(k-N_{retro}:k)} \tag{25}$$

$$R_k = r^2\sigma^2_{u(k-N_{retro}:k)} \tag{26}$$

Finding optimal values for q^2, q_f^2 and r^2 is a complex trade-off between convergence speed, bias, standard deviation and VAF. The preliminary investigation (Part III) showed that this optimum lies in the domain $\{q^2,\ q_f^2,\ r^2\}$ = [1,100]. The dimensionality of the trade-off is too high for a complete Monte Carlo analysis. Therefore, three selected settings $\{3,15,60\}$ are studied for r^2, as well as for $q^2 = q_f^2$. It was chosen to investigate a rather sparse domain because the aim is to find settings that are accurate and robust enough to make the DEKF find feasible solutions at every condition. Complete optimization of these parameters is dependant on the task conditions, and computationally expensive. The gravity of this article is at the TV performance assessment rather than the DEKF fine-tuning. In this high-level optimization of q^2, q_f^2 and r^2, $\tau_{f,0} = 0.8 \cdot \tau_{f,ref}$. It is studied which settings produce the quickest convergence ($\tau_{f,est} - \tau_{f,ref} < 0.025\ s$) with an acceptable bias and variance.

B. *Fixing Estimated HO Parameters (Step 2)*

As suggested, other HO parameters can be fixed to improve τ_f estimation performance. The effects of τ_f offsets on tracking behavior are shown in Fig. 10 and Fig. 11. Fixing other HO parameters at a different point than their actual value can create a bias in the τ_f estimations. To study this sensitivity, baseline conditions have to be developed, from which the parameters can be varied systematically. Table III shows the mean and standard deviation of the LTI-determined HO parameters from Van der El's preview time study [23]. Again, the combined lead and error rejection gain K_v is excluded due to the SI dynamics nature of the research. The mean values can serve as starting points for the baseline conditions, and the standard deviations can help determining the step sizes.

TABLE III: Mean / std of HO parameters (LTI) [23].

HO par.	τ_p = 0.25 s $\mu \mid \sigma$	τ_p = 0.50 s $\mu \mid \sigma$	τ_p = 0.75 s $\mu \mid \sigma$
τ_f [s]	0.23 | 0.057	0.44 | 0.032	0.54 | 0.088
K_f [-]	0.98 | 0.017	0.99 | 0.029	1.01 | 0.020
$\omega_{b,f}$ [rad/s]	1.2e14 | 3.4e14	2.2e8 | 3.6e8	14.09 | 9.34
K_p [-]	1.28 | 0.27	1.26 | 0.14	1.28 | 0.17
ω_{nms} [rad/s]	15.00 | 3.60	12.02 | 0.97	10.72 | 2.16
ζ_{nms} [-]	0.17 | 0.073	0.17 | 0.14	0.19 | 0.19
τ_v [s]	0.27 | 0.066	0.21 | 0.022	0.18 | 0.033

The three central conditions – corresponding to τ_p = $\{0.25,\ 0.50,\ 0.75\}$ s – are once more considered for simulations and experiments. To determine the variation range of the non-τ_f parameters for the simulations, all LTI parameter estimations from Van der El's study of preview time effect were analyzed (Table III). Based on these statistical data, Table IV summarizes the baselines and step sizes for the HO parameter variations. Assuming normal distributions, three standard deviation comprises approximately the entire data set. A standard deviation can thus be an indicative value for determining the step sizes of HO parameter variations in a feasible domain. The data set is not large enough to confirm information about the distribution, thus the step sizes should still be heuristically selected. To analyze the parameter sensitivity in the simulated environment, three steps are taken, both in negative and in positive direction. For experimental data, the baseline parameter values are the LTI-identified values for a specific HO-condition combination. From this experimental baseline, only two steps are taken to ensure that no physically impossible values are used, because some baseline values are already at the fringes of the feasible range.

TABLE IV: HO parameter base and step size.

HO par.	Base			Step Size
	τ_p = 0.25 s	τ_p = 0.50 s	τ_p = 0.75 s	
τ_f [s]	**0.25**	**0.45**	**0.55**	n.a.
K_f [-]	1.00	1.00	1.00	0.02
$\omega_{b,f}$ [rad/s]	**40.00**	**20.00**	**15.00**	6.00
K_p [-]	1.30	1.30	1.30	0.20
ω_{nms} [rad/s]	**15.00**	**12.00**	**10.50**	2.00
ζ_{nms} [-]	0.20	0.20	0.20	0.05
τ_v [s]	**0.27**	**0.21**	**0.18**	0.04

To study the HO parameter fixation, the bias and standard deviation are calculated for the τ_f estimation and the VAF is calculated for the re-simulated $\hat{\hat{u}}(t)$. For both simulations (100 realizations) and experiments (40 realizations), the median value and first and third quantile values are collected for each performance indicator. The ultimate non-outlier values are saved as well, following the definition for whiskers in Matlab's `boxplot.m` function. Every fixed HO parameter in the DEKF model is varied over the range determined by the step sizes from Table IV. All results for bias, standard deviation and VAF are normalized with respect to the median result value of the condition where the non-τ_f parameters are fixed at their baseline value. The baseline is in simulations the actual designed HO parameter value, and in experiments the LTI-identified parameter value. Due to the normalization, purely the effect of under- or over-estimating a parameter is shown. This can show the potential relative effect of fixing HO parameters at an arbitrary value, in terms of increase or decrease of look-ahead time estimation performance.

C. *Estimating τ_f With Time-Varying Preview (Step 3)*

Knowing the possible effects of the DEKF's initialization and only letting τ_f free for estimation, it is possible to assess the performance for TV conditions. The DEKF's capability of estimating τ_f is studied on simulated HO data. The experiments serve as validation cases for specific simulated conditions, analyzing whether these simulated HO parameter variations represented reality in the first place. The eight experimental conditions, of which five are TV, are outlined below the Latin Square in Table II. To minimize complexity and possible confounding factors, TV analyses include simple variations: sigmoid steps and single sines. For sigmoid steps, the influence on look-ahead time estimation bias and standard deviation is registered, as well as the effect on the VAF of re-simulated bahavior compared to the original. For sine variations, the amplitude and phase of the estimated traces is compared to that of the simulated τ_f traces or experimental τ_p traces, respectively.

*1) **Sigmoid Step Analyses:*** Sigmoid steps (Fig. 15) in preview during simulations (τ_f) and experiments (τ_p) influence HO tracking behavior. It is relevant to study how quickly the algorithm can reach a new equilibrium after the behavior changes, since the ultimate goal for shared control applications would be real-time human identification. For simulations, convergence time in a TV condition can be studied by comparing it to results of a TI condition. If the remnant seed and forcing function realization are equal for both the TV and TI simulations, the DEKF's τ_f estimation trace should approach the TI values at some point. For experiments, the LTI values are used as the reference instead of the simulated TI parameter values, which make the results less precise than for the simulations. Another interesting insight is how the performance (bias, standard deviation, VAF) after the step and following re-convergence compares to the initial equilibrium. To visually show the distribution of the data set, these performance indicators are shown in terms of a median, the first and third quantile, and the ultimate non-outlier values.

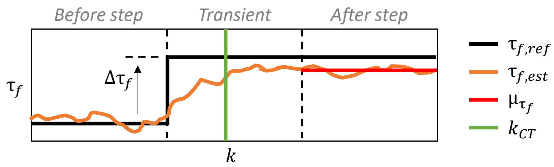

Fig. 15: Schematic representation of how a sigmoid step estimation progresses, and how the convergence time and bias are obtained.

*2) **Sine Variation Analyses:*** Periodic variations in preview can provide knowledge on the DEKF's performance as a function of frequencies. It is studied whether sinusoidal τ_f variations (Fig. 16) cause a response of the same nature in the DEKF's estimations. If the estimations are also sine-shaped, a fitting function can be used to extract the gain and delay in the estimated look-ahead time $\tau_{f,est}$ compared to the original variations of τ_f or τ_p. This can express how the DEKF performs in the frequency domain. An ordinary least squares (OLS) regression is performed on the estimated look-ahead time trace for every run, using Matlab's `fmincon.m` function. The regression procedure outputs a mean, amplitude, phase and frequency of the regressed sine signal $\tau_{f,reg}$. To assess the validity of the regressed signal results, the normalized root mean squared error between $\tau_{f,est}$ and $\tau_{f,reg}$ is collected for every condition. This value is expected to be low when the estimation trace indeed is sine-shaped, and high when this assumption does not hold.

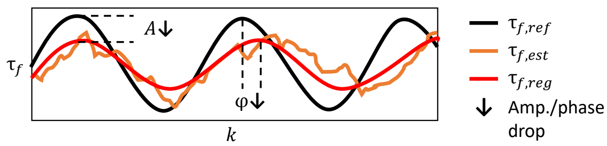

Fig. 16: Schematic representation of how a sine estimation progresses, and how the gain and phase are obtained.

V. Results

A. Initializing the DEKF (Step 1)

In Fig. 17, the convergence time T_{conv} ($= k_{CT}/f_{sp}$) is shown as a function of the $\tau_{f,0}$ initialization offset $\Delta\tau_f$. The blue lines represent the simulations and the box plots are experimental validation data. Looking at the median values, initialization of $\tau_{f,0} = \tau_f - 0.25$ s, causes the algorithm to converge in approximately 17 seconds. Conversely, if $\tau_{f,0} = \tau_f + 0.25$ s, it takes nominally 29 seconds to converge. The spread in the convergence time significantly increases as well for $\Delta\tau_f > 0$. The validation with experimental data appears to be in line with the simulations, looking at the median values. Also, the lower margins of the box plots coincide well with the simulated data. However, especially for the larger absolute $\Delta\tau_f$ values, the error margins are significantly larger. This means that either humans show unanticipated variable behavior, causing the convergence time threshold not being reached, or that this threshold should be defined to be less sensitive to behavior changes. Based on Fig. 17, it is decided to initialize the DEKF with $\tau_{f,0} = 0.8 \cdot \tau_f$ (simulations) or $\tau_{f,0} = 0.8 \cdot \tau_p$ (experiments).

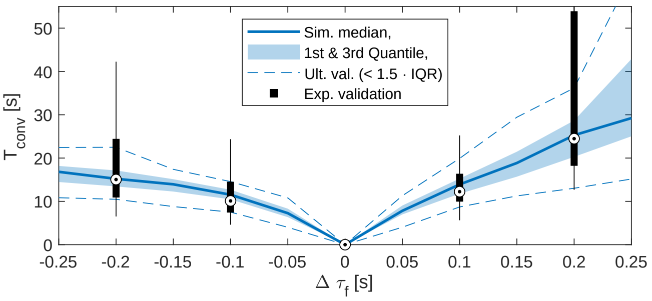

Fig. 17: Simulations and experimental validation for the effect of initial look-ahead time on convergence time.

As explained in Subsec. IV-A, a concise Monte Carlo study was performed for the initialization of r^2, q^2 and q_f^2, showing the convergence time, bias and standard deviation for different settings. All simulations are performed with $\tau_{f,0} = 0.8 \cdot \tau_f$. Fig. 18 shows the estimation time traces with the best compromise between performance indicators. The DEKF sensitivity parameters are $r^2 = 3$ and $q^2 = q_f^2 = 15$. Within 20 seconds, all three conditions are converged. Furthermore, both in terms of bias and standard deviation, the expected estimations stay within the +/- 0.025 s confidence interval of the simulated τ_f value. Even the ultimate, non-outlier boundaries (dotted estimation lines) show reasonable comparison with the actual look-ahead time values. All other investigated combinations of DEKF sensitivity parameters showed either a significantly higher convergence time, an undesired larger spread in the results, or both. The nine plots of the complete Monte Carlo analysis can be found in Appendix D (Part II). The selected settings, combined with the results of $\tau_{f,0}$ will be used to initialize the DEKF for the TV research.

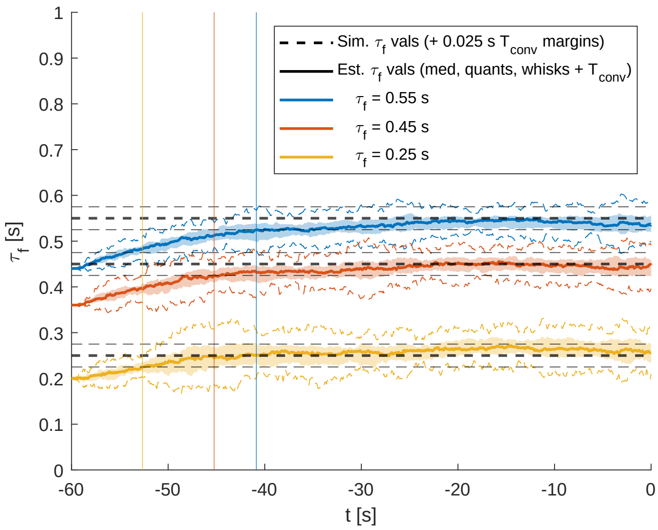

Fig. 18: Simulations for the sensitivity analysis of Q and R covariance matrices. Best τ_f estimation result obtained with $r^2 = 3$, $q^2 = q_f^2 = 15$.

B. Fixing Estimated HO Parameters (Step 2)

In order to facilitate convergence and prevent the interchanging of signal information, the DEKF is designed to only estimate τ_f and fix the other HO parameters. Van der El's preview model counts seven HO parameters in total for SI tracking tasks [34], possibly making this a rather limiting constraint. Analyzing the impact of offsetting the parameters directly quantifies possible confounds in TV analyses. Furthermore, it provides insights into the risks associated with either underestimating or overestimating the fixed HO parameters. The normalized effect of fixing HO parameters at incorrect values on the τ_f estimation bias is presented in Fig. 19a. Fig. 19b and Fig. 19c show the effects on τ_f estimation standard deviation and the re-simulated behavior's VAF, respectively. For the simulated data, the lines represent the estimated medians, the first and third quantiles and ultimate non-outlier values from simulations. The box plots show the validation based on the experimental TI HO tracking data from Van der El's preview time research [23].

Looking at the bias (Fig. 19a), what immediately stands out is the high risk of underestimating $\omega_{b,f}$ and ω_{nms}, compared to overestimating them. Both simulated data and experiment data point out that for underestimation, the bias in τ_f grows exponentially and the predictability decreases. It is thus safer to fix these HO parameters at a value known to be too high, than to choose a value that is possibly too low. This way, although overestimating could increase the τ_f estimation bias slightly, the chances of an extremely large bias in the τ_f estimation is minimized. The values for K_p and τ_v show a linear effect on the τ_f estimation bias. The gain K_p appears to be fairly constant for different preview conditions (Table III), providing the option to identify the value once per HO and keeping it constant during the TV analyses. In contrast, the delay τ_v varies more with the display preview time τ_p (Table III). Depending on the sigmoid step variation's extreme values, the effects of fixing τ_v on the τ_f estimation bias can range from negligible up to approximately 0.15 s. The damping ratio ζ_{nms} shows a moderate linear slope for the estimation bias compared to τ_v. The preview gain K_f has little effect on the τ_f estimation and can be fixed at an LTI-determined – possibly even arbitrary – value.

The simulations suggest that the estimation's standard deviation is also affected by incorrectly fixing HO parameters, as shown in Fig. 19b. Comparable to the bias, the standard deviation is asymmetrically influenced by $\omega_{b,f}$ and ω_{nms}. Again, overestimating these parameters mitigates the risk for unreliable τ_f estimations. In simulations, the gain K_p and delay τ_v have a symmetrical increase in standard deviation for both under- and overestimation. For damping ratio ζ_{nms} and gain K_f, the same observations hold as for the bias. However, the experimental validation's box plots suggest that the effects described above are in real-life less pronounced than the simulations predict. This can be explained by the generally much higher values of DEKF estimation standard deviation for experimental data. Additional variability of the estimations due to incorrectly fixed parameters do not add to the standard deviations of the DEKF in experimental conditions.

In some cases, behavior can change seemingly minimally, while significantly impacting the DEKF's τ_f estimations. On other occasions, the opposite holds, where behaviour appears to drastically change, while τ_f estimations remain accurate. Representing behavior by tracking signal reconstruction ($u(t)$ vs. $\hat{u}(t)$), Fig. 19c shows the effect of incorrect HO parameter fixations on the VAF. The motivation for overestimating $\omega_{b,f}$ and ω_{nms} is once more supported looking at the lower left two plots. In the upper left plot, it can be seen that the behavior is reconstructed well over the entire offset range of K_f. This does not hold for the damping ratio ζ_{nms}, as the top right plot shows that the VAF drops significantly in case of underestimation. Underestimating K_p and τ_v has a small effect on the VAF, decreasing it with 10-20 %. Overestimation them decreases the VAF of the behavior re-simulation more significantly. However, the decrease in reconstructed signal similarity is expected to be manageable, because the VAF decreases no more than 20 %. The curves for K_p and τ_v show an interesting asymmetry, even increasing the VAF when they are slightly underestimated. This is only witnessed in the experimental validation, where the explanation can be attributed to an LTI determined value that is slightly incorrect.

Concluding, the best look-ahead time estimation results are found when the other parameters are fixed at their LTI-determined values. If the DEKF is not capable of correctly estimating τ_f, this is most probably due to $\omega_{b,f}$ or ω_{nms} being fixed at a too low value, or due to K_p or τ_v being fixed at a value that is far from the actual value. The relations found in Fig. 19 can help identify the origin of the τ_f estimation errors. These insights can be used to explain DEKF performance during the TV estimations.

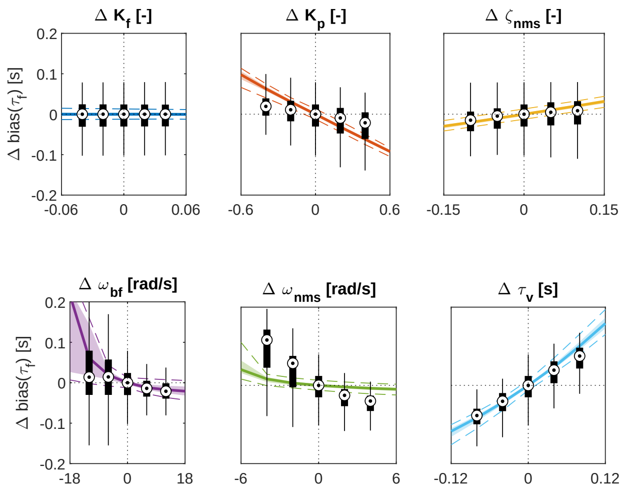

(a) bias($\tau_{f,est}$) sensitivity.

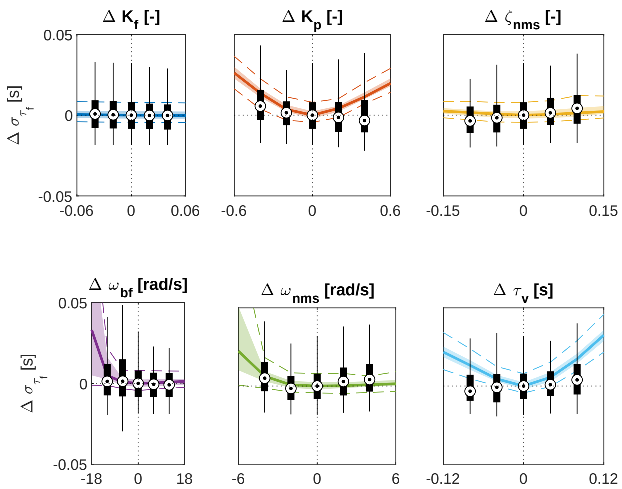

(b) $\sigma_{\tau_{f,est}}$ sensitivity.

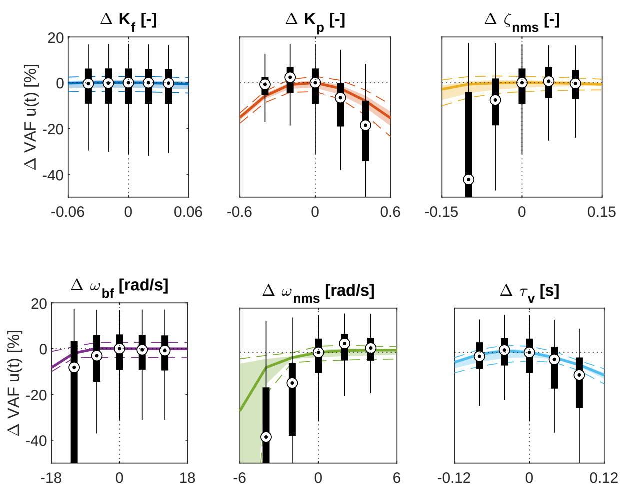

(c) VAF sensitivity.

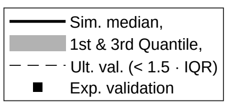

Fig. 19: Simulated (lines) and experimental (box plots) normalized sensitivity of fixing parameters on bias (a), standard deviation (b) and VAF (c).

C. Estimating τ_f With Time-Varying Preview (Step 3)

Besides observing how well the DEKF can estimate τ_f in time-varying preview tasks, it is desirable to find patterns in its performance. For the sigmoid steps, both transient (e.g., time to re-convergence after step) and static (e.g., bias before and after step) performance is studied. Here, the non-τ_f values can be fixed at either their initial (before step) or terminal (after step) values while estimating τ_f. For the sine variations, making the assumption that the DEKF's τ_f estimation traces are sinusoidal as well, it is studied how these fitted sine estimations compare to the originally designed signals. In Fig. 20, five simulated examples can be found of the look-ahead time estimations in the time domain.

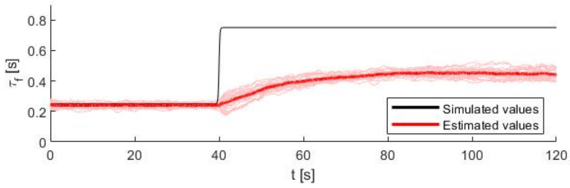

(a) Large step up, HO parameters fixed at initial values.

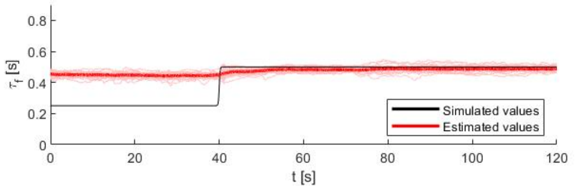

(b) Small step up, HO parameters fixed at terminal values.

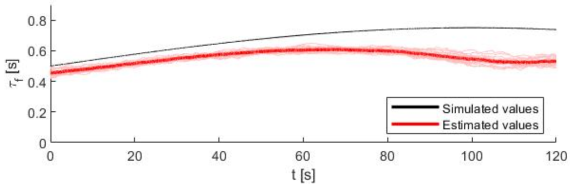

(c) Low frequency ($\frac{\pi}{200}$ rad/s), large amplitude.

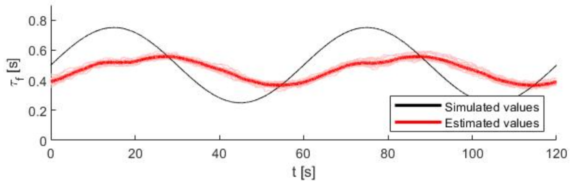

(d) Mid frequency ($\frac{\pi}{30}$ rad/s), large amplitude.

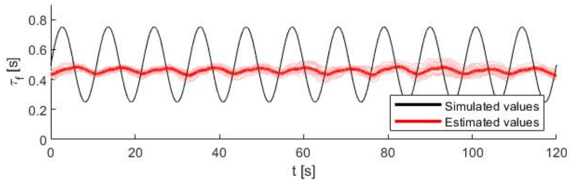

(e) High frequency ($\frac{11\pi}{60}$ rad/s), large amplitude.

Fig. 20: Simulated estimation traces (25x, and mean) of a large (a) and small (b) sigmoid step up, and of a low (c), mid (d), and high (e) frequency sine variation in τ_f. Other HO parameters fixed at their initial (a), terminal (b), and mean (c,d,e) values.

*1) **Sigmoid Step Results (Fig. 21–24)**:* Fig. 20a–b show examples of the DEKF estimation in reaction to a sigmoid step in preview. It takes time for the filter to converge to a new look-ahead time estimation and bias remains in these estimations. In Fig. 21, the re-convergence time to a new τ_f estimate after sigmoid steps is shown. This figure validates that the filter managed to find a new equilibrium and it quantifies the time this takes. This is comparable to the initialization step (Fig. 17), but now the initial state is already converged around an operating point, rather than set arbitrarily. In the simulations, the non-τ_f parameters are fixed at the value that they have after the behavior step change. For the experiments, these HO parameter values were fixed at an LTI-determined value based on the TI conditions that have the same display settings as the TV conditions after the step. The simulated results in the figure base convergence on staying between a +/- 0.025 s margin of a trace where no step occurred. For the experimental box plots, LTI-estimated values of the TI conditions were used for the fixed HO parameter values and an expected bias (Fig. 22) after the step is calculated. The LTI estimate and the expected bias together form the estimation target value. Convergence is defined by staying within a +/- 0.050 s margin from the target value, because σ_{τ_f} is approximately twice as high for experiments as for simulations. Because the measurement domain for convergence time is [40,80] s, the maximum registered values are 40 s. The plot shows a similar pattern to the DEKF initialization study (Fig. 17). The median T_{conv} for $\Delta\tau_f = 0$ s for simulations shows zero as expected, but the experimental data do not have zero convergence time, because of operator variability during the run, breaking with the convergence threshold. The results show that the DEKF is expected to re-convergence within approximately 30 s for $\Delta\tau_f$ = [-0.3,0.5] using its current settings.

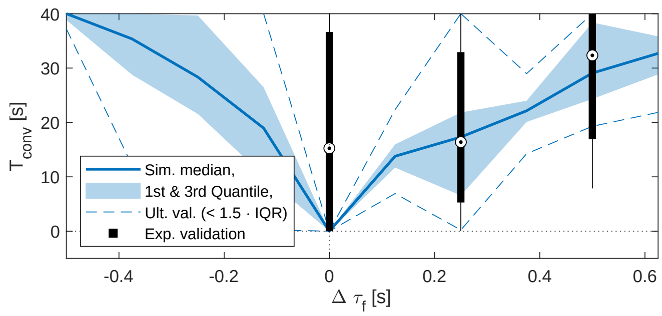

Fig. 21: Effect of sigmoid step size on convergence time. Other HO parameters fixed at their terminal value.

After the transient domain has passed and the DEKF has re-converged, it is studied how the performance of the DEKF after the sigmoid step in τ_f compares to before the step. In Fig. 22–24, the bias, standard deviation and VAF are shown, respectively. The other HO parameters are fixed at either their initial value (a), or their terminal value (b). The total measurement domain, starting after the run-in time, is 120 seconds, of which the first 40 and the last 40 seconds are compared. The transient domain in between – used for T_{conv} calculations (Fig. 21) – is excluded from the analysis, since it can confound the equilibrium performance analysis.

The effect of a look-ahead time sigmoid step on the DEKF bias performance is shown in Fig. 22. The blue results correspond to the first 40 seconds of the measurement domain and the red points to the last 40 seconds. Near-perfect symmetry is observed for the two parameter fixation options. Almost no estimation bias is witnessed when the other HO parameters are fixed at their scheduled (simulations) or LTI-estimated (experiments) values. In other words, when the parameters are fixed at their initial values, no bias is expected before the step, and when fixed at their terminal values, this holds for after the step. From the simulated estimations, a linear relation between sigmoid step size and bias is concluded with a slope of approximately 0.04 s ($|\tau_{f,est}|$) per 0.1 s ($|\Delta\tau_f|$). The three experimental validation points overlap well with the simulations, although the bias slope appears to be steeper for the HMI experiment data. The bias is an artifact of the fixed HO parameters during estimations, but the linear relation implies that a mapping between estimated and true values can be synthesised for the DEKF. For example, plots like Fig. 22 can be created for a large range of non-τ_f HO parameter fixations and many sigmoid preview time variations. Then, when certain step changes in look-ahead time are detected by the DEKF while knowing the fixed non-τ_f parameter settings, the expected bias in τ_f can be determined and used for estimation correction. This computationally heavy procedure would require further research before implementation.

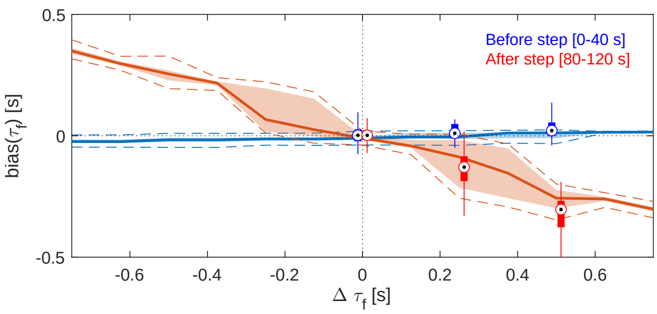

(a) Other HO parameters fixed at initial value.

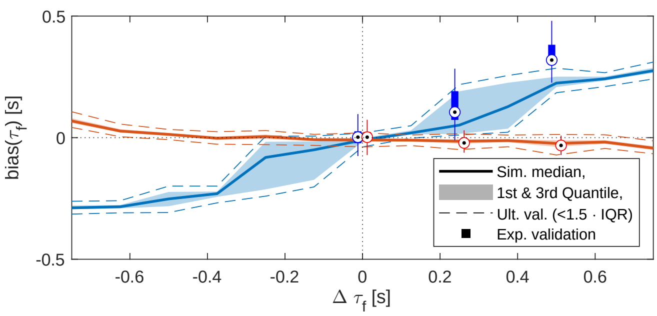

(b) Other HO parameters fixed at terminal value.

Fig. 22: Effect of sigmoid step size on bias($\tau_{f,est}$). Other HO parameters fixed at their initial (a) or terminal (b) value.

In Fig. 23, the effect is shown of different sigmoid step sizes on the standard deviation of the estimated look-ahead time (σ_{τ_f}). Looking at the simulations, there seems to exist a square relation between the standard deviation and the size of the step. For large steps in τ_f of +/- 0.75 s, σ_{τ_f} is expected to increase by a factor three to four. In the case that a step up is made and the other HO parameters are fixed at their terminal value (right side of Fig. 23b), σ_{τ_f} is high both before and after the sigmoid step. This suggests that the way in which the parameter values are fixed has an effect on the consistency of the results. When fixing the non-τ_f HO parameters at their terminal values, the estimation performance is expected to be better after the sigmoid step. However, the left side of Fig. 23b shows that this is not the case. This is because the τ_f estimation standard deviation generally decreases when the parameter approaches zero (pursuit tracking). The DEKF has more difficulty in consistently estimating the look-ahead time, most probably due to the much rougher tracking input of the HO. For the experimental validation box plots, the same relation seems to be present as for the simulations. However, generally, σ_{τ_f} is significantly higher, because the variability of the DEKF and of the HO are accumulated here. Understanding how the standard deviation changes can help understanding the variability of DEKF results in TV conditions. It also has an immediate effect on analyses, for example on how convergence can be determined (Fig. 21).

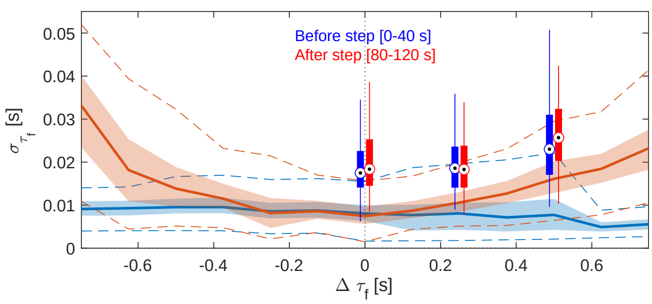

(a) Other HO parameters fixed at initial value.

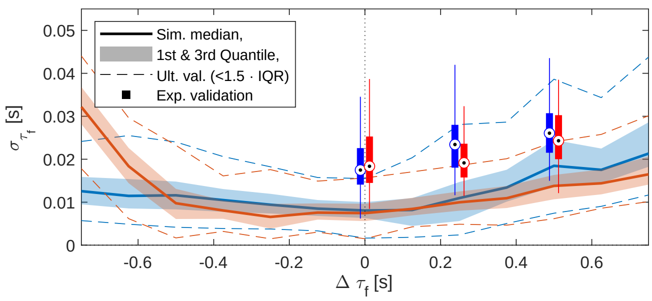

(b) Other HO parameters fixed at terminal value.

Fig. 23: Effect of sigmoid step size on $\sigma_{\tau_{f,est}}$. Other HO parameters fixed at their initial (a) or terminal (b) value.

In Fig. 24, the effects of sigmoid steps in τ_f on the VAF of the reconstructed signal ($\hat{u}(t)$) are shown. It is expected that the re-simulated tracking input corresponds well with the simulated or measured tracking input, when the non-τ_f parameters are fixed at their simulated or LTI-determined values. Comparable to the bias plots (Fig. 22), a constant and higher VAF value is expected for the first 40 seconds if the HO parameters are fixed at the initial value, and for the last 40 seconds if they are fixed at the terminal value. However, both the simulation plots and the validation boxplots have unexpected results. The size of $\Delta\tau_f$ seems to make impact, but this time on both the initial and terminal 40 seconds. This can be explained by the values at which the non-τ_f HO parameters are fixed. If the HO parameters are fixed at a value corresponding to large preview times, the reconstruction of the tracking input ($\hat{u}(t)$) coincides better with the original signal ($u(t)$). The preview model is harder to identify when less display preview time is available. This is why the left hand side in Fig. 24a and the right hand side in Fig. 24b show higher VAF values. Which HO parameters exactly contributes how much to this phenomenon is left for future research. The expected VAF values of the reconstructed tracking input remain higher than 70% for even the largest sigmoid step changes in display preview. This means that the DEKF is capable of capturing nearly all signal information by purely estimating the look-ahead time.

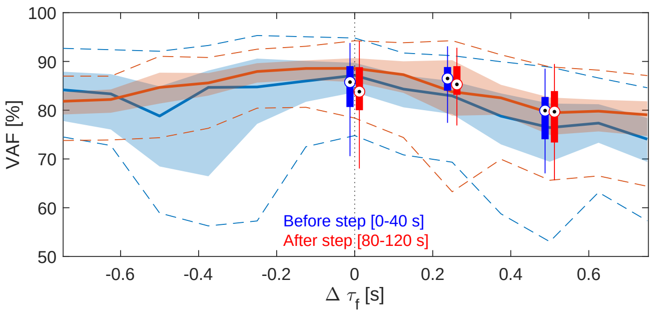

(a) Other HO parameters fixed at initial value.

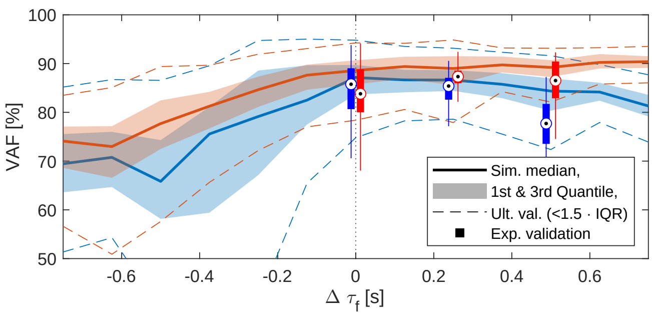

(b) Other HO parameters fixed at terminal value.

Fig. 24: Effect of sigmoid step size on VAF. Other HO parameters fixed at their initial (a) or terminal (b) value.

*2) **Sine Variation Results (Fig. 25–28)**:* The sigmoid step analyses showed mostly equilibrium performance, both before and after the change in look-ahead time. Furthermore, it provided knowledge on how fast the transition between these equilibria occurred. The sine variation results provide additional insights in the transient behavior of the DEKF. As input, the HO look-ahead time is varied with a sine schedule. After the preliminary phase of this research (Part III), the DEKF estimation response $\tau_{f,est}$ to sinusoidal variation in τ_f is assumed to be sine-shaped as well. This means that the $\tau_{f,est}$ data can be fitted to a sine wave to form the regressed estimation signal $\tau_{f,reg}$, with a specific amplitude A_{reg}, phase ϕ_{reg}, mean μ_{reg} and frequency ω_{reg}. These fitted sine parameters can then be compared to the simulated τ_f values or the experiment τ_p values, respectively.

The HO parameter amplitudes in the simulations are based on the LTI estimated values of TI runs. The means for the experimental data are the LTI estimated values for the sine TV experiments. The gain and phase between the estimated sine-fitted estimation $\tau_{f,reg}$ and the originally sine variations of the preview are shown in Fig. 25. For the experiment data, the reference amplitude is based on the TI estimations and the reference phase is assumed to be equal to the τ_p variations.

Based on the sigmoid step findings on convergence speed, the DEKF is expected to be capable of keeping track of relatively slow changes in τ_f. Every sine variation that takes 30 seconds or more to move from its mean to its peak – thus with a period of more than 120 seconds – should be identifiable (Fig. 21) without a delay. The response gain is expected to be dependent on the amplitude of the HO τ variations, because fixing the non-τ_f parameters introduces an estimation bias. However, this bias is not expected to be larger than 0.1 s (Fig. 22). Looking at the Bode plot domain of Fig. 25, the gain is expected to be slightly lower than 1, and the delay is expected to be 0 for the extremely low frequencies ($< 0.052\ rad/s = 1/120\ Hz$). From that point onward, the reactive nature of the DEKF would suggest a lag function in the response. This is expected to continue until the response is completely out of phase with the preview variations of the task.

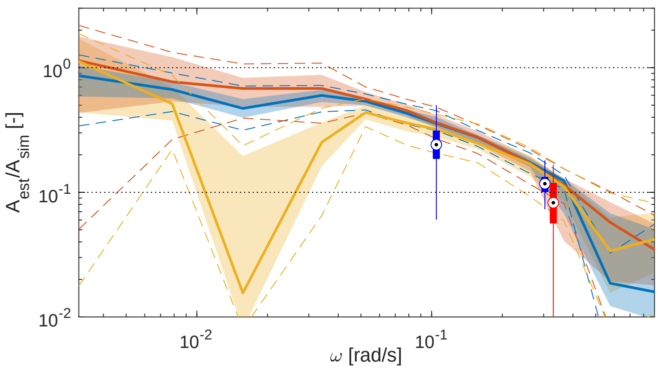

(a) Amplitude gain.

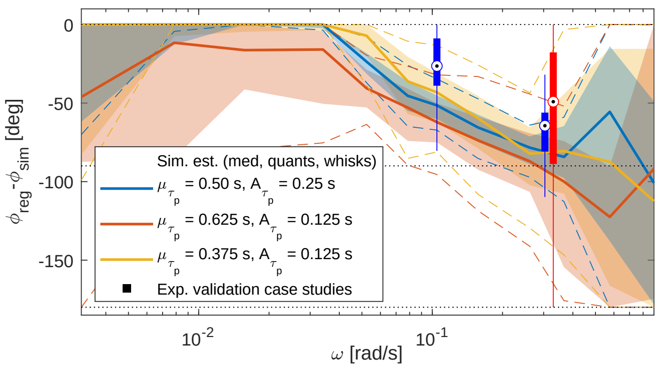

(b) Phase delay.

Fig. 25: Effect of sine frequency on amplitude gain (a) and phase delay (b) between regressed $\tau_{f,reg}$ and (expected) original τ_f. Other HO parameters fixed at their mean values.

Looking at the results in Fig. 25, the first observation is how well the experiment data overlap with the simulations. Both the experimental amplitude gain and phase delay seem to follow the same trend as their simulated counterparts. The gain is systematically lower for the experiments, which could be explained by the fact that the sine-fitted estimations amplitude A_{reg} is compared to the amplitude of the preview time in the display. Humans are expected to use less preview than provided [23], which can explain the offset with regard to the simulations. The difference between the fitted sine phase ϕ_{reg} and the phase of the display preview time is smaller for the experiments than for the simulations. A possible explanation for this could be that, during the tracking experiments, the participants created more lead than was expected in the simulations. This higher lead is then of course also reflected in the DEKF estimations for look-ahead time.

In the bode plot, the values at 0.016 rad/s for the condition with a mean of $\mu_{\tau_p} = 0.375\ s$ and an amplitude of $A_{\tau_p} = 0.125\ s$ (yellow) are inconsistent with the rest of the results. The estimation results of these unexpected values are presented in the time domain in Fig. 26. The estimation trace does not manage to follow the small look-ahead time estimations. When the estimation batch for this specific frequency was constructed, the only presented scenario is the black line from Fig. 26, and the DEKF shows a consistent response to this variation. The estimation first seems to follow the simulated values, after which it dips back to its original value. In the sine fitting calculations, an extremely low amplitude was recorded because the estimations appear fairly constant, resulting in the unexpected low values for the yellow line in Fig. 25.

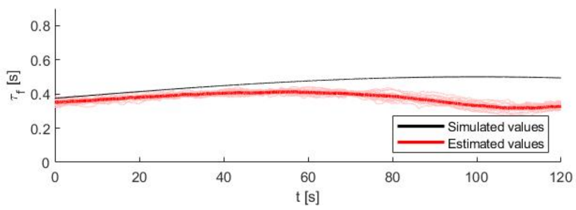

(a) Simulated estimations (x25, and mean).

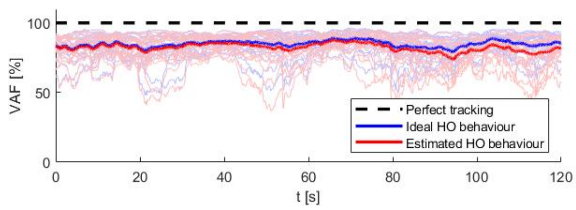

(b) VAF trace during estimation.

Fig. 26: Simulated case study of anomaly in Fig. 25 at 0.016 rad/s with μ_{τ_p} = 0.375 s and A_{τ_p} = 0.125 s.

Additional to the anomaly described above, for the frequencies lower than 0.052 rad/s, the spread in the results of the Bode plot is unexpectedly increasing instead of decreasing. This is an artefact of the sine fitting method, because no more than the 120 s measurement domain is used for the regression. If the sine waves are larger than this domain (Fig. 20c), not even one entire period can be used, impeding the regression quality. From a mathematical perspective, longer runs could have been simulated for the lower frequencies. However, with a factor 10 to 30 computational expense increase for these frequencies, it was decided to keep the plots as they are. The τ_f estimation time traces of different low-frequency estimations support the expectation that the look-ahead time tracking is synchronous to the preview variations.

For frequencies between 0.03 rad/s and 0.4 rad/s, the Bode plots seems to follow the trend of a lag function (Fig. 27). Within this domain, the response gain and phase delay gradually decrease to 0.08 and -100 degrees, respectively. This effectively means that nearly no variation is identified compared to the actual preview variations. When the frequencies become higher than 0.4 rad/s, the spread of the fitted sine parameters becomes as large as the entire physically possible phase delay domain [-180,0] degrees, and the median values stop following the lag trend. This is because the DEKF is too slow to adapt its estimation strategy and starts to show a random walk for τ_f between the scheduled sinusoidal values. For the higher frequencies, it becomes clear that the assumption of a sine response might be insufficient to accurately fit the τ_f estimations. The asymmetrical convergence time plots (Fig. 17, Fig. 21) support this finding. Future research could be done to investigate what type of periodical function better fits the DEKF estimation response to sine variations in preview time.

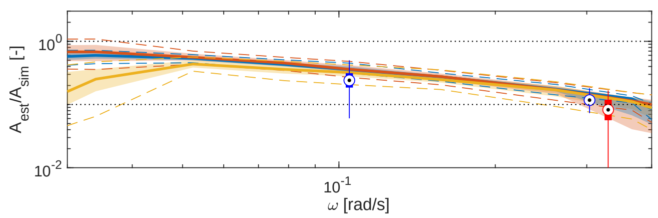

(a) Amplitude gain.

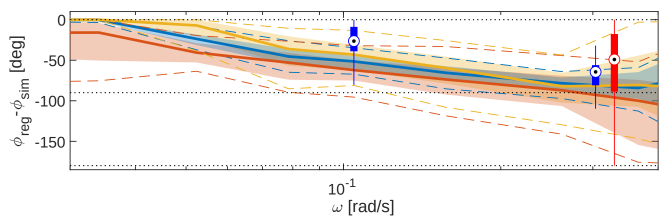

(b) Phase delay.

Fig. 27: Scoped copy of Fig. 25, domain: [0.03,0.4] rad/s.

The experimental data points for gain and phase seem to coincide well with the results from simulated data. However, the combined assumptions of a linear relation between the display and HO behavior on the one hand and a simple lag relation between HO look-ahead time variations and the DEKF estimations on the other, can accumulate to estimation confounds. To check the validity of these assumptions, the normalized root mean squared error (RMSE) between $\tau_{f,est}$ and $\tau_{f,reg}$ is presented in Fig. 28. From simulations, it is clear that the lowest frequencies show irregularities because the domain for the sine fitting was to small. The highest frequencies come with increased RMSE values, because the assumption for a sinusoidal DEKF response appears to be insufficiently accurate. Regardless of the frequency, these RMSE values are significantly higher for experimental data, meaning that the sine response assumption's fidelity is lower for actual HMI applications than for simulations. All results from the TV analyses point out that the DEKF can be effectively used for TV HO look-ahead time estimation. As long as the effect of constraining assumptions is understandable, it could be a powerful tool for future identification applications.

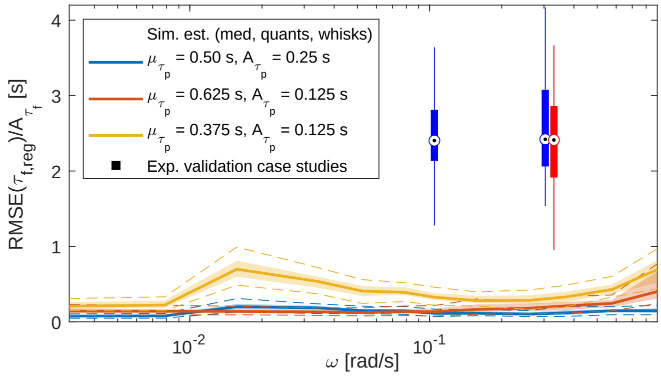

Fig. 28: Effect of sine frequency on normalized RMSE between regressed $\tau_{f,reg}$ and estimated $\tau_{f,est}$. Other HO parameters fixed at their mean values.

VI. Discussion and Recommendations

A. Discussion of Results

Finding the optimal settings for the DEKF can be a tedious process and depends – amongst other aspects – on the controlled element dynamics. To make a deep-dive in the time-varying identification performance, it was decided to select only one type of controlled element. The promising DEKF performance for single integrator tracking data in Vertregt's study [14] motivated to focus on the results and conclusions of single integrator dynamics tasks. Fundamental cybernatics research by McRuer [19], [22], [36] often also included gain and double integrator dynamics. Later, Van der El showed in a range of studies [34] that the preview parameters are highly dependent on controlled element dynamics. Human operators show more pronounced low-pass filtering behavior while processing gain and double integrator signals. For this reason, the results presented in this article cannot be directly transferred to other dynamics types. Still, a large step is made by quantitatively showing the DEKF's estimation performance during time-varying human operator tracking tasks. The knowledge gained can be used as a starting point for the analysis methodology of other controlled element dynamics.

For single integrator tracking data, seven human operator parameters from Van der El's preview model have to be identified [12]. During the initial time-varying analyses by Vertregt [14], it was shown that DEKF-estimating all seven parameters simultaneously comes with a considerable bias and variance. He proposed to keep other parameters fixed while studying the identification of a specific human operator parameter. Quantitative and repeatable results for all seven preview model parameters could not be acquired within the researcher's available time and computational capacity. For that reason, this study focuses on the highly influential look-ahead time parameter. Possibly, this scoping operation could reduce the flexible and complete potential of the DEKF [13], [31], [32]. This is because behavior variations are in this case only attributed to the look-ahead time parameter, whereas they might have originated from other parameters that are fixed. Fortunately, the constraining effect of this assumption is much less than expected. With all other human operator parameters fixed, the DEKF is well capable of identifying time variations in preview behavior. The results are consistent, and the simulations match well with reality. For the first time, performance of the DEKF during time-varying preview tracking tasks has been quantified, and these insights can be used to improve the algorithm.

The sigmoid step results show that the DEKF is not yet capable of real-time human operator identification. The algorithm can take up to 40 seconds to reach a new estimation equilibrium after a large step change in preview time has occurred. No initialization settings were found that can reach an equilibrium faster, while maintaining the desired estimation accuracy and consistency. Reflecting on the DEKF tuning strategy, only the sensitivity of the adaptive process and measurement noise covariance matrices has been quantified with a limited Monte Carlo analysis. This implies that the measured convergence speed is not the optimal result. Other tuning operations could be revisiting the state and parameter covariance matrices, or the number of measurements included to update the adaptive process and measurement noise covariance matrices. Furthermore, it can be investigated whether the optimal tuning parameters are variable with the of preview time. Artificial intelligence could be used link the measurable signals of the preview tracking task to optimal DEKF initialization and tuning. The current DEKF design is a baseline that can be used for the optimization for time-varying look-ahead time identification. Improving the convergence speed would facilitate reaching the ultimate goal of real-time human operator identification in shared control applications [4].

Also for the sine analyses, the DEKF's convergence speed is visible in the results. Up until a certain frequency, a lag function trend can be expected between the variation of preview time and the look-ahead time estimation. This lag function is sustained to a frequency of approximately 0.4 rad/s, after which the results on gain and phase become less predictable while their spread increases. This drop in predictability is most likely caused by the assumptions that there is a linear relation between the display preview time and the human operator look-ahead time variations and that the estimations can be fitted to a simple sine wave. However, both the operator's reaction to display variations and the algorithm's reaction to parameter variations can very well be non-linearly related. The root mean squared error values of the sine-fitted DEKF response suggest that more complex fitting functions could enable a better understanding of the DEKF over a larger preview variation frequency bandwidth. The performance in the lower frequencies is already well-understood, now the challenge remains for the higher bandwidths.

It was impossible to fix human operator parameters other than look-ahead time at their correct values, because all parameters vary with the preview. Therefore, it was assumed that the time-varying parameters can be related to the time-invariant data traces. For the two sigmoid step experiments, a time-invariant run was performed for the conditions before and after the step. The human operator parameters from the time-invariant run could be identified with the frequency-domain method from Van der El [12], [23]–[26]. These identified parameters then served as the baseline for fixing the parameters in the time-varying estimations. In the seeded simulations, the parts where the tracking tasks of the time-invariant and the time-varying simulations overlap result in identical behavior. For that reason, the simulated time-invariant human operator parameters can be safely used for time-varying analyses. For the human control experiments, every estimation trace has a unique stochastic realization, thus it is possible that the HO parameters are fixed at an incorrect value during the time-varying experiments. Nonetheless, looking at the time-varying estimation results, the validation experiments show a striking resemblance with the simulations. This supports the procedure of performing a calibration frequency-domain human operator parameter estimation for a time-invariant experiment prior to a time-varying estimation run.

The researcher encountered a limitation in the available computational power and memory capacity. Because the time-domain simulation and estimation algorithms are computationally expensive, a trade-off was made between the number of investigated conditions and the statistical validity per condition. The results could be refined by allowing longer run times, more sustainably coding the DEKF identification algorithm, and using more powerful computers. Although the results are not as smooth as the actual distributions should be, they indicate clearly the trends of the DEKF performance.

Based on earlier research by Vertregt [14], the DEKF was expected to be a promising candidate for time-varying human operator look-ahead time identification in single integrator tracking tasks. Fixing other human operator parameter estimates was suggested to make the look-ahead time estimations faster and more accurate. The study in this article systematically investigated the performance following these hypotheses. It was found that the DEKF indeed can identify preview time variations for experimental human operator tracking data. To improve the DEKF output, the algorithm is constrained to only estimate the look-ahead time. A limitation is that not the full scope of human operator parameters can be described. Fortunately, even when making this assumption, the filter seems to respond predictably and consistently for a wide range of conditions. From the smallest to the largest preview time sigmoid steps, the DEKF manages to identify the look-ahead time variations. Based on the step size, the estimation delay and bias linearly increase to 40 seconds and 0.4 seconds, respectively. Sinusoidal variations in preview are identified as well, where the DEKF behaves comparable to a lag function. In its current design, the DEKF's look-ahead time estimation performance is still rather dependent on fixation of other parameters. Because these fixed parameters correspond to a specific preview time condition, the DEKF performs best around this operating point. A key next step would be to make this initialization and tuning adaptive to the tracking task. This way, the DEKF truly becomes a competing time-varying identification algorithm for preview tracking tasks, that can enable advanced shared control applications.

B. Recommendations for Further Research

A next step in the DEKF validation procedure is to investigate performance for double integrator dynamics tasks. It can be analyzed what the transient and equilibrium performance is during sigmoidal and sinusoidal preview time variations in the display. The initial case studies for double integrator dynamics look-ahead time estimations by Vertregt [14] were less promising than their single integrator counterparts. The estimations had difficulty converging to the correct value for both time-invariant and time-varying conditions. Pointed out by Vertregt and repeated in the preliminary investigation of this study (Part III), the double integrator identification requires a revision of how the remnant is modeled. For double integrator tasks, human remnant is modeled by low-pass filtering white noise with a much lower break frequency than the forcing function bandwidth. Because of the remnant interfering with the target signal, crucial signal information might be lost, which can be accounted for if the remnant is included in the DEKF's human operator model.

For the further validation of all future algorithms, more time-varying experimental preview tracking data should be collected. As shown in this research, the acquisition of such data sets is a time-consuming process. The limited number of eight time-varying experiments required minimally eight – and always a multiple of eight – participants for a balanced within-subject data set. Every participant's tracking behavior was recorded for 100 minutes in total, making the experiment last three hours to complete. The box plots in the results section suggest that not many conditions have been validated and that the tested conditions' data are still relatively sparse. Ideally, a larger range of sigmoid steps in preview time is experimentally studied, moving both up and down. It would be interesting to confirm whether there is a linear relation between step size and estimation bias, or that other dynamics might be underlying. Additionally, more sine variation experiments could be performed, including results for a larger range of frequencies, and for sines with a different mean and amplitude. This way, it can be analyzed whether the lag function hypothesis holds, and what order lag can be expected.

Regarding the validation methodology, it is insightful to compare the DEKF's results to other time-varying identification algorithms. Especially because the actual time variations of the look-ahead time are not yet identifiable with a validated estimation tool, different algorithms should be put side by side in order to gain understanding in human behavior. A summarizing study can be performed, where the state-of-the-art time-varying algorithms [15]–[18] estimate human parameters for a few basic time-varying conditions. The strengths and points of improvements of the different methods can be systematically analyzed, which can provide lessons for the DEKF. For example, if the lag of the DEKF is considerably larger than for other methods, the comparative study can show the potential gain for future algorithm implementations. This way, the DEKF will be more efficiently improved to a desired optimum, capable of real-time human identification.

VII. Conclusion

This study investigated the performance of a *Dual Extended Kalman Filter* (DEKF) for human look-ahead time parameter estimations during single integrator tracking tasks with a time-varying display preview time. Both for realistic simulation data and for human-subject experiment data, the algorithm initialization sensitivity and the performance for sigmoid and sine preview variations were analyzed. The results suggest that a linear relation between look-ahead time initialization offset and convergence time exists. Underestimated initial look-ahead time values appear to be converging faster than overestimated values. Initialization that is 0.25 s away from the correct value is expected to converge within 30 s. When fixing human operator parameters that are not look-ahead time, it should be ensured that the preview break frequency and the neuromuscular break frequency are not underestimated. The human processing delay should be fixed at a value that is estimated for a specific human operator with a linear time-invariant algorithm. If these notions are not taken into account, this can result in 0.1 seconds look-ahead time biases and a factor three to four increase in standard deviation of the DEKF estimations. For sine variations in preview time with the lowest frequencies, the DEKF shows a synchronous response in the look-ahead time estimations. For the middle frequencies (one to ten periods in the 120 s measurement domain), the DEKF behaves as a lag function, decreasing the estimation gain and phase delay to 0.08 and -100 degrees, respectively, compared to the preview time variations. The higher frequencies result in an estimation response that is better described as random walk. This research included realistic simulations and validation experiments to quantify the capabilities of the DEKF for the time-varying identification during preview tracking. It can serve as a starting point for future improvements to the algorithm and for investigating additional task variable variations. This way, the findings contribute to the development of a time-varying human identification algorithm, which in turn enables automated shared control applications to increase safety and efficiency of vehicle operations.

Acknowledgment

The author would like to thank his supervisors D.M. Pool, M. Mulder and K. van der El for the time and effort they invested in the progress of this project. Their critical views on the methods and results ensured the quality of the research. Their sincere interest in and advice for well-being helped keeping the author motivated. Their constructive feedback throughout to process helped with the personal and professional development of the author.

References

[1] R. Parasuraman, T. B. Sheridan, and C. D. Wickens, "A Model for Types and Levels of Human Interaction with Automation," *IEEE Transactions on Systems, Man, and Cybernetics - Part A: Systems and Humans*, vol. 30, no. 3, pp. 286–297, 2000.

[2] L. Li, D. Wen, N.-N. Zheng, and L.-C. Shen, "Cognitive Cars: A New Frontier for ADAS Research," *IEEE Transactions on Intelligent Transportation Systems*, vol. 13, no. 1, pp. 395–407, 2011.

[3] S. Barendswaard, "Modelling Individual Driver Trajectories to Personalise Haptic Shared Steering Control in Curves," Ph.D. dissertation, Delft University of Technology, Delft, March 2021.

[4] M. Mulder, D. M. Pool, D. A. Abbink, E. R. Boer, P. M. T. Zaal, F. M. Drop, K. van der El, and M. M. van Paassen, "Manual Control Cybernetics: State-of-the-Art and Current Trends," *IEEE Transactions on Human-Machine Systems*, vol. 48, no. 5, pp. 468–485, 2018.

[5] Z. Xu, K. Zhang, H. Min, Z. Wang, X. Zhao, and P. Liu, "What Drives People to Accept Automated Vehicles? Findings From a Field Experiment," *Transportation Research Part C: Emerging Technologies*, vol. 95, pp. 320–334, oct 2018.

[6] A. Shariff, J.-F. Bonnefon, and I. Rahwa, "Psychological Roadblocks to the Adoption of Self-Driving Vehicles," *Nature*, vol. 10, pp. 694–696, 2017.

[7] W. Scholtens, S. Barendswaard, D. M. Pool, M. M. van Paassen, and D. A. Abbink, "A New Haptic Shared Controller Reducing Steering Conflicts," in *Proceedings - 2018 IEEE International Conference on Systems, Man, and Cybernetics, SMC 2018*. Institute of Electrical and Electronics Engineers Inc., jan 2019, pp. 2705–2710.

[8] D. A. Abbink, M. Mulder, and E. R. Boer, "Haptic Shared Control: Smoothly Shifting Control Authority?" *Cognition, Technology and Work*, vol. 14, no. 1, pp. 19–28, mar 2012. [Online]. Available: https://link.springer.com/article/10.1007/s10111-011-0192-5

[9] F. Flemisch, M. Heesen, T. Hesse, J. Kelsch, A. Schieben, and J. Beller, "Towards a Dynamic Balance Between Humans and Automation: Authority, Ability, Responsibility and Control in Shared and Cooperative Control Situations," *Cognition, Technology and Work*, vol. 14, no. 1, pp. 3–18, mar 2012. [Online]. Available: https://link.springer.com/article/10.1007/s10111-011-0191-6

[10] J. Rasmussen, "Skills, Rules, and Knowledge; Signals, Signs, and Symbols, and Other Distinctions in Human Performance Models," *IEEE Transactions on Systems, Man and Cybernetics*, vol. SMC-13, no. 3, pp. 257–266, 1983.

[11] B. Strauch, "Ironies of Automation: Still Unresolved after All These Years," *IEEE Transactions on Human-Machine Systems*, vol. 48, no. 5, pp. 419–433, oct 2018.

[12] K. van der El, D. M. Pool, H. J. Damveld, M. M. van Paassen, and M. Mulder, "An Empirical Human Controller Model for Preview Tracking Tasks," *IEEE Transactions on Cybernetics*, vol. 46, no. 11, pp. 2609–2621, 2016.

[13] A. Popovici, P. M. T. Zaal, and D. M. Pool, "Dual Extended Kalman Filter for the Identification of Time-Varying Human Manual Control Behavior," *Proceedings of the AIAA Modeling and Simulation Technologies Conference, Denver (CO)*, 2017.

[14] C. Vertregt, "Estimation of Time-Varying Human Manual Control Behaviour in Preview Tracking Tasks using a Dual Extended Kalman Filter," 2020, preceding work to this DEKF validation study.

[15] P. M. T. Zaal, "Manual Control Adaptation to Changing Vehicle Dynamics in Roll-Pitch Control Tasks," *Journal of Guidance, Control, and Dynamics*, vol. 39, no. 5, pp. 1046–1058, 5 2016. [Online]. Available: https://arc.aiaa.org/doi/10.2514/1.G001592

[16] P. M. T. Zaal and B. T. Sweet, "Estimation of Time-Varying Pilot Model Parameters," *AIAA Modeling and Simulation Technologies Conference 2011*, 2011.

[17] H. A. Van Grootheest, D. M. Pool, M. M. van Paassen, and M. Mulder, "Identification of Time-Varying Manual-Control Adaptations with Recursive ARX Models," in *Proceedings of the AIAA Modeling and Simulation Technologies Conference, Kissimee*, no. AIAA-2018- 0118. American Institute of Aeronautics and Astronautics Inc, AIAA, 2018. [Online]. Available: https://doi.org/10.2514/6.2018-0118

[18] J. Rojer, D. M. Pool, M. M. van Paassen, and M. Mulder, "UKF-based Identification of Time-Varying Manual Control Behaviour," in *Proceedings of the 14th IFAC Symposium on Analysis Design and Evaluation ofHuman Machine Systems Tallinn, Estonia*, vol. 52, no. 19. Elsevier B.V., 1 2019, pp. 109–114.

[19] D. T. McRuer and H. R. Jex, "A Review of Quasi-Linear Pilot Models," *IEEE Transactions on Human Factors in Electronics*, vol. HFE-8, no. 3, pp. 231–249, 1967.

[20] R. W. Allen and J. F. O'hanlon, "Effects of Roadway Delineation and Visibility Conditions on Driver Steering Performance," *Transportation Research Record*, vol. 739, pp. 5–8, 1979. [Online]. Available: https://www.semanticscholar.org/paper/EFFECTS-OF-ROADWAY-DELINEATION-AND-VISIBILITY-ON-Allen-O%27hanlon/eb0484614672f1b84c2db3a5f70e46e075cff8b4
[21] M. F. Land and J. Horwood, "How Speed Affects the Way Visual Information Is Used in Steering," *Vision in Vehicles - VI*, pp. 43–50, 1998. [Online]. Available: https://trid.trb.org/view/492266
[22] D. T. McRuer, D. Graham, E. Krendel, and W. Reisener Jr, "Human Pilot Dynamics in Compensatory Systems-Theory," *Models, and Experiments with Controlled Element and Forcing Function Variations. AFFDL-TR-65-15*, 1965.
[23] K. van der El, S. Padmos, D. M. Pool, M. M. van Paassen, and M. Mulder, "Effects of Preview Time in Manual Tracking Tasks," *IEEE Transactions on Human-Machine Systems*, vol. 48, no. 5, pp. 486–495, 10 2018. [Online]. Available: https://doi.org/10.1109/THMS.2018.2834871
[24] K. van der El, *How Humans Use Preview Information in Manual Control*, 2018. [Online]. Available: http://repository.tudelft.nl/
[25] K. van der El, D. M. Pool, and M. Mulder, "Analysis of Human Remnant in Pursuit and Preview Tracking Tasks," in *Proceedings of the 14th IFAC Symposium on Analysis Design and Evaluation ofHuman Machine Systems Tallinn, Estonia*, vol. 52, no. 19. Elsevier B.V., 1 2019, pp. 145–150.
[26] K. van der El, D. M. Pool, M. M. van Paassen, and M. Mulder, "Effects of Target Trajectory Bandwidth on Manual Control Behavior in Pursuit and Preview Tracking," *IEEE Transactions on Human-Machine Systems*, vol. 50, no. 1, pp. 68–78, 2 2020.
[27] G. J. Silva, A. Datta, and S. P. Bhattacharyya, "Controller Design via Padé Approximation can Lead to Instability," in *Proceedings ofthe 40th IEEE Conference on Decision and Control (Cat. No. 01CH37228)*, vol. 5, 2001, pp. 4733–4737.
[28] E. R. Boer and R. V. Kenyon, "Estimation of Time-Varying Delay Time in Nonstationary Linear Systems: An Approach to Monitor Human Operator Adaptation in Manual Tracking Tasks," *Systems and Humans*, vol. 28, no. 1, pp. 89–99, 1998.
[29] R. F. M. Duarte, D. M. Pool, M. M. van Paassen, and M. Mulder, "Experimental Scheduling Functions for Global LPV Human Controller Modeling," *IFAC-PapersOnLine*, vol. 50, no. 1, pp. 15 853–15 858, 2017, 20th IFAC World Congress. [Online]. Available: https://www.sciencedirect.com/science/article/pii/S2405896317331440
[30] J. Steen, H. J. Damveld, R. Happee, M. M. van Paassen, and M. Mulder, "A Review of Visual Driver Models for System Identification Purposes," in *Conference Proceedings - IEEE International Conference on Systems, Man and Cybernetics*, 2011, pp. 2093–2100.
[31] C. You, J. Lu, and P. Tsiotras, "Nonlinear Driver Parameter Estimation and Driver Steering Behavior Analysis for ADAS Using Field Test Data," *IEEE Transactions on Human-Machine Systems*, vol. 47, no. 5, pp. 686–699, oct 2017.
[32] X. Li and R. Kennel, "General Formulation of Kalman-Filter-Based Online Parameter Identification Methods for VSI-Fed PMSM," *IEEE Transactions on Industrial Electronics*, vol. 68, no. 4, pp. 2856–2864, apr 2021.
[33] R. E. Kalman, "A New Approach to Linear Filtering and Prediction Problems," *Journal of Basic Engineering*, vol. 82, pp. 35–45, 3 1960.
[34] K. van der El, D. M. Pool, M. M. van Paassen, and M. Mulder, "Effects of Preview on Human Control Behavior in Tracking Tasks With Various Controlled Elements," *IEEE Transactions on Cybernetics*, vol. 48, no. 4, pp. 1242–1252, 4 2018. [Online]. Available: https://doi.org/10.1109/TCYB.2017.2686335
[35] W. H. Levison, S. Baron, and D. L. Kleinman, "A Model for Human Controller Remnant," *IEEE Transactions on Man-Machine Systems*, vol. 10, no. 4, pp. 101–108, 1969.
[36] D. T. McRuer, "Human Dynamics in Man-Machine Systems," *Automatica*, vol. 16, no. 3, pp. 237–253, may 1980.

II

Scientific Article Appendices

A

State-Space Representation of Preview Model

$$\frac{F_t^*(s)}{F_t(s)} = \frac{-\tau_f^{*3}s^3 + 12\tau_f^{*2}s^2 - 60\tau_f^*s + 120}{\tau_f^{*3}s^3 + 12\tau_f^{*2}s^2 + 60\tau_f^*s + 120} \cdot K_f \frac{\omega_{b,f}}{\omega_{b,f} + s} \tag{A.1}$$

$$\frac{\hat{U}(s)}{F_t^*(s)} = (K_p + K_v s) \cdot \frac{\omega_{NM}^2}{s^2 + 2\zeta_{NM}\omega_{NM}s + \omega_{NM}^2} \cdot \frac{-\tau_v^3s^3 + 12\tau_v^2s^2 - 60\tau_v s + 120}{\tau_v^3s^3 + 12\tau_v^2s^2 + 60\tau_v s + 120} \tag{A.2}$$

$$\frac{\hat{U}(s)}{Y(s)} = -1 \cdot (K_p + K_v s) \cdot \frac{\omega_{NM}^2}{s^2 + 2\zeta_{NM}\omega_{NM}s + \omega_{NM}^2} \cdot \frac{-\tau_v^3s^3 + 12\tau_v^2s^2 - 60\tau_v s + 120}{\tau_v^3s^3 + 12\tau_v^2s^2 + 60\tau_v s + 120} \tag{A.3}$$

$$\begin{aligned}
\underline{\dot{x}_s} &= \begin{bmatrix} 0 & 1 & 0 & 0 & 0 & 0 & 0 & 0 & 0 \\ 0 & 0 & 1 & 0 & 0 & 0 & 0 & 0 & 0 \\ 0 & 0 & 0 & 1 & 0 & 0 & 0 & 0 & 0 \\ 0 & 0 & 0 & 0 & 1 & 0 & 0 & 0 & 0 \\ -a_{2,0} & -a_{2,1} & -a_{2,2} & -a_{2,3} & -a_{2,4} & b_{1,0} & -b_{1,1} & b_{1,2} & -b_{1,3} \\ 0 & 0 & 0 & 0 & 0 & 0 & 1 & 0 & 0 \\ 0 & 0 & 0 & 0 & 0 & 0 & 0 & 1 & 0 \\ 0 & 0 & 0 & 0 & 0 & 0 & 0 & 0 & 1 \\ 0 & 0 & 0 & 0 & 0 & -a_{1,0} & -a_{1,1} & -a_{1,2} & -a_{1,3} \end{bmatrix} \underline{x_s} + \begin{bmatrix} 0 & 0 \\ 0 & 0 \\ 0 & 0 \\ 0 & 0 \\ 0 & -1 \\ 0 & 0 \\ 0 & 0 \\ 0 & 0 \\ 1 & 0 \end{bmatrix} \begin{bmatrix} f_t \\ y \end{bmatrix} \\
\hat{u} &= \begin{bmatrix} b_{2,0} & b_{2,1} & b_{2,2} & -b_{2,3} & -b_{2,4} & 0 & 0 & 0 & 0 \end{bmatrix} \underline{x_s} + \begin{bmatrix} 0 & 0 \end{bmatrix} \begin{bmatrix} f_t \\ y \end{bmatrix}
\end{aligned} \tag{A.4}$$

$$a_{2,0} = \frac{120\omega_{NM}^2}{\tau_v^3} \qquad b_{2,0} = \frac{120K_p\omega_{NM}^2}{\tau_v^3}$$

$$a_{2,1} = \frac{60\tau_v\omega_{NM}^2 + 240\zeta_{NM}\omega_{NM}}{\tau_v^3} \qquad b_{2,1} = \frac{120K_v\omega_{NM}^2 - 60K_p\omega_{NM}^2\tau_v}{\tau_v^3}$$

$$a_{2,2} = \frac{12\omega_{NM}^2\tau_v^2 + 120\zeta_{NM}\omega_{NM}\tau_v + 120}{\tau_v^3} \qquad b_{2,2} = \frac{12K_p\omega_{NM}^2\tau_v^2 - 60K_v\omega_{NM}^2\tau_v}{\tau_v^3}$$

$$a_{2,3} = \frac{\omega_{NM}^2\tau_v^3 + 24\zeta_{NM}\omega_{NM}\tau_v^2 + 60\tau_v}{\tau_v^3} \qquad b_{2,3} = \frac{K_p\omega_{NM}^2\tau_v^3 - 12K_v\omega_{NM}^2\tau_v^2}{\tau_v^3}$$

$$a_{2,4} = \frac{2\omega_{NM}\zeta_{NM}\tau_v^3 + 12\tau_v}{\tau_v^3} \qquad b_{2,4} = K_v\omega_{NM}^2$$

$$a_{1,0} = \frac{120\omega_{b,f}}{(\tau_f^*)^3} \qquad b_{1,0} = \frac{120K_f\omega_{b,f}}{(\tau_f^*)^3}$$

$$a_{1,1} = \frac{60\omega_{b,f}\tau_f^* + 120}{(\tau_f^*)^3} \qquad b_{1,1} = \frac{60K_f\omega_{b,f}}{(\tau_f^*)^2}$$

$$a_{1,2} = \frac{12\omega_{b,f}(\tau_f^*)^2 + 60\tau_f^*}{(\tau_f^*)^3} \qquad b_{1,2} = \frac{12K_f\omega_{b,f}}{\tau_f^*}$$

$$a_{1,3} = \frac{\omega_{b,f}(\tau_f^*)^3 + 12(\tau_f^*)^2}{(\tau_f^*)^3} \qquad b_{1,3} = K_f\omega_{b,f}$$

B

Complete DEKF Algorithm

1) Parameter Prediction

$$\begin{aligned}\theta_k^- &= \theta_{k-1}^+ \\ P_{p,k}^- &= \Phi_{p,k-1} P_{p,k-1}^+ \Phi_{p,k-1}^T + \Gamma_{p,k-1} Q_p \Gamma_{p,k-1}^T\end{aligned} \tag{B.1}$$

2) State Prediction

$$\begin{aligned}x_{s,k}^- &= x_{s,k-1}^+ + f(x_{s,k-1}^+, \theta_k^-, f_{t,k+N_s}, y_{k-1})\Delta t \\ P_{s,k}^- &= \Phi_{s,k-1} P_{s,k-1}^+ \Phi_{s,k-1}^T + \Gamma_{s,k-1} Q_{s,k} \Gamma_{s,k-1}^T\end{aligned} \tag{B.2}$$

3) State Correction

$$\begin{aligned}S_{s,k} &= G_{s,k} P_{s,k}^- G_{s,k}^T + R \\ r_k &= u_k - g(x_{s,k}^-, \theta_k^-) \\ K_{s,k} &= P_{s,k}^- G_{s,k}^T S_{s,k}^{-1} \\ x_{s,k}^+ &= x_{s,k}^- + K_{s,k} r_k \\ P_{s,k}^+ &= (I - K_{s,k} G_{s,k}) P_{s,k}^- (I - K_{s,k} G_{s,k})^T + K_{s,k} R K_{s,k}^T\end{aligned} \tag{B.3}$$

4) State Limitation

$$\tilde{x}_{s,k}^+ = x_{s,k}^+ - D_{s,k}^T (D_{s,k} D_{s,k}^T)^{-1} (D_{s,k} x_{s,k}^+ - d_{s,k}) \tag{B.4}$$

5) Parameter Correction

$$\begin{aligned}S_{p,k} &= G_{p,k}^{tot} P_{p,k}^- (G_{p,k}^{tot})^T + R \\ K_{p,k} &= P_{p,k}^- (G_{p,k}^{tot})^T S_{p,k}^{-1} \\ \theta_k^+ &= \theta_k^- + K_{p,k} r_k \\ P_{p,k}^+ &= (I - K_{p,k} G_{p,k}^{tot}) P_{p,k}^- (I - K_{p,k} G_{p,k}^{tot})^T + K_{p,k} R K_{p,k}^T\end{aligned} \tag{B.5}$$

6) Parameter Limitation

$$\tilde{\theta}_k^+ = \theta_k^+ - D_{p,k}^T (D_{p,k} D_{p,k}^T)^{-1} (D_{p,k} \theta_k^+ - d_{p,k}) \tag{B.6}$$

C
Human-Subject Experiment Briefing and Consent Form

See next pages

Experiment Briefing

Human operator response to time-varying preview times in display

Thank you for your participation. This experiment is part of cybernetics research focusing on human behavior identification for tracking tasks with *preview*, i.e. tasks where the operator aims to align a system's state with a target trajectory ahead. The experiment is performed in the Human-Machine Interaction Laboratory (HMI Lab) at TU Delft's Faculty of Aerospace Engineering. This briefing will give an overview of the experiment and explains what is expected from the participants. Please read this document carefully. Should any questions or comments remain, always feel free to discuss these with the researcher conducting the experiment.

Experiment Objective

Originating from the desire to understand human behavior for a range of time-varying tracking tasks, efforts are being made to apply time-domain identification methods accurately. This experiment collects data on how humans adapt their behavior to time-variations in the display's available preview time. The data can be used to validate results of simulations of time-domain identification tools. Such time-varying identification methods are an essential enabler for detecting and understanding how humans adapt their behavior over time due to task variations.

Experiment Set-up

HMI Lab (Fig. 1) is used to investigate interaction between human operators and controlled elements. You are asked to take place in the right chair, where you can control the side-stick with your right hand. On the display in front of you, you will find a preview tracking task (Fig. 2), with the objective to align the state with the target trajectory. Throughout the experiments, you will encounter different scenarios with either time-invariant or time-varying settings of the display preview time. Several runs per scenario are collected, and per run, your tracking input will be measured for 150 seconds, where the first 30 seconds compose the run-in time needed to calibrate the identification software.

Figure 1: Illustration of HMI Lab. The participant will be sitting on the right (blue) seat and controls the side-stick.

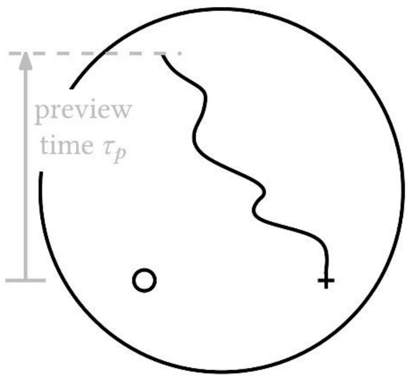

Figure 2: Sketch of HMI Lab tracking display (Van der El). The goal is to steer the state (circle) to the target (plus). The preview time (line) is varied over a range of conditions.

Experiment procedure

During the experiment, you are tasked with making the controlled element state (circle) follow the target trajectory (plus and line) by giving tracking input to the side-stick. These tasks always include a *preview display, and a single integrator controlled element*. During the experiments, a specific condition is scheduled for the display preview time, which can be either time-invariant or time-varying. The display time-variations can be either one step change, or one periodic sine variation. Besides the variations of the target, there exists a small disturbance on the controlled element. While these variations occur, you will keep focusing on tracking the target and rejecting the disturbance. In total, you will be performing the tracking task for 8 different display conditions. All tracking runs collect performance in a specific score, which will be communicated to you by the researcher. Every display condition is repeated until 5 consistent runs are collected, before proceeding to the next condition. When 4 out of the 8 conditions have been completed, a 15 minute break is held. Should more breaks be required, you can request them at any moment. Conducting the experiment for all display conditions takes approximately 2-3 hours.

Covid-19 Protocol

Due to the COVID-19 pandemic, several measures are taken to reduce the spreading risk. Generally, the Dutch governmental guidelines[1] are to be followed. This means that both researcher and participants confirm they do not have symptoms related to COVID-19, and that they regularly disinfect their hands. The experiment-specific measures following "COVID-19 Protocols for Human Subject Experiments" (V1.9) of the Control and Simulation department are as follows:

- **Entering HMI Lab:** The experimenter and participant will avoid being both in the same room. This will be achieved by having the participant enter first, and continue directly to the experiment room, while the experimenter enters second. Exiting happens in reversed order.
- **Briefing:** The (de)briefing of the participant will be performed at standing tables outside HMI Lab, for which it is recommended to still maintain sufficient distance between experimenter and participant (e.g. separate tables for experimenter and participant).
- **Experiment:** All surfaces and objects the participant and experimenter handle during the experiment, shall be disinfected between participants, after each break and after the experiment. This includes the side-stick, control room devices and standing tables.

Your Rights & Consent

Experiment participation is voluntary. Should you feel uncomfortable, you can decide to stop your participation at any time. By participating in the experiment you agree that the collected data may be published. Your personal data will remain confidential and anonymous, only the researcher can link the collected data to a specific participant. To ensure you understand and comply with the conditions of the experiment, you will be asked to sign an informed consent form.

Contact information researcher:	Contact information research supervisor
[name] [e-mail] [phone]	[name] [e-mail] [phone]

Thank you again for participating!

[1] https://www.rijksoverheid.nl/coronavirus

Experiment Consent Form

Adaptation to time-varying display preview during tracking tasks

I hereby confirm, by ticking the box, that:

1. I volunteer to participate in the experiment conducted by the researcher (**[name]**), under supervision of **[name],** from the Faculty of Aerospace Engineering of TU Delft. I understand that my participation in this experiment is voluntary and that I may withdraw ("opt-out") from the study at any time, for any reason. ☐

2. I have read the briefing document and I understand the experiment instructions, and have had all remaining questions answered to my satisfaction. ☐

3. I understand that taking part in the experiment involves performing manual tracking tasks under varying display conditions in the HMILab simulator at TU Delft. I understand that only the recorded time traces of the tracking tasks I perform are saved. ☐

4. I confirm that the researcher has provided me with detailed safety and operational instructions for the HMILab simulator (simulator setup, electro-hydraulic side stick, emergency procedures) used in the experiment. Furthermore, I understand the researcher's instructions for guaranteeing the experiment's compliance with current COVID-19 guidelines, and that this experiment shall at all times follow these guidelines. ☐

5. I confirm that I currently do not have any COVID-19 symptoms and that I have performed a '*Self-Quarantaine Check*' (https://quarantainecheck.rijksoverheid.nl/en) no more than 24 hours before my experiment session. ☐

6. I understand that the researcher will not identify me by name in any reports or publications that will result from this experiment, and that my confidentiality as a participant in this study will remain secure. Specifically, I understand that any demographic information I provide (gender, handedness, age range, ***see next page***) will only be used for reference and always presented in aggregate form in scientific publications. ☐

7. I understand that this research study has been reviewed and approved by the TU Delft Human Research Ethics Committee (HREC). To report any problems regarding my participation in the experiment, I know I can contact the researchers using the contact information below. ☐

My Signature	Date
My Printed Name	Signature of researcher

Contact information researcher:	Contact information research supervisor:
[name]	[name]
[e-mail]	[e-mail]
[phone]	[phone]

Participant Demographic Information

Adaptation to time-varying display preview during tracking tasks

Age range:

- 18 – 19
- 20 – 24
- 25 – 29
- 30 – 34
- 35 – 39
- 40 – 44
- 45 – 49
- 50 – 55
- 55+

Handedness:

- Left handed
- Right handed
- Ambidextrous

Gender: __________

Participant number: __________
(filled out by the researcher)

Contact information researcher:	Contact information research supervisor:
[name]	[name]
[e-mail]	[e-mail]
[phone]	[phone]

D
Trade-Off Graphs for Determining Q and R Sensitivity Values

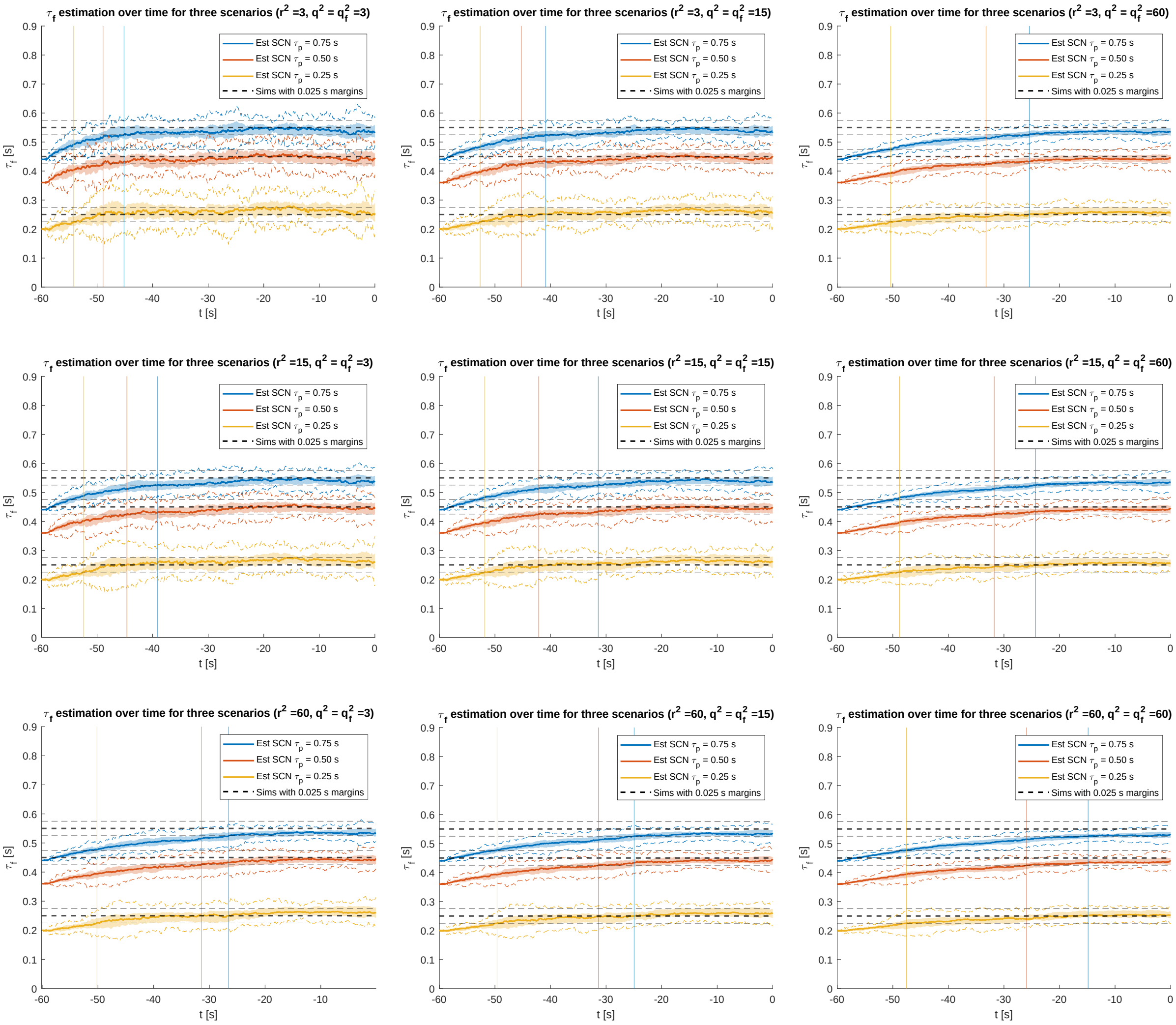

Figure D.1: Limited Monte Carlo trade-off to establish the noise matrix settings of the DEKF. From these nine combinations, r^2 =3 and $q^2 = q_f^2$ =15 is optimal combination of convergence speed and estimation stability.

III

Preliminary Report (Already Graded)

1
Introduction

In control tasks, available infrastructure should be used as efficiently as possible, and safety for the vehicle operators should be maximized. Most of these tasks rely on a human operator (HO) that tries to influence the future state of a controlled element (CE). Optimised efficiency and safety could be reached by introducing automation in the human-machine interaction (HMI) control loop [1]. However, due to operator responsibility [2] and complex operating environments, the human in the loop should stay well-informed [3], and be able to adapt to input [4]. Currently, automation is introduced to aid operators in their manual control tasks [5, 6], such as lane assistance in a car. Many operators choose to disable such functionalities, since the suggestions can feel counter-intuitive [7, 8]. Even though a control system suggests the most fuel-efficient and safest actions, it is a sub-optimal strategy when a human rejects it. Furthermore, however smart artificial intelligence is becoming, full autonomy is still something unique for biological operators like humans [9]. The control system must be intuitively cooperative with the HO, by identifying the human control strategy at any moment, and adapting the feedback accordingly [8, 10, 11].

Human controllers show variable and adaptive control behaviour [12, 13]. A specifically interesting human behaviour feature is how much future information is processed. This varies with the available future signals, but also due to intrinsic aspects, such as fatigue and learning [14]. The definition for anticipation on the future, or *preview*, is effectively a negative delay, with additional cognitive smoothing or filtering. How much preview is used can be described by the *look-ahead time* parameter, which is a variable human characteristic, significantly affecting control behaviour [15]. Look-ahead time can vary due to external factors (e.g. obstruction on road, mist), and due to HO variability (e.g. distraction). Acquiring real-time estimations of this look-ahead time during a control task would be a large step towards the prediction of human control strategies [12], comparably relevant to online HO identification during sudden vehicle stability degradation [16].

In preceding research, the Dual Extended Kalman Filter (DEKF) has proven to be a powerful tool for the estimation of HO parameters during tracking tasks [17]. These tracking tasks involved a *compensatory display*, where no future information is presented, and merely the error between the state and the target is visible. Many real-life manual control tasks use a *preview display*, which includes three observable signals: the state, target (including future) and error between the two [18]. Processing a preview tracking task is more complex, resulting in more HO parameters, and a more sophisticated identification procedure [15]. Recently, a definition of the DEKF in preview tracking tasks has been developed [19]. This algorithm showed promising first results for time-invariant experiments. If the algorithm works well for preview tracking experiments with time-varying display preview time, this would be a step towards intuitive adaptive control systems [12].

The main goal of this research is to validate the implementation of a DEKF for the time-varying identification of look-ahead time in preview tracking tasks. Only the measurable state, target, error and tracking input signals are to be used. By means of a simulation phase, the working principles and sensitivity of the Kalman Filter are investigated. Furthermore, the DEKF tuning is optimised, in order to achieve sufficient performance in scenarios where the HO look-ahead time is varied. Then, by designing and executing HMI experiments, real data will be acquired on variable preview time. With this HMI experiment data, it can be validated whether the DEKF is capable of reconstructing the look-ahead time parameter in a time-varying scenario. As part of the preliminary report, the Literature Review can be found in Chapter 2, followed by the Research Objective and Methodology in Chapter 3. The most important Preliminary Analyses Results are compiled in Chapter 4, and in the concluding Chapter 5 the Proposed Final Analyses are outlined.

2

Literature Review

Research in the field of human operator (HO) behaviour while performing **preview tracking tasks** and while exposed to **time-varying conditions** has recently been identified as one of the key areas of improvement for the global Cybernetics efforts [12]. This call for increased focus on preview tracking and time-varying conditions has lead to a significant amount of scientific literature being published [14, 20, 21, 22, 23, 24, 25, 26]. In order to contribute to the state-of-the-art in this field of research, it is of paramount importance to become acquainted with the fundamentals of the theory and the most recent developments. Van der El's preview model [14] and Popovici's Dual Extended Kalman Filter (DEKF) [17] can be combined for the time-varying identification of HO strategy during preview display tracking tasks. Vertregt has developed such a DEKF for preview tracking tasks in preceding research [19]. In this chapter, the preview model and DEKF are elaborated upon in Section 2.1 and Section 2.2, respectively.

2.1. Preview Model

In the early stages of manual control and cybernetics research, it was distinguished that humans may encounter three different types of visual displays: compensatory, pursuit and preview [18]. The compensatory tracking task – which does not provide information on a state or a target but merely on the difference between the two – has been studied and modeled most elaborately [15]. However, it should be noted that for real-life applications, the compensatory tracking framework can only be applied to a selection of cases, and an understanding of pursuit and preview is desired [12]. Below, an elaborate description can be found on preview displays, the pilot-vehicle system, Van der El's preview model and simulations with preview.

2.1.1. Preview Displays

The concept of preview can be explained in real-life examples, such as car driving or flying. Such vehicle control tasks are highly complex, and due to many internal and external uncertainties playing part in these human actions, it is difficult to acquire cybernetic models from the operator behaviour. Without sufficiently accurate modelling based on controlled preview tracking experiments, no simulations can be created to reproduce the human behaviour [14]. For that reason, experimental preview displays are abstracted from the familiar tasks. Both the real-life and experimental displays are further explained.

Real-Life Preview

A relatively well-understood visual display is found in *compensatory* tracking tasks. Here, the HO only observes the error between its state and the target of the controlled element (CE). An example of a compensatory tracking task would be keeping an aircraft level with the horizon using the elevators. However, most real-life human objectives executed with visual cues would be best described by a *pursuit* tracking task or a *preview* tracking task. A pursuit tracking task entails matching a state and target combination without a predefined path. A preview tracking task requires steering a state to a predefined future target, e.g. driving a car, where the road is the visual trajectory [18]. In human-machine interaction (HMI) applications, and especially when it includes vehicle operation, one usually finds preview displays with which humans can assess their performance [24]. This previewed target does not necessarily have to be a physical boundary such as a road, but can also be a virtually imposed trajectory such as an augmented primary flight display (PFD) with a navigational tunnel superimposed [27]. Even the concept of a road-to-follow is not a requirement, as long as the operator can distinguish its state, and the target to follow including preview. Figure 2.1 shows two examples of preview encountered in real life. Looking at the two figures, it immediately stands out that there exists variability and coupling in the perception of states. For example, the preview time can be changed with other vehicle states, such as velocity and heading, since the time difference between the HO state and the previewed target is a function of e.g. the velocity [28]. Additionally, the perceived preview can be variable with external factors, such as rain, lighting, obstructions on or delineation of the road [29]. Note that the coupled or derivative states (e.g. velocity and heading) can be variable by external factors (e.g. road quality and wind) as well, which in turn has effect on the preview time. In real-life applications, a human reacts to more than just visual input, but also to vestibular and somatosensory cues. Besides that, every sensory system might react to several cues simultaneously and the reactions could be coupled, such as roll and pitch input [30]. Even more complex, there can be coupled cross-sensor reactions. Different types of displays in the same tracking experiment can also create variable behaviour. In the virtual navigational tunnel display (Figure 2.1) there exists a preview tracking task of following the trajectory, but also a secondary compensatory tracking task (in both roll and pitch) of keeping level with the horizon. This altogether introduces many non-linearities and a poorly observable pilot-vehicle system while investigating real-life preview applications [14].

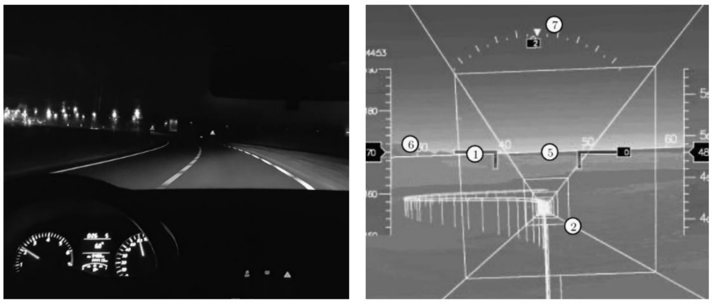

(a) *(b)*

Figure 2.1: Two examples of real-life preview. (a) physical preview, (b) virtual preview [24].

Experimental Preview

As explained, the understanding of human perception and behaviour in real-life pursuit and preview tracking exercises is complicated by the variable conditions, the multi-sensory information feed and the multi-loop observations [30]. Moreover, the human nervous system's precognitive nature enables operators to anticipate on signals that are not even provided by the display, which introduces another non-linearity for actual physical applications [13]. This occludes the insights in the purely visual response of a human operator (HO) for specific tasks. Therefore, a specific visual tracking task has been developed, which is since its introduction and application by McRuer [18] a widely accepted display for experimental preview tracking tasks (see Figure 2.2). This display contains one optional reference point, one point representing the CE output (state) and one target signal which is to be followed by the CE as a function of the HO input. Should no preview be available (preview time $\tau_p = 0$ s), this display is one-dimensional and would be classified as a pursuit tracking task. Should the preview time increase, the future trajectory of the target signal will be extended further away from the reference, such that the preview display becomes two-dimensional. Note that the speed at which the signal seems to approach the HO is a design parameter, which is out of the HO's control. The CE dynamics is constrained to move in a single direction, so that only the instantaneous target is to be matched. Using such an experimental preview tracking set-up comes with advantages [18, 14]:

- There is one single observable CE output (state) signal, which can be directly controlled by one single HO control input signal
- The HO only responds to visual input, thus there exists no sensory signal coupling, since the dynamics of the CE are invariable with the state and the simulator is stationary
- The presented states and actions are one-dimensional, simplifying the preview task to a single-axis experiment, mitigating the need for abstracting multiple responses
- The display is easy to reproduce, verify and implement in many different cybernetics experiments and for many different purposes

A sufficient understanding of human behaviour during real-life preview tracking tasks starts with fundamental research into the isolated feedback and feedforward responses to specific visual cues [18]. Instead of cues from a driver's point of view (e.g. the tangent line of a road [31]), this study focuses on how much future information is used in terms of time. Ideally, a model is constructed that can predict this behaviour. The display presented in Figure 2.2 facilitates designing a quasi-linear model of a HO subjected to preview, which will be elaborated upon in Section 2.1.3. Before explaining the complete model, a short introduction is given into the pilot-vehicle system and the expected signals in the control loop.

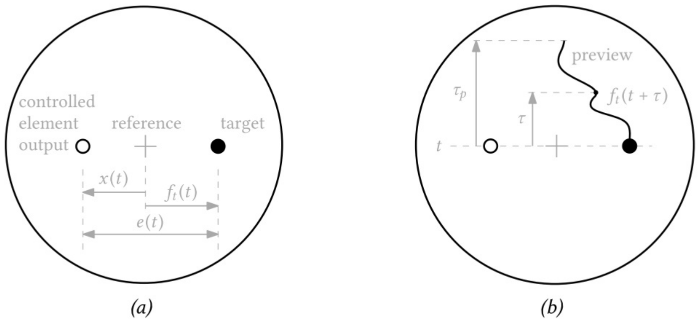

Figure 2.2: Pursuit and preview tracking [14].

2.1.2. Pilot-Vehicle System for Preview Tracking Tasks

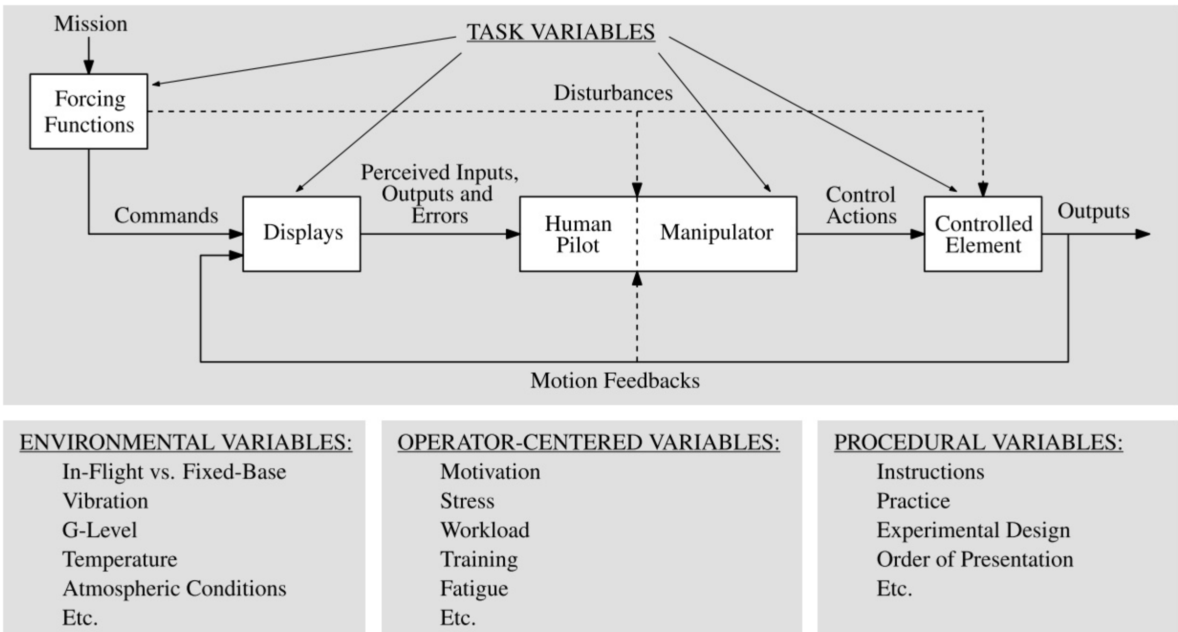

Figure 2.3: The complete pilot vehicle system to be modelled [18].

To ensure a fundamental understanding of the HO preview model, and to become acquainted with its underlying assumptions, one should oversee the complete pilot-vehicle system. Figure 2.3 showcases a schematic representation of this system [18]. Central in this system is the Human Pilot (same as HO), which is exposed to a range of task variables and conditional variables. To facilitate finding a causal relation between the variables of interest and the HO, all variables except the ones under investigation are to be kept constant as much as possible. For clarity, the system is elaborated upon with the experimental preview tracking task as leading example, but in essence, this applies also to real-life applications with preview. The objective in this case is trying to match the CE output (system state) with the target trajectory (see Figure 2.2). This target signal progresses in time following a certain path, which can for experimental purposes be controlled with a Forcing Function (FoFu) [32]. To suppress precognitive behaviour [33], it is advised to make these signals appear random while still being in control of them, i.e. pseudo-random. This is done by summing a range of sine functions of a known bandwidth. Another uniquely distinguishable FoFu can be injected into the system to simulate the noisy character of a real-life preview tracking system. Note that this FoFu is not taken up into the previewed target, making the disturbance rejection a compensatory task. The pilot vehicle system is now comparable to McRuer's environment [18], but fundamental differences exist in the modeling procedures of compensatory and preview tracking tasks [15], which will become clear in the next section.

As can be seen in Figure 2.2, three unique cues of information are available from a preview tracking display [18]. The target signal $f_t(t)$ and the current CE output signal $x(t)$ with respect to the reference on the one hand, and the tracking error between the two $e(t)$ on the other [14]. This corresponds to the perceived inputs, outputs and errors presented by the display to the HO in Figure 2.3. It is known that humans use these three information feeds to form a response with the manipulator (e.g. side stick), which in this case is the control action $u(t)$ exerted on the CE. This HO response from the display signals to the tracking action on the manipulator is exactly what should be captured in the preview tracking model. Figure 2.4 shows in its upper part a schematic representation of the HO [15]. Ideally, it is aimed to find the linear conversion of each signal and its contribution to the human operator stick input. However, humans are known to be highly time-varying and adaptive controllers, which inherently show non-linear behaviour. This combination of linear frequency response functions (FRFs) and a non-linear remnant injection is called a quasi-linear model [18].

As explained, there are only two controllable FoFus in this modelled environment: one injected as the previewed target signal, and one disturbance signal injected somewhere in the control loop. These are the only two signals that can be related to the human control action in a frequency response function (FRF) [15]. This means that just two of the three visual signals can be directly related to HO output, and the third is to be lumped in the other responses. A substantiated choice is to be made which two out of the three input signals $(f_t(t), x(t), e(t))$ are modeled to be related to the output signal $(u(t))$. Due to the interrelation of the input signals ($e = f_t - x$), it is possible to sum FRFs, as can be seen in the center equations of Figure 2.4. The FRFs relating the target signal and the CE state to the human control action are most suited (see the bottom part of Figure 2.4) [15], since here two distinguishable FoFus can be injected; one for preview tracking, one for disturbance rejection. It should be remembered that, due to this underlying assumption, the direct response to the visual error cue is not observable, but partially included in the other two responses.

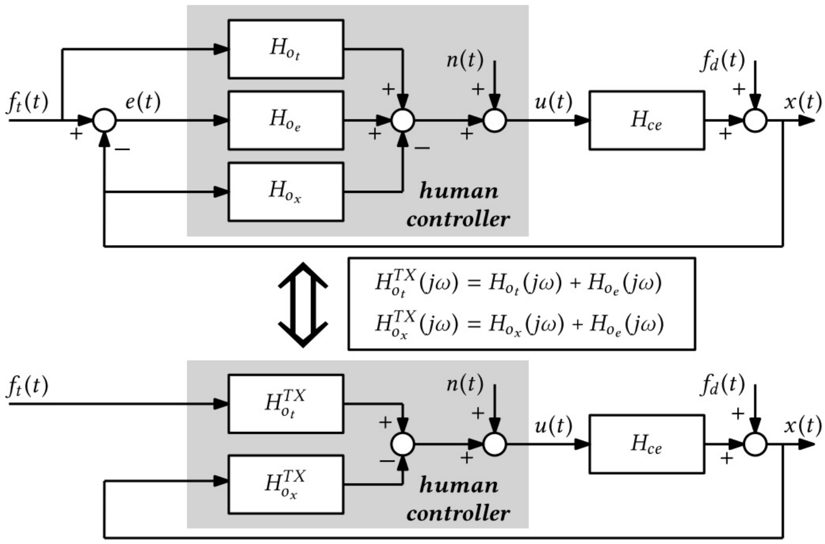

Figure 2.4: Upper: human preview control diagram based on available input signals to the operator (f_t, e, x). Lower: simplified lumped human control diagram based on identifiable signal responses. [15]

Looking at the lower part of Figure 2.4, it becomes clear that the HO model should describe a feed-forward response to the target (FoFu 1, $f_t(t)$), and a feedback response to the state disturbance (FoFu 2, $f_d(t)$). Like in McRuer's work for compensatory tracking tasks [18], [34], it would be preferred to have a decent physiological parameterisation, which can predict the behaviour of any HO in varying scenarios with preview [15].

2.1.3. Van der El's Preview Model

In the late sixties, McRuer's Crossover Model for compensatory tracking tasks enabled researchers to estimate HO control actions for given error signal inputs [18]. By means of a parameterised FRF, the model was able to predict how the HO would adapt when exposed to different task variables. In such tracking tasks, only the error signal is visually presented to the HO. Essentially, the state of the CE is constantly perturbed by a FoFu, and the HO tries to reject this disturbance to keep the CE state level around a reference point. Figure 2.5 showcases a compensatory display and McRuer's parameterised Crossover Model. In Equation (2.1) and Equation (2.2), the formulation of the FRFs can be found relating the error signal to the control action. In this formula, K_e represents the HO's static gain to the error signal. $T_{L,e}$ and $T_{l,e}$ represent the lead-time and lag-time constant, respectively. The HO's neuromuscular response is described by its natural frequency ω_{NM}, and its damping ratio ζ_{NM}. The signal processing delay that is present in the complete HO response to the error signal is accumulated to the delay time τ_v. In the closed loop pilot-vehicle system, the CE dynamics are outside the control of the HO. However, the response of the vehicle state to the error signal will often show similar results. This was found during research into compensatory tracking with CE dynamics differing between gains, single integrators (SI), and double integrators (DI). Humans were concluded to adapt their control strategy to the presented tasks. For this, HOs can vary their static gain, lead-time constant and lag-time constant [18].

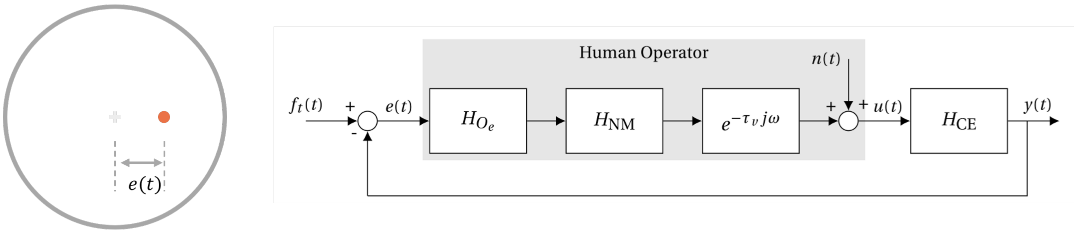

Figure 2.5: Overview of compensatory display and Crossover Model [18].

$$H_{O_e}(j\omega) = K_e \frac{1 + T_{L,e} j\omega}{1 + T_{l,e} j\omega} \tag{2.1}$$

$$H_{NM}(j\omega) = \frac{\omega_{NM}^2}{(j\omega)^2 + 2\zeta_{NM}\omega_{NM} j\omega + \omega_{NM}^2} \tag{2.2}$$

This CE-adaptive HO behaviour is found for all types of sensory processing and for all types of displays [13]. McRuer's parameterisation proved to be an extremely powerful tool, which increased the general understanding of compensatory operations. Therefore, it will be a significant contribution to technology when the preview tracking tasks could be parameterised comparably [12]. Some research regarding preview control models for driver steering tasks have been studied in the past [35], however, this was not as fundamental as McRuer's Crossover Model. A state-of-the art preview tracking model has been comprised by Van der El [15]. The two key aspects that distinguish preview displays from compensatory displays are that **the HO can anticipate on the target, rather than only react**, and that **the HO is presented three visual signals, rather than only one**. It was already explained that merely two FRFs can be established, and that the error response will be lumped to the state-target response. Also, it was elaborated upon that the tracking objective is designed as a combined target tracking and disturbance rejection task. The target tracking task includes information on the future (preview), meaning that a feed-forward FRF can be expected there. The state disturbance rejection task shows similarities with compensatory tracking, where the new reference point coincides with the state rather than being static. For that reason, this feedback FRF is expected to be comparable to the FRFs found in the Crossover Model. Figure 2.6 shows a preview display and Van der El's parameterised preview model. The FRFs relating the previewed target signal and CE state signal to the control action are outlined in Equation (2.3) until Equation (2.5). What immediately stands out is the striking similarity between the closed loop part of the preview model and the Crossover Model. In the preview model, however, the HO sees no error, but creates an internal representation of the error $e^*(t)$ using the processed target signal $f_{t,f}^*(t)$ and the state signal $y(t)$. Clearly visible in the grey area of the preview model, the target is presented to the HO as a signal some time in the future. How much future information is included in the current tracking behaviour is described by the look-ahead time τ_f. Even when the HO is presented a display with a preview time far ahead, how much of this preview is used – defined by the look-ahead time – hardly ever extends until further than a critical point. Furthermore, if the display showcases constant preview time, the look-ahead time can still vary considerably and inconsistently. This is exactly the reason why this τ_f parameter is decided to be the focus point of this research. The processed target signal is produced by passing the previewed target signal $f_t(t+\tau_f)$ through the low-pass filtering H_{O_f}. For SI dynamics, this FRF is mostly described by the target response gain K_f, due to the relatively low values of the preview smoothing time-constant $T_{l,f}$ $(1/\omega_{b,f})$. From HMI experiments examining the influence of preview time τ_p on K_f [14], this response gain shows to be approximately invariant to preview changes. Variation of $T_{l,f}$ is more pronounced for DI dynamics, inducing a shift in the weight of the response gain K_f on the tracking action. In this DI case, the preview FRF is effectively a low-pass filter which can dampen much of the conventional FoFu bandwidth. This is the main reason for focusing on CE dynamics of SI nature, which will be further elaborated upon in the rest of this section. The option for an equalising lag time-constant is not included in the preview model, because it has been validated for SI – requiring pure gain – and DI – requiring lead – control tasks [15]. In the preview model, there are thus three additional physically interpretable HO parameters that can vary compared to the Crossover Model. This can be induced by task variation, but it can also occur due to intrinsic HO variability. The model enables cybernetics researchers to not only predict the outcome, but also illuminate the human strategy causing behaviour. The remaining challenge is finding an identification method that can recursively estimate these preview parameters while the HO is performing a preview tracking task [19].

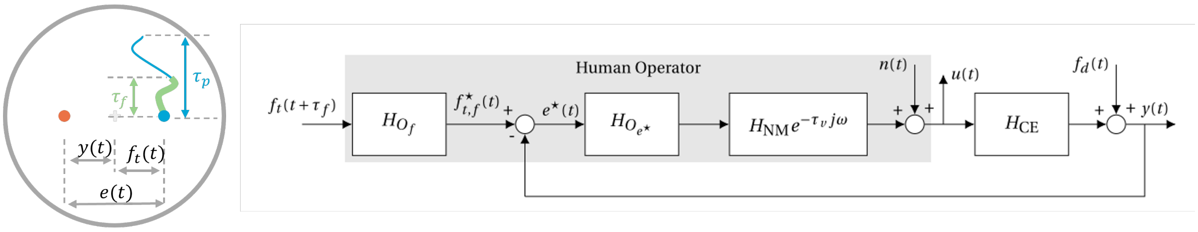

Figure 2.6: Overview of preview display and preview model [14].

$$H_{O_f}(j\omega) = \frac{K_f}{1+T_{l,f}\,j\omega} = K_f\,\frac{\omega_{b,f}}{\omega_{b,f}+j\omega} \tag{2.3}$$

$$H_{O_{e^*}}(j\omega) = K_{e^*}(1+T_{L,e^*}\,j\omega) \tag{2.4}$$

$$H_{NM}(j\omega) = \frac{\omega_{NM}^2}{(j\omega)^2+2\zeta_{NM}\omega_{NM}\,j\omega+\omega_{NM}^2} \tag{2.5}$$

2.1.4. Time-Varying Simulations with Preview Model

Although preview could be conceptually straightforward to understand, care should be taken from a modelling perspective. This is because look-ahead time – essentially a negative delay – is accompanied by a state that has not yet been visited [19]. The central problem is how to find characteristics of a signal which has not yet passed the control loop. Due to the time-varying research focus, it would be wise to model the look-ahead time compliant with time-domain calculations. Especially for the approximation of time delays in this time-varying fashion, a negative delay is not preferred [36]. With the reference point in time at the current CE output and target, the look-ahead time will always be a negative delay. This reference point in time can be shifted, however, without interacting with the values of the tracking. If one shifts this reference point until past the look-ahead horizon, the look-ahead time with respect to that reference will be a positive delay. The amount the reference is translated into the future is called the suspension time τ_s (sometimes in literature referred to as anticipation time τ_a). Using this suspension, the new value representing the look-ahead time is called the apparent time delay τ_f^* [19] (see Figure 2.7). If the suspension time is stored, the look-ahead time and apparent time delay can always be related to each other by $\tau_f = \tau_s - \tau_f^*$. Note in Figure 2.8 that this virtually created delay introduces an extra FRF block to the HO model chain.

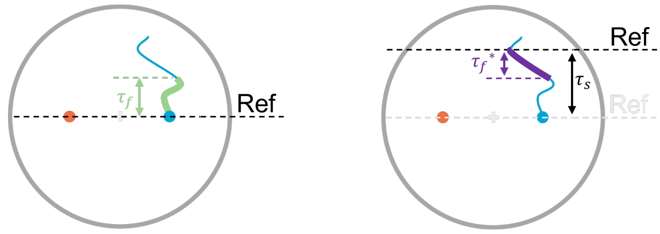

Figure 2.7: Converting look-ahead time to apparent delay time with suspension time [19].

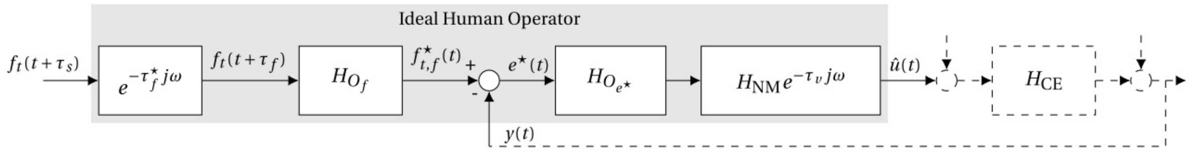

Figure 2.8: Isolated human operator model as implemented in the time-varying simulations [15] (edited by Vertregt).

In the frequency domain, calculations are based on how the signals progress through the FRFs, using a summation of uniquely identifiable input frequencies, and analysing the output signals at these same frequencies. This can provide a solid estimation of the HO parameters over the entire run of the experiment [15]. For such a frequency-domain calculation base to hold, a range of underlying assumptions are to be regarded:

- The input signals' frequencies should fit an integer number of times in the measurement domain
- The frequency, phase and amplitude of the input signals are agreed upon before and fixed throughout the experiment
- The HO parameters to be estimated are constant values throughout the measurement, specific for the provided task variables

Such assumptions will occlude essential aspects of HO strategy as described in the preview model. Already elaborated upon, a HO exposed to a real-life preview tracking task can encounter a highly variable environment. Additionally, even in a controlled experimental environment such as the preview tracking task presented here, humans could portray intrinsic time-varying behaviour. Here one can think of learning capabilities and fatigue, which induce less effortful strategies. This motivates for the conversion of the HO model from Figure 2.8 to a state-space (SS) representation which can capture all the presented parameters in the time domain [17]. With the SS system at hand, it becomes possible to find the inter-dependency between the internal system states and the model parameters at every time step. While investigating the isolated HO model with the FRF blocks, two challenges arise for a time-domain conversion. First, the exponential functions related to both the look-ahead time (in simulations represented by apparent time delay) and the response time delay have no direct translation into a time-domain transfer function (TF), meaning that an adequate approximation is to be made [36]. Second, the combination of different order FRF blocks and two different points of input into the system slightly complicate the direct conversion into a state space system. It is preferred to represent the system in controllable canonical form, and for identification purposes, the number of states should be kept to a minimum [19]. The time delay representation with Padé approximations and the derivation of the minimal state-space function of the HO model are elaborated upon below.

The Padé Approximation for Time-Domain Delay Functions

To convert a control theoretical block diagram into a controllable canonical state-space system, the blocks are to be described with fractional TFs. This is already in place for the preview target processing block $H_{O\,f}$, the HO equalization block $H_{O_{e*}}$ and for the neuromuscular limitations H_{NM}. However, the blocks describing the conversion from suspended target signals to previewed target signals and the physical HO response time delay contain an exponential TF. These can be converted to a fractional alternative by means of a Padé approximation [36]. When deciding upon the order of the fractional block, one has to consider the approximation accuracy, the extent to which the TF would be distinguishable from the other blocks, and the number of resulting canonical states in the state-space equation that are to be kept at a minimum. After a trade-off between these factors, the preferred order of this fractional approximation is 3, meeting the accuracy requirements while keeping the number of canonical states relatively low [19]. After this, it can be found that the Padé approximations still account for a large part of the canonical states (see Equation (2.7) and Equation (2.11)). The description of this model's Padé approximation is presented in Equation (2.6), where m and r both represent the maximum order assumed for the approximation, in this case 3.

$$H_{delay}(j\omega) = e^{-\tau j\omega} \approx \frac{\sum_{i=0}^{m} \frac{(2r-i)!}{i!(r-i)!}(-\tau j\omega)^i}{\sum_{k=0}^{m} \frac{(2r-k)!}{k!(r-k)!}(\tau j\omega)^k} \tag{2.6}$$

Looking at Equation (2.6), the primary motivation for the virtually negative representation of the look-ahead time becomes evident once more. In the description of the Padé approximation, a positive time delay is to be included [36]. Look-ahead time is essentially a negative time delay [15], which cannot be incorporated in the complete state-space equations without making the solution unstable [36]. By means of suspending the target tracking signal further away than the preview signal, the look-ahead time can be presented as a time delay, stabilising the estimation procedure [19].

Derivation of the Minimal State-Space Representation

During the identification phase of this research, it is essential to keep the differential representation of the control problem as small as possible. In order to align the simulation and identification phase, it is chosen to apply the same differential equations for the simulations as the identification requires. This means that the dynamics should be described in as few states as possible, defined as the *minimal realisation*. The time-varying identification tool should perform a parallel system state and HO parameter estimation. Ambiguity in explanation of HO control behaviour can be avoided by only keeping the strictly necessary states. At this point, all FRFs that can be found in Figure 2.8 have a fractional TF description, enabling a controllable canonical SS transformation. These descriptions are summarized in Equation (2.7) until Equation (2.11). The first and last equation are the third order Padé approximated TFs of both time delays [15, 19].

$$e^{-\tau_f^* s} \approx \frac{-\tau_f^{*3} s^3 + 12\tau_f^{*2} s^2 - 60\tau_f^* s + 120}{\tau_f^{*3} s^3 + 12\tau_f^{*2} s^2 + 60\tau_f^* s + 120} \tag{2.7}$$

$$H_{O_f}(s) = \frac{K_f}{1 + T_{l,f}s} = K_f \frac{\omega_{b,f}}{\omega_{b,f} + s} \tag{2.8}$$

$$H_{O_{e^*}}(s) = K_{e^*}(1 + T_{L,e^*}s) = K_p + K_v s \tag{2.9}$$

$$H_{NM}(s) = \frac{\omega_{NM}^2}{s^2 + 2\zeta_{NM}\omega_{NM}s + \omega_{NM}^2} \tag{2.10}$$

$$e^{-\tau_v s} \approx \frac{-\tau_v^3 s^3 + 12\tau_v^2 s^2 - 60\tau_v s + 120}{\tau_v^3 s^3 + 12\tau_v^2 s^2 + 60\tau_v s + 120} \tag{2.11}$$

Looking at the equations, the resulting HO parameters that need to be estimated by means of a system identification method are thus: τ_f^* $(= \tau_s - \tau_f)$, K_f, $\omega_{b,f}$ $(= 1/T_{l,f})$, K_p $(= K_{e^*})$, K_v $(= K_{e^*} T_{L,e^*})$, ω_{NM}, ζ_{NM}, and τ_v. To find a causal interaction between the states and the parameters of the HO model, the system should be converted to a differential format, preferably in state-space form. Converting a block scheme to a controllable canonical state-space system is a particularly powerful operation. This creates a reproducible result with unique states that relate to each other as derivatives [19]. For a linear control block diagram with a single point of input and a single point of output (SISO), the conversion to the state-space system presented in Equation (2.12) and Equation (2.13).

$$\frac{Y(s)}{U(s)} = \frac{b_2 s^2 + b_1 s + b_0}{s^3 + a_2 s^2 + a_1 s + a_0} \tag{2.12}$$

$$\begin{aligned} \begin{bmatrix} \dot{x}_1 \\ \dot{x}_2 \\ \dot{x}_3 \end{bmatrix} &= \begin{bmatrix} 0 & 1 & 0 \\ 0 & 0 & 1 \\ -a_0 & -a_1 & -a_2 \end{bmatrix} \begin{bmatrix} x_1 \\ x_2 \\ x_3 \end{bmatrix} + \begin{bmatrix} 0 \\ 0 \\ 1 \end{bmatrix} u \\ y &= \begin{bmatrix} b_0 & b_1 & b_2 \end{bmatrix} \begin{bmatrix} x_1 \\ x_2 \\ x_3 \end{bmatrix} + \begin{bmatrix} 0 \end{bmatrix} u \end{aligned} \tag{2.13}$$

The SISO calculations do not directly reflect the general form of multiple-input-single-output (MISO) and multiple-input-multiple-output (MIMO) systems. However, they provide a solid basis, since the more complex systems can be constructed with the aid of the SISO logic. The general description of a MIMO state-space system can be found by looking at which points the signals are injected and at which points they are retreived with regard to the TFs. A simple case would be two input signals ($u(t)$ and $v(t)$) passing through the same TF as used in Equation (2.12), to form a single output signal ($y(t)$). The resulting state-space derivations are presented in Equation (2.14) and Equation (2.15), which essentially represents a summation of the TFs.

$$\frac{Y(s)}{U(s)} = \frac{b_{1,2} s^2 + b_{1,1} s + b_{1,0}}{s^3 + a_{1,2} s^2 + a_{1,1} s + a_{1,0}} \quad \& \quad \frac{Y(s)}{V(s)} = \frac{b_{2,2} s^2 + b_{2,1} s + b_{2,0}}{s^3 + a_{2,2} s^2 + a_{2,1} s + a_{2,0}} \tag{2.14}$$

$$\begin{aligned} \begin{bmatrix} \dot{x}_1 \\ \dot{x}_2 \\ \dot{x}_3 \\ \dot{x}_4 \\ \dot{x}_5 \\ \dot{x}_6 \end{bmatrix} &= \begin{bmatrix} 0 & 1 & 0 & 0 & 0 & 0 \\ 0 & 0 & 1 & 0 & 0 & 0 \\ -a_{1,0} & -a_{1,1} & -a_{1,2} & 0 & 0 & 0 \\ 0 & 0 & 0 & 0 & 1 & 0 \\ 0 & 0 & 0 & 0 & 0 & 1 \\ 0 & 0 & 0 & -a_{2,0} & -a_{2,1} & -a_{2,2} \end{bmatrix} \begin{bmatrix} x_1 \\ x_2 \\ x_3 \\ x_4 \\ x_5 \\ x_6 \end{bmatrix} + \begin{bmatrix} 0 & 0 \\ 0 & 0 \\ 1 & 0 \\ 0 & 0 \\ 0 & 0 \\ 0 & 1 \end{bmatrix} \begin{bmatrix} u \\ v \end{bmatrix} \\ y &= \begin{bmatrix} b_{1,0} & b_{1,1} & b_{1,2} & b_{2,0} & b_{2,1} & b_{2,2} \end{bmatrix} \begin{bmatrix} x_1 \\ x_2 \\ x_3 \\ x_4 \\ x_5 \\ x_6 \end{bmatrix} + \begin{bmatrix} 0 & 0 \end{bmatrix} \begin{bmatrix} u \\ v \end{bmatrix} \end{aligned} \tag{2.15}$$

The conversion of the HO control model presented in Figure 2.8 is different from the general MISO/MIMO calculations. This is mostly because the two feeds of input are injected at a different point. Looking at the flow of information, the suspended target signal ($f_t(t+\tau_s)$) passes through all HO blocks and the CE dynamics output ($y(t)$) only feeds through the equalization and limitation sequence. The two points of signal influx can be used to divide the model in two state-space systems that interact [19]. The first state-space system is designed to translate the suspended target signal ($f_t(t+\tau_s)$) to a perceived (or internal) current target signal ($f^*_{t,f}(t)$) based on the preview information. The second state-space system converts this perceived target signal and the CE dynamics output ($y(t)$) – the difference is the internal error ($e^*(t)$) – into the HO control action. Note that the output of the first state-space system is a direct input to the second. Creating a separate controllable canonical state-space block for both input-output TFs ($\frac{\hat{U}(s)}{F_t(s)}$ and $\frac{\hat{U}(s)}{Y(s)}$) would thus yield an unnecessary high number of canonical states [19]. Remember that for identification purposes, it is desired to have a minimal realisation of the state-space system. There are three input-output TFs that are to be incorporated in this minimal representation: $\frac{F^*_t(s)}{F_t(s)}$, $\frac{\hat{U}(s)}{F^*_t(s)}$ and $\frac{\hat{U}(s)}{Y(s)}$. Noting that the the first two TFs are directly connected as a feedthrough illuminates that the state-space representation should have 2 inputs and 1 output. Equation (2.16) until Equation (2.19) show how the state space system of the isolated HO model is constructed using the TFs of Equation (2.7) until Equation (2.11).

$$\boxed{\frac{F_t^*(s)}{F_t(s)} = \frac{-\tau_f^{*3}s^3 + 12\tau_f^{*2}s^2 - 60\tau_f^* s + 120}{\tau_f^{*3}s^3 + 12\tau_f^{*2}s^2 + 60\tau_f^* s + 120} \cdot K_f \frac{\omega_{b,f}}{\omega_{b,f} + s}} \tag{2.16}$$

$$\frac{\hat{U}(s)}{F_t^*(s)} = (K_p + K_v s) \cdot \frac{\omega_{NM}^2}{s^2 + 2\zeta_{NM}\omega_{NM}s + \omega_{NM}^2} \cdot \frac{-\tau_v^3 s^3 + 12\tau_v^2 s^2 - 60\tau_v s + 120}{\tau_v^3 s^3 + 12\tau_v^2 s^2 + 60\tau_v s + 120} \tag{2.17}$$

$$\boxed{\frac{\hat{U}(s)}{Y(s)} = -1 \cdot (K_p + K_v s) \cdot \frac{\omega_{NM}^2}{s^2 + 2\zeta_{NM}\omega_{NM}s + \omega_{NM}^2} \cdot \frac{-\tau_v^3 s^3 + 12\tau_v^2 s^2 - 60\tau_v s + 120}{\tau_v^3 s^3 + 12\tau_v^2 s^2 + 60\tau_v s + 120}} \tag{2.18}$$

$$\begin{bmatrix} \dot{x}_1 \\ \dot{x}_2 \\ \dot{x}_3 \\ \dot{x}_4 \\ \dot{x}_5 \\ \dot{x}_6 \\ \dot{x}_7 \\ \dot{x}_8 \\ \dot{x}_9 \end{bmatrix} = \begin{bmatrix} \underbrace{\begin{matrix} 0 & 1 & 0 & 0 & 0 \\ 0 & 0 & 1 & 0 & 0 \\ 0 & 0 & 0 & 1 & 0 \\ 0 & 0 & 0 & 0 & 1 \\ -a_{2,0} & -a_{2,1} & -a_{2,2} & -a_{2,3} & -a_{2,4} \end{matrix}}_{A_2} & \begin{matrix} 0 & 0 & 0 & 0 \\ 0 & 0 & 0 & 0 \\ 0 & 0 & 0 & 0 \\ 0 & 0 & 0 & 0 \\ \underbrace{b_{1,0} \quad b_{1,1} \quad b_{1,2} \quad b_{1,3}}_{C_1} \end{matrix} \\ \begin{matrix} 0 & 0 & 0 & 0 & 0 \\ 0 & 0 & 0 & 0 & 0 \\ 0 & 0 & 0 & 0 & 0 \\ 0 & 0 & 0 & 0 & 0 \end{matrix} & \underbrace{\begin{matrix} 0 & 1 & 0 & 0 \\ 0 & 0 & 1 & 0 \\ 0 & 0 & 0 & 1 \\ -a_{1,0} & -a_{1,1} & -a_{1,2} & -a_{1,3} \end{matrix}}_{A_1} \end{bmatrix} \begin{bmatrix} x_1 \\ x_2 \\ x_3 \\ x_4 \\ x_5 \\ x_6 \\ x_7 \\ x_8 \\ x_9 \end{bmatrix} + \begin{bmatrix} \begin{matrix} 0 \\ 0 \\ 0 \\ 0 \\ \underbrace{0}_{D_1} \end{matrix} & \underbrace{\begin{matrix} 0 \\ 0 \\ 0 \\ 0 \\ -1 \end{matrix}}_{B_2} \\ \underbrace{\begin{matrix} 0 \\ 0 \\ 0 \\ 1 \end{matrix}}_{B_1} & \begin{matrix} 0 \\ 0 \\ 0 \\ 0 \end{matrix} \end{bmatrix} \begin{bmatrix} f_t \\ y \end{bmatrix}$$

$$\hat{u} = \begin{bmatrix} \underbrace{b_{2,0} \quad b_{2,1} \quad b_{2,2} \quad b_{2,3} \quad b_{2,4}}_{C_2} & 0 & 0 & 0 & 0 \end{bmatrix} \begin{bmatrix} x_1 \\ x_2 \\ x_3 \\ x_4 \\ x_5 \\ x_6 \\ x_7 \\ x_8 \\ x_9 \end{bmatrix} + \begin{bmatrix} 0 & \underbrace{0}_{D_2} \end{bmatrix} \begin{bmatrix} f_t \\ y \end{bmatrix} \tag{2.19}$$

The equations above show how the flow of inputs to outputs is handled internally. Note that the state-space representation is presented in generalised parameterisation, which can be directly calculated by creating a controllable canonical form of the TFs highlighted in red and in blue. In Equation (2.16) (highlighted in red), it is shown how the suspended target signal ($f_t(t+\tau_s)$) is converted to an internal instantaneous target signal ($f_{t,f}^*(t)$). The output of this TF is only virtually expressed, since it feeds straight in the second chain of calculations. Looking at Equation (2.17), the opposite holds, where the input is the virtual internal target signal, and the output is the explicit HO control action ($\hat{u}(t)$). The third equation (Equation (2.18)) shows how the CE dynamics state ($y(t)$) converts to the HO control action. Note the negative sign, which is necessary to represent the calculation of the internal error ($e^*(t) = f_{t,f}^*(t) - y(t)$). There are only two actual input-output relations in Equation (2.16)-Equation (2.18), and the hand-over of the internal error signal ($e^*(t)$) can be cleverly incorporated by a restructuring of the controllable canonical state-space systems. As showcased in Equation (2.19), the state matrix and input matrix (A_1, B_1) resulting from Equation (2.16) (highlighted in red) can be explicitly expressed. However, since the output is only a virtual representation, which is directly fed into the new calculation sequence, it has no explicit contribution in the output equation. To still account for this feed-through effect, the output matrix and feed-through matrix (C_1, D_1) can be appended to the state representation (A_2, B_2) of Equation (2.18). This immediately fits Equation (2.17) in the overall state-space sytem. The state matrix and input matrix (A_2, B_2) resulting from Equation (2.18) (highlighted in blue) are accompanied by the explicit output equation. The output matrix and the feed-through matrix (C_2, D_2) here fully describe the simulation of the HO control action.

At this point, the minimal state-space representation is derived, which entails 9 canonical states. It should be noted that a different approximation order is accompanied by a different number of canonical states. Since the third order Padé approximations were concluded to provide the minimal feasible solution space for the state and parameter estimation, the HO identification is expected to have the form of Equation (2.19). In the next section, the identification procedure is elaborated upon.

2.2. Dual Extended Kalman Filter

Now that the preview model of Van der El [15] has been explained, it should be possible to describe the behaviour of a HO by means of physically interpretable parameters. In more conventional frequency-domain analyses and prediction methods, data collection over the entire measurement time frame is required to find single values for the states and parameters [12]. The human capability to adapt to environments and tasks, and the human limitation of inconsistent behaviour, make the frequency-domain calculations inherently obscure some of the control responses. Ideally, for preview tracking applications, a time-domain analysis method is used to identify the states and the parameters of the pilot vehicle system, comparable to Popovici et al. [17]. This section describes a range of time-varying identification techniques, Popovici's DEKF for compensatory tracking [17], and Vertregt's updated DEKF for preview tracking [19].

2.2.1. Time-Varying System Identification

The isolated HO SS system allows for the time-domain – potentially real-time – estimation procedure of states and parameters [19]. As previously discussed, the most interesting HO parameter is look-ahead time τ_f, which can also be described as the apparent time delay τ_f^*. There exists a range of methods for this time-domain estimation, which all have their advantages and inadequacies. The ideal estimation method should be able to (1) estimate time-delays [37], (2) converge even when exposed to remnant [19], (3) allow for free parameter variation [19] or scheduling in line with experimental data [38], and (4) directly identify HO preview model parameters [39]. In car driving experiments, non-linear parameter estimations have been performed with a Dual Extended Kalman Filter (DEKF) to study advanced driver-assist systems [40]. Additionally, recent research into parameter identification for permanent magnet synchronous machines has proven that the DEKF is promising for online identification [41]. The considerations regarding different identification methodologies for preview tracking tasks are briefly summarized to substantiate choosing DEKF as the most suitable option [19].

- **Maximum Likelihood Estimations (MLE)** [30] can only express the parameter variations in terms of predefined progressions, which have to be designed beforehand
- **Wavelets** [42] prove to be too sensitive to HO remnant and the parameters can not be directly estimated during the procedure, but have to be acquired with frequency response analyses
- **Recursive ARX Models** [22] have their own representation of parameters, and time delays cannot be estimated, which impedes the desired HO parameterisation for preview tracking tasks
- **Unscented Kalman Filters (UKF)** [23] are relatively costly with regard to computational expenses, which can possibly introduce difficulties for real-time applications
- **Dual Unscented Kalman Filters (DUKF)** could facilitate the reliability and computational efficiency increase with regard to the UKF, but have not yet found a sophisticated application in cybernetics
- **Dual Extended Kalman Filters (DEKF)** [17] are a good compromise between power and expense, although the initialisation and the tuning should be carefully monitored for convergence

2.2.2. Popovici's DEKF for Compensatory Tracking

The dual Kalman Filter concept has been incorporated for a range of research applications already. Here one can think of state and parameter estimation for vehicles [43], or batteries [44], but also of compensatory tracking research using the states and parameters from the Crossover Model [17]. To gain relevant insights in the application of a DEKF for preview tracking parameter estimation, the past implementations in TU Delft cybernetics are outlined in this section.

Working Principles of a Kalman Filter [45], [46], [47]

To formally introduce the Kalman Filter, and to establish some initial understanding of the algorithm, it is explained using the application it was originally designed for: state estimation. In modern technology, research is highly relying on sensor readings for adequately valid results. Even after calibration, sensors can be expected to provide readings with the necessary noise and bias. Evidently, smoothing operations can be implemented for the data, in order to create more rigid results, but this will provide no insights in measurements accuracy. State estimation aims for finding a state vector, for which all the noise and bias features have been mitigated. In order to reach this goal, the Kalman Filter makes an educated prediction of the signal's next data point, based on the current data point and readings of the signal variance. Depending on its confidence in its prediction, it will make an weighed decision between measurements and predictions [45]. Fundamental for the Kalman Filter to work optimally, it is required to provide it with statistical information of the system noise Q and measurement noise R. Q is constructed by placing the expected variances of all system states on the diagonal, and R is described by the sensor variance.

As initialisation of the Kalman Filter, a value is chosen for the state estimate $x_{k,k}$ and the covariance matrix corresponding to the state prediction error $P_{k,k}$. The value of $P_{k,k}$ essentially describes $x_{k,k}$'s uncertainty. Using an internal model of the system (e.g. the SS system for preview control tracking), the Kalman Filter's predictor tries to make a calculation for the next data point's state $x_{k+1,k}$. Again, the uncertainty is evaluated with a state covariance matrix $P_{k+1,k}$, which is constructed using the state prediction and the process noise statistics that are fed into the algorithm. For this to hold, it is assumed that the system noise and state error are uncorrelated. With the variables at hand, the Kalman Gain K_k can be constructed. The Kalman Gain is meant as an optimisation step, where a penalty is given for the offset between the measured and predicted state. The larger the offset, the larger the penalty, and the higher the associated value for the Kalman Gain. This gain is expected to decrease until a value is reached corresponding to a converged algorithm. This means that the Kalman Filter is not more uncertain than the noise statistics that were seeded before. Using the Kalman Gain, the Kalman Filter's corrector makes educated estimation for the next time step's state $x_{k+1,k+1}$, which in turn allows the calculation for the next step state error covariance matrix $P_{k+1,k+1}$. This process is repeated for every step in time. This filtering process requires several data points to converge, increasing the state estimation accuracy to an optimum over time. The state estimation principle can also be applied to more advanced applications, such as fusing data of different sensors to increase estimation fidelity, and the simultaneous identification of states and parameters in a system identification problem. Two powerful features are combined to form the DEKF, which are – as the name suggests – *Extended Kalman Filtering* and *Dual Kalman Filtering*. Both these aspects are slightly elaborated upon to create better understanding of the HO parameter identification algorithm. Furthermore, due to the generally accepted domain of some parameter values under investigation, a solution space limiting feature is included in the algorithm, called *Estimate Projection Limitation* which will be described as well.

Extended Kalman Filtering [47]

After the introduction of the Linear Kalman Filter (KF), it was quickly discovered that the algorithm was not applicable to many real-life scenarios. The main drawbacks are that the KF (1) is based on the assumption that the states to be estimated are linearly related, and (2) requires the system to be fully observable in order to converge to the optimal solution. Looking at HMI applications, the system and measurement equations are mostly of non-linear nature. To still adequately estimate the state vector, the EKF has been designed, which locally linearises the system before the estimation procedure is performed. For this to hold, the state equation and the output equation are assumed to be a continuous function of the input and the output signals. With this assumption, it is possible to calculate the Jacobians of both the state differential equation and the output equation of the state-space system. These Jacobians (F_x, H_x) can be used to find a discretized version of the perturbation equations, including the discrete state transition and input matrices ($\Phi_{k+1,k}, \Gamma_{k+1,k}$). It should be noted that the EKF is not guaranteed to converge to a global optimal solution. Due to the low approximation order of the estimation procedure, only fairly small perturbations can be adequately identified, which can only be realised if the initial conditions are estimated to be close to their actual values. Later in this research, it will become evident that the initialisation of the final filter can still be a tedious process before it provides convergent results. Another disadvantage of the original joint – meaning that all variables to be estimated are included in the same state vector – EKF is that the convergence is highly dependent on the length of the state vector. As can be expected, the more states and parameters introduced, the more the algorithm will explain certain readings with these newly introduced variables. This can even increase to the extent that the algorithm cannot uniquely identify a solution space that can explain the readings, leading to a diverging solution. Splitting the states and the parameters over two individual EKFs (dual filtering) and introducing boundaries to the solution space (state and parameter limitation) can re-enable convergence of the EKF algorithm. The EKF is shown in algorithm format while explaining Vertregt's DEKF algorithm.

Dual Kalman Filtering

In the field of cybernetics, the DEKF has been succesfully applied by Popovici et al. for a compensatory tracking task [17]. For Popovici's research, a comparable state-space system as in Section 2.1.4 was constructed based on McRuer's Crossover Model [18], rather than Van der El's preview model [15]. In this case, the dynamics of the HO executing a compensatory tracking task can be described with 5 canonical states ($x_{s,1},...,x_{s,5}$) and 5 HO parameters ($K_p, K_v, \omega_n, \zeta_n, \tau_v$). In Figure 2.9, it can be seen that the DEKF consists of a state filter (EKF) investigating the faster varying canonical states and pilot gains and a parameter filter (EKF) assessing the less variable HO limitation features. The decision of which states and parameters are attributed to which filter are a design choice, also creating the possibility for parameter estimation in the state filter. The two estimation procedures run simultaneously, and they interact with each other during the dual estimation sequence. Rather than one combination of large sparse covariance matrices for the joint estimation procedure, two smaller sets can be constructed, gaining significantly in computational efficiency and likeliness of convergence [17].

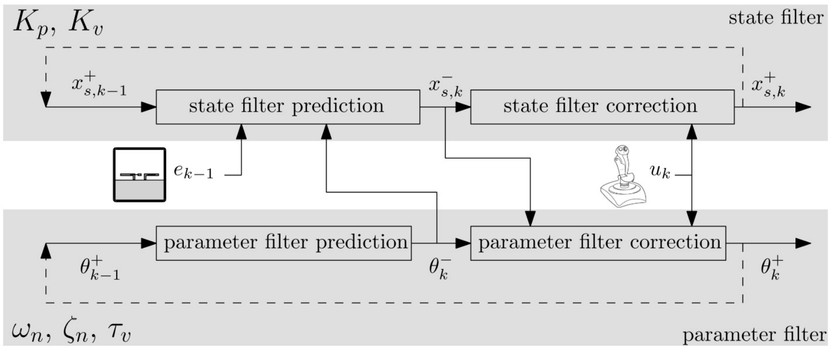

Figure 2.9: The DEKF applied with McRuer's compensatory crossover model [17]

As shown in Figure 2.9, the HO equalization gains are included in the state filter, because of their higher expected variability and more direct expected relation with the internal canonical states of the system [17]. When designing the case-specific state vector and parameter vector, which states and which parameters are assigned to which vector can be chosen arbitrarily. However, one should clearly keep in mind which assumptions are present for the state and parameter dynamics. Both the state filter and the parameter filter have an individual state equation, with the main difference that the parameter filter's equation is described as random walk. For this reason, the equalization gains are included in the more variable state vector [17]. The entire estimation procedure has a single output equation, describing the HO control action. Equation (2.20) until Equation (2.22) show the state and output equations corresponding to Figure 2.9. Usage of the dual estimation procedure decreases the covariance matrix size of the states and parameters and of the accompanying process noise ($7x7$ and $3x3$ matrices rather than $10x10$ matrices). This immediately facilitates the convergence of the process. Note that, although convergence took place, the resulting solution can still be infeasible when the states and parameters exceed values that are physically possible. For this reason, an optional solution limitation step is elaborated upon [48].

$$\dot{x}_s(t) = f(x_s(t), e(t), \theta(t)) + w_s(t) \tag{2.20}$$

$$\dot{\theta}(t) = w_p(t) \tag{2.21}$$

$$u(t) = g(x_s(t), \theta(t)) + v(t) \tag{2.22}$$

Estimate Projection Limitation

In the trade-off between time-varying estimation methods, the DEKF's main advantage over MLE methods was its ability to freely vary the states and parameters based on the pilot-vehicle dynamics [30, 17]. However, in the solution space of the states and parameters, some values would not make sense from a physical or physiological perspective. For example, humans have been witnessed to show only a slight variation in their expected visual time delay, with a clear minimum and maximum [14]. Converging values for these parameters beyond their expected ranges essentially means that behaviour is explained by the wrong parameters. Limiting the solution space to stay within the feasible boundaries might facilitate the trustworthiness of the results. In previous research within the field of cybernetics, estimate projection has been applied to limit the states and parameters [19]. In the results, this is reflected by hard floors and ceilings for the states and parameters under investigation [48]. When this method is applied, it should be kept in mind that the mathematical steps before the final result (e.g. Kalman Gains, Covariance Matrices) are not yet limited, possibly occluding an infeasible intermediate solution [19]. This is mainly a problem when the parameters approach their boundaries when the Kalman Filter has already converged. If the limitation step is only used as a tool to ensure convergence of the filter in the initial phase, than the method can be safely implemented. Estimate Projection is a relatively simple matrix operation, where the amount that a generic state surpasses the imposed limit is substracted from the estimation again. In Vertregt's DEKF algorithm below, the limitation step is described both for state and parameter estimations [19].

2.2.3. Vertregt's DEKF for Preview Tracking [19]

For the HO parameter estimation procedure while the pilots are being exposed to a preview tracking task, the theory above is combined to form a DEKF with fixed parameter boundaries. As explained, the canonical states ($x_{s,1},...,x_{s,9}$), and optionally the equalization gains (K_p, K_v), are assigned to the state filter. The less variable human limitation factors ($\omega_{nms}, \zeta_{nms}, \tau_v$) and the preview task-driven parameters ($K_f, \omega_{b,f}, \tau_f^*$) find their identification in the parameter filter. It can clearly be seen in Figure 2.10 that the filters show interdependency and thus have to be run in parallel. The steps taken regarding prediction, correction and limitation are highly comparable looking at the two individual filters. The greatest difference is the assumed differential basis of the state equations (see Equation (2.20) and Equation (2.21)).

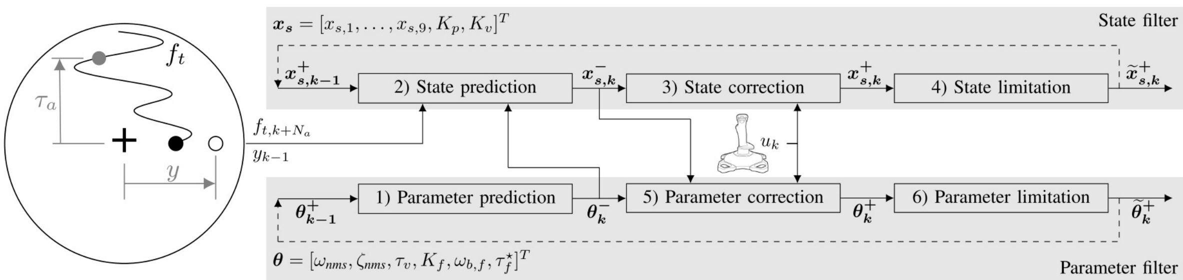

Figure 2.10: The interaction between the state filter and the parameter filter [19].

Both the state and the parameter prediction steps are used to find an initial prediction (a priori) of the values, as a function of the previous best estimate (a posteriori). The parameter progression was assumed to only depend on noise (random walk), which motivates for the most sensible prediction (θ_k^-) to be the previous corrected value (Equation (2.23)). This a priori parameter prediction is accompanied by a calculation of the parameter covariance matrix ($P^-_{p,k}$). Since the state progression is a function of the states, the parameters, the preview target signal and the CE output signal, the current-step prediction ($x^-_{s,k}$) is a function of these values and time (Equation (2.24)). Hereafter, the state covariance matrix ($P^-_{s,k}$) is calculated. The state correction steps as showcased in Equation (2.25) are introduced to make a more substantiated estimation (a posteriori) of the new state ($x^+_{s,k}$). This is done by taking into account the system output and its progression, and by assessing the prioritisation between the a priori state and the measurements with a Kalman gain ($K_{s,k}$). With the new state estimation comes a new state covariance matrix ($P^+_{s,k}$). The state limitation step (Equation (2.26)) introduces a ceiling or floor to the estimated values by means of the D an d matrices, resulting in a bounded a posteriori state estimation ($\tilde{x}^+_{s,k}$). The parameter correction step (Equation (2.27)) and the parameter limitation step (Equation (2.28)) work similarly. An important difference between the state filter and the parameter filter is the definition of Jacobian matrix for the observations $G_{s/p,k}$. As explained by Popovici et al. [17] and

Vertregt [19], the *total derivative* $G_{p,k}^{tot}$ is applied for the parameter filter in the correction step. For both the state filter and the parameter filter, this should a step where the Jacobian is calculated for the output equation $g(x_s, \theta)$ with respect to either the states or the parameters. However, in Section 2.1 it was already shown that the parameters corresponding to the preview processing (τ_f, K_f, $\omega_{b,f}$) are not explicitly represented in the output equation. To still provide sensible values for this variable, it is chosen to calculate the total derivative $\frac{d\bullet}{d\theta}$, rather than the Jacobian matrix. The latter is possible for the canonical states: $\frac{\delta\bullet}{\delta x_s}$.

1) Parameter Prediction

$$\begin{aligned} \theta_k^- &= \theta_{k-1}^+ \\ P_{p,k}^- &= \Phi_{p,k-1} P_{p,k-1}^+ \Phi_{p,k-1}^T + \Gamma_{p,k-1} Q_p \Gamma_{p,k-1}^T \end{aligned} \tag{2.23}$$

2) State Prediction

$$\begin{aligned} x_{s,k}^- &= x_{s,k-1}^+ + f(x_{s,k-1}^+, \theta_k^-, f_{t,k+N_s}, y_{k-1})\Delta t \\ P_{s,k}^- &= \Phi_{s,k-1} P_{s,k-1}^+ \Phi_{s,k-1}^T + \Gamma_{s,k-1} Q_{s,k} \Gamma_{s,k-1}^T \end{aligned} \tag{2.24}$$

3) State Correction

$$\begin{aligned} S_{s,k} &= G_{s,k} P_{s,k}^- G_{s,k}^T + R \\ r_k &= u_k - g(x_{s,k}^-, \theta_k^-) \\ K_{s,k} &= P_{s,k}^- G_{s,k}^T S_{s,k}^{-1} \\ x_{s,k}^+ &= x_{s,k}^- + K_{s,k} r_k \\ P_{s,k}^+ &= (I - K_{s,k} G_{s,k}) P_{s,k}^- (I - K_{s,k} G_{s,k})^T + K_{s,k} R K_{s,k}^T \end{aligned} \tag{2.25}$$

4) State Limitation

$$\tilde{x}_{s,k}^+ = x_{s,k}^+ - D_{s,k}^T (D_{s,k} D_{s,k}^T)^{-1} (D_{s,k} x_{s,k}^+ - d_{s,k}) \tag{2.26}$$

5) Parameter Correction

$$\begin{aligned} S_{p,k} &= G_{p,k}^{tot} P_{p,k}^- (G_{p,k}^{tot})^T + R \\ K_{p,k} &= P_{p,k}^- (G_{p,k}^{tot})^T S_{p,k}^{-1} \\ \theta_k^+ &= \theta_k^- + K_{p,k} r_k \\ P_{p,k}^+ &= (I - K_{p,k} G_{p,k}^{tot}) P_{p,k}^- (I - K_{p,k} G_{p,k}^{tot})^T + K_{p,k} R K_{p,k}^T \end{aligned} \tag{2.27}$$

6) Parameter Limitation

$$\tilde{\theta}_k^+ = \theta_k^+ - D_{p,k}^T (D_{p,k} D_{p,k}^T)^{-1} (D_{p,k} \theta_k^+ - d_{p,k}) \tag{2.28}$$

An immediate research contribution by Vertregt [19] is that there now exists an identification tool that can provide a preview model parameter reading at every time step. In sigmoid step time-varying scenarios, the DEKF is shown to lag significantly behind the original parameter trace. Also, a significant amount of variance is present in the individual estimations. These are aspects that will impede the performance when the algorithm is applied to time-varying HMI experimental data. In Figure 2.11 until Figure 2.14, simulation results of Vertregt's DEKF are presented [19]. Figure 2.11 and Figure 2.12 show a SI scenario and a DI scenario, respectively. In these scenarios, only τ_f was scheduled to vary, and all other parameters were simulated to be constant. During the DEKF estimation, only the neuromuscular delay τ_v was fixed to its scheduled value, and all other parameters were free to vary. For the SI case, the DEKF seems promising, with an estimation spread of approximately +/- 0.1 s, and a delay of slightly more than 25 s. In the DI scenario, it is harder to evaluate the DEKF's performance. The estimation spread is in this case +/- 0.2 s, and within the measurement time frame, it is inconclusive whether the filter is capable of converging to a constant value. In an attempt to reach more reliable τ_f estimations, all other parameter estimations can be fixed at their simulated values in the DEKF. Effects of such measures are shown for SI and DI dynamics in Figure 2.13 and Figure 2.14, respectively. The effect in the SI case is positive, reducing the spread and bringing down the time to reach the terminal estimate to approximately 15 s. For DI scenarios, the opposite holds, as the spread nearly doubles, and it is uncertain whether the filter reacts to the changes in τ_f at all. As shown in Figure 2.11 until Figure 2.14, in its current form, the DEKF has potential for time-varying estimations of HO parameters in preview tracking tasks. In the initial research, applying the filter to SI dynamics experiments, and leaving only τ_f free for estimation, produces the most reliable results. In the progression of that research, SI tasks and τ_f estimation will be focus areas in the validation of the DEKF.

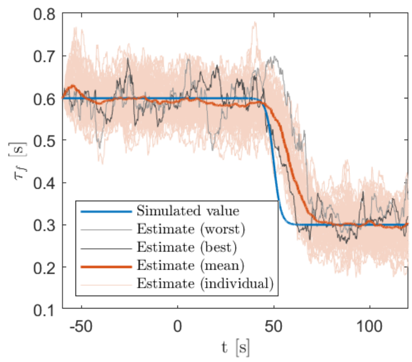

Figure 2.11: Estimating τ_f, while fixing τ_v (SI) [19]

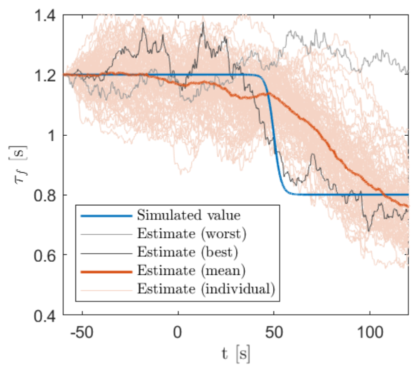

Figure 2.12: Estimating τ_f, while fixing τ_v (DI) [19]

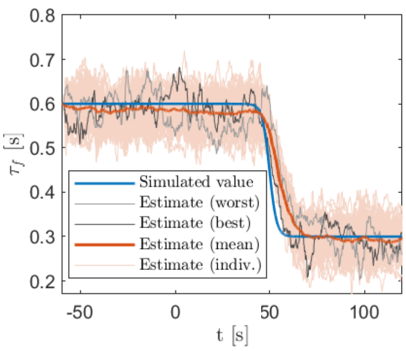

Figure 2.13: Estimating τ_f, fixing all other parameters (SI) [19]

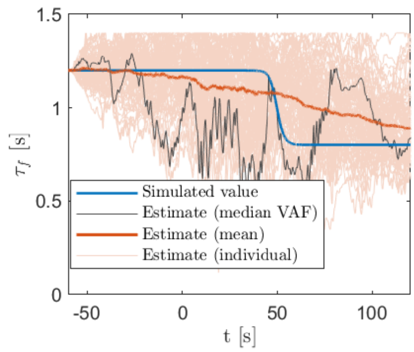

Figure 2.14: Estimating τ_f, fixing all other parameters (DI) [19]

For iterations of the DEKF design, Vertregt suggests to focus on the remnant [19]. For the simulation environment, the remnant is injected in the measurable output signal as a colored noise signal. In experimental applications, the remnant cannot be known. Just as all preview model parameters, remnant can be time-varying. If the remnant is explicitly modelled as a low-pass filtered noise signal, these parameters could be included in the DEKF description. This way, the influence of remnant might less easily be attributed to the preview model parameters. Another point of focus for the future application of the DEKF is its initialisation. Especially evident for double integrator dynamics, the algorithm's performance relies on the first estimate that is presented. Rather than a unique optimal setting, the DEKF is expected to have specific optimal settings for different scenarios. Effort could be invested in establishing some heuristics that determine the initialisation based on measurable scenario characteristics. Before moving straight to finding one generalised optimal DEKF, it is desired to validate it in its current form for the estimation of look-ahead time τ_f.

2.3. Conclusion for Future Studies

The identification of human control in preview display tracking tasks has been described as a focus area in future cybernetics research. In vehicle operation, human operators are expected to remain responsible for the years to come. In order to still increase safety and efficiency, human-machine shared control will become a more pronounced part of vehicle operations. Such applications require accurate understanding and identification of human behaviour, and a real-time or time-domain nature of the calculations. Van der El's preview model has become a widely accepted describing function of human behaviour in preview tracking tasks. It is particularly powerful due to the physically interpretable parameters. As addition to McRuer's crossover model, human behaviour can now be predicted accurately when preview is available. A promising candidate for the time-domain estimation of the parameters is the Dual Extended Kalman Filter, as Popovici proved for compensatory displays. Its main advantages are the capability of time delay estimation, the robustness to remnant interference, the unconstrained variation of parameters, and the preservation of the original parameter definitions. Vertregt's DEKF, using the parameterisation of the preview model, shows promising first results for the time-varying identification of human strategy during preview tracking tasks. At this point, HO parameter estimation with a DEKF seems feasible for a specific range of preview tracking task applications. The look-ahead time τ_f is shown to be the most variable parameter as function of variations in display preview time τ_p. Additionally, τ_f shows most sensitivity towards the HO tracking behaviour compared to other parameters, within their variation boundaries. For these reasons, the research in this study will primarily focus on the estimation of τ_f, and time-varying estimation of all parameters simultaneously is left as an option for future studies. Vertregt was able to show that the DEKF can accurately estimate τ_f, when the HO is subjected to tracking tasks with single integrator dynamics. When double integrator dynamics was implemented in the controlled element, the τ_f estimation proved to be significantly more difficult. The low-pass filtering properties of the remnant definition and the HO preview response function seem to impede the accurate estimation of HO parameters.

The knowledge compiled in this literature review can be used to continue the research regarding time-varying estimation of HO preview parameters. Before trying to create a robust and consistent DEKF for all possible scenarios in simulation environment, here, focus will be on validating its capability in the research domain where it seems to operate well. This has motivated the decision to scope the study around SI dynamics tracking experiments, where purely the look-ahead time τ_f is estimated, and all other parameter are fixed during the time-varying identification. The goals are to understand the behaviour of the DEKF, and to investigate what levers can be pulled to influence the filter performance. Furthermore, it will be studied what assumptions can be made, and what the effect of these assumptions is on the identification. This should prepare the researchers for applying the DEKF on data from experiments with time-varying display preview time. While assessing the DEKF's operation, both the variation of parameters, as well as the effect on HO behaviour should be taken into account. During the identification with HMI experiment data, it should be studied whether the filter can be set up arbitrarily, or whether some knowledge regarding the HO and the scenario are to be included in the filter definition. This experimental phase can prove whether the DEKF can identify changes in τ_f as function of time-varying τ_p.

3

Research Objective and Methodology

3.1. Research Objective

The Literature Review has provided insights in the working principles of the human operator preview model and the Dual Extended Kalman Filter. In the variation of human strategy, a parameter of particular interest is the look-ahead time τ_f. The look-ahead time indicates exactly which part of the previewed trajectory is used by the operator for control. After the proven potential of the DEKF for parameter identification of the Crossover Model, a research gap exists for its application with the preview model. For this reason, the research objective can be formulated as follows:

> **"To investigate the application of a Dual Extended Kalman Filter for the time-varying identification of human operator look-ahead time during preview tracking tasks."**

As explained in Chapter 2, the preview model is based on the HO response to input signals, consisting of a bandwidth of uniquely distinguishable sines. Although it is impossible to find out what exactly is the human strategy, by means of a parameterisation, predictions can be made of human behaviour. Unfortunately, there will remain non-linearities which cannot be accounted for by a linear model, requiring the introduction of the non-linear remnant in the signal. The DEKF tries to attribute values to the canonical states and the parameters of the system's state-space representation. In this representation, assumptions are made, and some states or parameters are correlated in terms of their effect on the output. Due to the parameterisation and the accompanying estimation, the performance of a DEKF cannot be directly linked to human strategy in a HMI experiment. For this reason, the research question should be split in a preliminary analysis (SIM) and an in-depth analysis including a HMI experiment (EXP). The main questions are based on the following two research areas:

SIM: DEKF identification of time-varying HO look-ahead time using simulated scenarios

EXP: DEKF identification of time-varying HO look-ahead time based on HMI experiment data

The first research area is purely regarding the DEKF applied to the preview model, without using any actual human data. The main goal here is finding the filter's sensitivity to certain preview model parameters, to tune the filter to be as effective as possible for the estimation of look-ahead time, and to create some expectations for the performance for actual HO data. The second research area tries to find a relation between the variation of the display preview time and the variation in estimated HO preview model look-ahead time. As said, the actual strategy cannot be found, but it can become evident what the filter detects when certain variations occur. This could later be linked to human strategy with more elaborate research. The SIM research area will be supported by the preliminary analyses results found in Chapter 4. These analyses are mostly based on the simulated variation of preview model parameters, and specifically the influence of varying look-ahead time. The EXP research area will be addressed by the proposed further analyses as discussed in Chapter 5. During this phase of the research, emphasis is put on the variation of all preview parameters simultaneously, and on experiments with time-varying preview time in the display. The research questions aiming to reach the main objective are summarised below.

SIM (Preliminary Analyses)

1. **How should a simulation environment be constructed?**
   (a) What assumptions are to be made?
   (b) How should the stochastic simulations be executed?
   (c) How should the simulation environment's signals be verified?
2. **What are the most important performance indicators?**
   (a) What is the sensitivity of look-ahead time to output signals?
   (b) What simulated signals provide insights in DEKF performance?
   (c) How can performance indicators be acquired to compare scenarios?
3. **How can the DEKF be set up for time-invariant scenarios?**
   (a) What TI scenarios should be introduced for optimal performance?
   (b) What is the effect of DEKF initialisation on performance?
   (c) What is the effect of covariance matrix sensitivity changes on DEKF?
4. **How does the DEKF perform in time-varying scenarios?**
   (a) What TV scenarios should be introduced for DEKF performance analysis?
   (b) How would these scenarios compare to actual human TV behaviour?
   (c) What is the effect of the TV scenarios on performance indicators?

EXP (Proposed Further Analyses)

5. **How will the DEKF perform if all HO parameters vary simultaneously?**
   (a) What variations in display preview time are relevant for the experiments?
   (b) What HO parameter variations are expected with TV display preview time?
   (c) Which stochastic features of the scenarios are required for validation?
   (d) Can look-ahead time be identified while all HO parameters are varying?
   (e) How does the DEKF performance compare to scenarios of SIM?
6. **How does the DEKF perform in time-invariant preview HMI experiments?**
   (a) Which time-invariant HMI experiment data should be used?
   (b) What are the expected values and limitations of the HO parameters?
   (c) How do the estimations compare to LTI signal analyses?
   (d) What insights in look-ahead time variations are relevant for TV analyses?
7. **How does the DEKF perform in time-varying preview HMI experiments?**
   (a) How should the TV preview HMI experiment be designed?
   (b) How do state and parameter estimations vary due to the display changes?
   (c) How do estimations for TV experiments (Q7) compare to TV simulations (Q5)?

3.2. Methodology / Approach

With the research questions defined in Section 3.1, the approach to answering the questions is explained here. As can be deduced from the research areas SIM and EXP, the goal can be reached by comparing simulations that have predefined HO parameter variations with experiments that have predefined display variations. This will aid the validation process of a DEKF for the time-varying identification of HO look-ahead time during preview tasks. Below, the methodology for the simulations and the experiments will be explained, accompanied by the graphically explained research process of Figure 3.1.

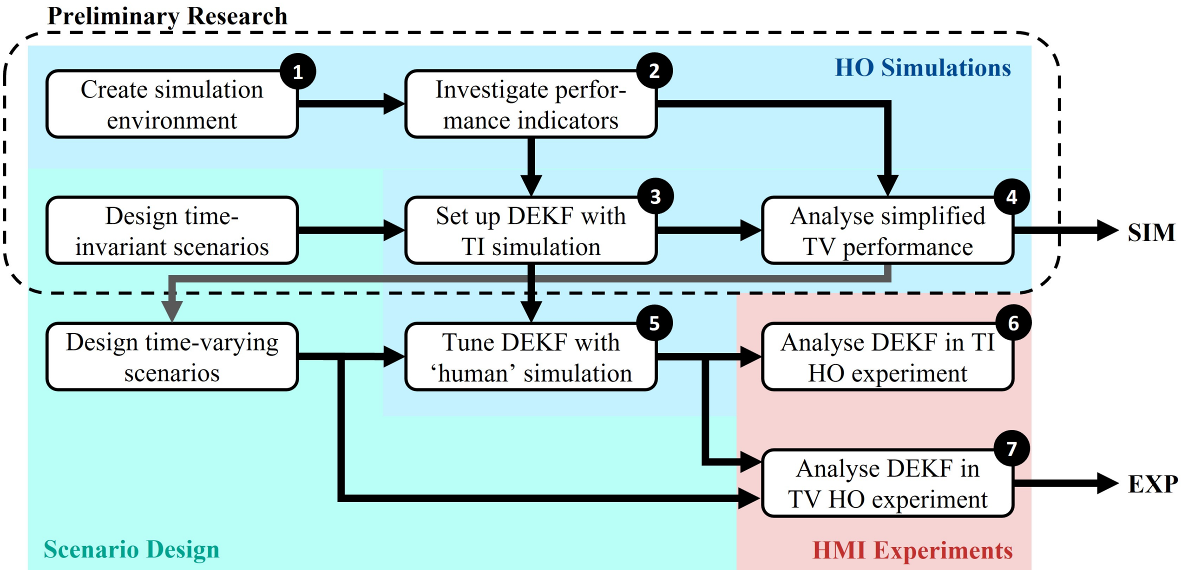

Figure 3.1: Schematic representation of the research process. The dashed box comprises the results included in this document.

Simulations

In previous research by Vertregt [19], a simulation environment including a DEKF algorithm was developed in Matlab, which enables to analyse the estimation performance in a controlled fashion. Vertregt's code structure is recycled in this research. Now, the primary research focus is validating the DEKF, finding its capability to estimate the look-ahead time, and identifying the origin of its behaviour. Some aspects of the code had to be restructured or added in order to perform the analyses. The environment should be able to perform a closed-loop pilot-vehicle simulation to generate HO behaviour using target inputs and HO strategy (parameters). Furthermore, it should be able to simulate open-loop remnant-free pilot behaviour based on the target and state inputs and HO strategy, which serves as verification of the DEKF. To keep track of the full performance at every time-step, the state-space structure of these two simulations should be identical to the one defining the DEKF. This way, all canonical states and HO parameters estimated by the DEKF can be compared to the original quasi-linear simulations, and to the perfect linear response. Although the definitions of the simulation and estimation environments now coincide theoretically, it is also important to verify the solver itself and the produced signals. The closed-loop simulation can also be performed with Matlab's Simulink, by including all transfer functions and process signals in a control diagram. Compared to Vertregt's Simulink scheme, the target signal processing block is restructured by removing the near-viewpoint signal and including the apparent time delay transfer function. Only including the far-viewpoint target and combining the equalization and the neuromuscular transfer function allowed for complete resemblance between the Simulink control diagram and the state-space system from Section 2.1. Simulink also has the possibility to include Padé approximations for time-delays, which are set to the same order as the state-space system. If the update frequency coincides with the newly created solver, all system signals can be verified in both the time domain and the frequency domain. With this updated simulation environment, it is possible to address all main questions of the SIM research area. Both the simulated scenarios and the DEKF algorithm can be altered individually. This will provide insights in the working principles and sensitivity of the DEKF for the application of HO parameter estimation in preview tracking tasks. It also enables further experimental research to start with an identification algorithm that is in the vicinity of its optimal initialisation and settings.

Experiments

Important in the DEKF's validation process is the analysis of the algorithm's behaviour when actual HMI signals are provided. Measurements of these signals will be collected in TU Delft's Human-Machine Interaction Laboratory (HMI-Lab). This is a fixed-base simulator, including a display and an electro-hydraulic servo-controlled side-stick. The side-stick can be limited to only move in controlled fashion around its roll axis. Human operators can provide input to the side-stick as a response to the previewed target signal and its disturbance on the display. The visual preview time of the target signal can be varied during the experiment. The acquisition of response data should last 120 second with an update rate of 100 Hz, which is in line with earlier research and the simulation phase. Note that the goal is not to understand human behaviour in time-varying tasks, since the DEKF estimations are not proven to be representative for HO strategy. Also, it is not the intention to analyse the accuracy of the parameter estimations, since there exists little knowledge yet on how human's change strategies in the time domain, and to what parameters it can be attributed. What is sought after is understanding what the DEKF's reaction is to HO behaviour changes, induced by time-varying preview time in the display. For this reason, the HMI experiments should be simple and limited to a small set of scenarios. The experiments should include significant display time-variance at clearly distinguishable moments, and should be in line with HO parameter time-variance that will be simulated. It would be interesting to see whether there are signs of filter convergence, and whether the estimations are in line with the expected parameter values based on the preview display.

Research Process

The research questions and sub-questions defined in Section 3.1 should together contribute to reaching the main objective of this thesis. Figure 3.1 shows in schematic fashion how the research activities will be performed consecutively. The preliminary research activities (dashed line) are already executed, and the results can be found in this report. The digits on the blocks correspond to the specific research questions 1-7. The entire research consists of simulations and HMI experiments, which together will show whether the DEKF can identify time-varying HO look-ahead time if it would be applied in preview tracking control tasks.

4

Preliminary Analyses Results

In this chapter, the results of the preliminary research phase are presented. The structure follows the work-flow of the research process in Figure 3.1. First, the preliminary research scoping process is elaborated upon and the decisions are presented in Section 4.1. Then, in Section 4.2, the creation of the simulation environment is described. After that, Section 4.4 shows the initial tuning process of the DEKF during time-invariant simulations. The DEKF's performance during time-varying simulations is analysed in Section 4.5. A reflection on the preliminary results can be found in Section 4.6.

4.1. Preliminary Research Scope

Although the display and assignment of this study's preview tracking task look simple, the pilot-vehicle system (Figure 2.3) is rather complex. This is mostly due to the wide range of variables influencing the behaviour of the HO. Furthermore, the simulation environment and the DEKF have many design settings that can be tuned during the analyses. All these variables and design choices influence the system and signals, meaning that drawing conclusions should always be limited to the researched domain. Because the entire research is performed in the time domain, and because time-variance is investigated, a single scenario analysis is computationally expensive. Due to the research time-frame, this requires an educated scoping of the scenario spaces. Remember that emphasis is put on the investigation of the DEKF, and showing its potential for the time-varying identification of HO parameters during preview tracking tasks. Below, the scope of the pilot-vehicle system, the preview model and the DEKF can be found.

Pilot-Vehicle System

In the Literature Review, the pilot-vehicle system is briefly touched upon, and showcased in Figure 2.3. In the description of the entire system, there are task variables and conditional variables. In quantitative cybernetics research, only the task variables of interest should be varied, and all others are to be kept constant as much as possible. The conditional variables, being environmental, operator-centered, or procedural should be kept constant at all times to not confound the results of the experiment. The task variables comprise of the Forcing Functions (FoFus), the Display, the Manipulator and the Controlled Element (CE). Central in this system are Human Pilots (HO), who adapts their behaviour to the presented task variables. All task variables can be varied over a range of options, and varying these options often heavily influence how the HO behaves. For that reason, if some generalised insights of HO behaviour are to be retrieved from the experiment, it is important to show that it is true for all the task variable design options. Since the main research focus is the DEKF's parameter estimation, and because the research time is limited, the pilot-vehicle system has been scoped to a small set. The decisions regarding the FoFus, Display, Manipulator and CE dynamics are presented below.

The DEKF is a time-domain identification tool, which is capable of making system estimations per time step. In this research, the goal is to find the tool's capability of estimating the look-ahead time parameter. It is not of interest what frequency bandwidth the HO can include in its response. Therefore, only one arbitrary bandwidth has to be selected for both the target tracking and the disturbance rejection. The only requirement is that these to multi-sines can be uniquely distinguished from each other. The FoFus used are the same as used in previous research by Vertregt [19]. For the preliminary analyses, three realisations are generated, which showed to be a decent trade-off between computational speed and reliability.

Since this research is about preview tracking tasks, the design options for the Display are limited to preview displays. Still, the display should show many realisations in this research, since time-variations of the display preview time are studied. To keep the scope manageable, the parameter traces in this study will be either time-invariant, single sigmoid steps, single sines or double sines. The maximum research precision, or minimum granularity in variations, will be 0.05 s for HO look-ahead time (SIM). The domain of the variation is determined by the boundaries as determined in earlier research (see Appendix A. The display's aestetiscs will be equal to earlier research by Van der El [14].

No specific vehicle control application is under investigation, meaning that the Manipulator can be chosen arbitrarily, as long as it complies with the tracking task. For that reason, the side-stick configuration in HMI-Lab is used, and it is limited to move around its roll axis, similar to Van der El's research [14].

HO tracking behaviour is vastly different in double integrator (DI) CE dynamics tasks, compared to single integrator (SI) tasks. The difference of this behaviour will be directly reflected in different HO parameters in the preview model. Ideally, the DEKF would operate adequately for both the SI and DI dynamics. Unfortunately, this performance aim quickly proved difficult due to HO adaptation in DI tracking tasks. To understand this, the preview processing transfer function (TF) from the preview model should be regarded again:

$$H_{O_f}(s) = \frac{K_f}{1 + T_{l,f}s} = K_f \frac{\omega_{b,f}}{\omega_{b,f} + s} \tag{2.8}$$

This TF behaves as a low pass filter, where the breaking point is determined by $\omega_{b,f}$ $(= 1/T_{l,f})$. This breaking point parameter can vary as a function of varying preview time in the display. For SI dynamics tracking tasks, this parameter's values stay sufficiently high, ensuring that all FoFu signal information is passed through to the closed-loop. This break-frequency is much more variable with preview time in DI dynamics tracking tasks, where it drops to values lower than the FoFu's bandwidth. This is detrimental for the signal observability. A vastly different design and optimisation procedure is to be executed to make the DEKF work for both SI and DI dynamics. Since first insights into the DEKF's estimation capabilities are to be investigated, and since it is not desired to re-design the filter at this stage, it is decided to only focus on SI tracking tasks.

Preview Model

In the modelling procedure, it is important as well to keep track of the relevant scope to reach the research objective. The assumptions underlying the preview model itself are already elaborated upon in Section 2.1. These include the error response being lumped to the CE state and preview target signals, and the definition of the new look-ahead reference point at 0.9 s before the current time reference. The additional scope of the remnant model definition and the Padé approximation are explained below.

The remnant in the quasi-linear preview model should represent all non-linear behaviour that still exists around the linearised point. In the input response, there is thus a linear model contribution and a remnant contribution, summing to the total signal u. In a study regarding HO remnant in preview tracking tasks [25], it was found that the power ratio P_n between the remnant contribution and the total signal is relatively invariant to display preview time. This remnant power ratio is defined as the remnant contribution variance divided by the total tracking input variance:

$$P_n = \frac{\sigma^2_{u,n}}{\sigma^2_u} \tag{4.1}$$

After the introduction of the fundamental Crossover Model, a first-order remnant model was developed by Levison [49], which is stated as TF in Equation (4.2). In [25], it was confirmed that this model also suffices for the preview model. The remnant gain K_n can be tuned in order keep the remnant power ratio at a constant predetermined value. In this research scope, K_n is only determined at the start of each simulation and kept constant afterwards. Constantly adapting the gain is computationally expensive, so in line with the finding that P_n is relatively invariable with preview time, this assumption was justified.

$$H_n(s) = \frac{K_n}{\omega_{b,n} + s} \tag{4.2}$$

In the equations above, both the remnant power ratio P_n and the break frequency $\omega_{b,n}$ proved to be invariable with preview time [25]. However, they are variable with the other task variables. Based on the preview time processing TF H_{O_f}, it was already determined to take only the SI CE dynamics scope into account. In the conclusions it should be remembered that the remnant scope should be revisited should the validation process be expanded to DI dynamics tasks.

Besides the remnant, another influential design choice is the definition of time-delays in the preview model. To make the two delays part of the controllable canonical state-space representation, Padé approximations [36] are introduced. The higher the order of approximation, the more precise the delay definitions, but also the more introduced canonical states. In initial research [19], it was determined that third order approximations for both delays are a compromise between signal precision and state estimation capability of the DEKF. For that reason, only third order approximations are included in the research scope.

DEKF

The Dual Extended Kalman Filter has a range of design features that influence its performance. Due to the computational expense and research focus on the capability of look-ahead time estimation, not the entire scope of design features is taken into account. The research is scoped in terms of the DEKF's set-up and in terms of its filtering characteristics.

While setting up the DEKF for state and parameter estimation, some design choices are made and fixed throughout the analysis. It is decided that the parameters are estimated in the first filter, and the states in the second. Because primarily focus will exist for look-ahead time estimation, it has no estimation advantage to move some parameters to the state filter. In the estimation procedure, all other parameter values are assumed fixed at a value they would have for half the critical preview time. This is because only the capability of look-ahead time estimation is studied. This is the parameter showing most variation and signal expression (Appendix A) due to varying display preview time. In the filter prediction initialisation, τ_f is always assumed to be 0.3 s, which half the expected critical preview time as described by Van der El [14]. The values for all 9 canonical states are initiated at the arbitrary value of 0. The suspension time is designed to be fixed at 0.9 s ahead of the current-time reference. This was decided to be far enough to cope with outliers in look-ahead time behaviour, an to be close enough to generate reliable results.

The initialisation of the parameter estimation variance $\sigma^2_{\tau_f}$ is set at an arbitrarily large value of 1. The parameter covariance matrix P_p is immediately described by this, since its diagonal contains all values for parameter variance. The initial guess for the signal variance of the canonical states $\sigma^2_{x,s}$ is 5, which directly describes the initialisation of the P_s matrix. During the estimation the HO parameters are limited to their physically possible range as determined in earlier research. The Q matrix and R value are designed to be a function of CE state $y(t)$ and tracking input $u(t)$. The variation and tuning of these two design features of the DEKF are described in Section 4.5.

4.2. Creating a Consistent Simulation Environment

It is determined what methods will be applied to complete the research objective, and the research scope is elaborated upon. To facilitate the further preliminary research questions, a consistent simulation environment should be developed. In this section, the transition from control diagram to state-space system is graphically showcased, after which figures are presented verifying the simulation environment.

From Control Diagram to State-Space System

In Section 3.2 and Section 4.1 it has been discussed that this research builds on earlier thesis work [19], and that only a specific scope will be addressed. The closed-loop and open-loop control diagrams in this research are always in line with Figure 4.1. Only third order Padé approximations will be encountered, and only SI dynamics will be investigated. The closed-loop simulations are necessary for generating all updates for state and human tracking values. The HO open-loop simulations are relevant because they the best performance a DEKF can reach, since the remnant is not modeled. It aimed for to design simulations with a solver that produces nearly exactly the same results as Matlab's Simulink would. Simultaneously, the underlying dynamics (canonical states, parameters) should be designed exactly like the DEKF estimates them. Remember that the DEKF requires the state-space realisation to be the minimal, since the canonical states to be estimated should be kept at a minimum. On the next page, one can find the translation between the open-loop control diagram and a minimal state-space system in controllable canonical form.

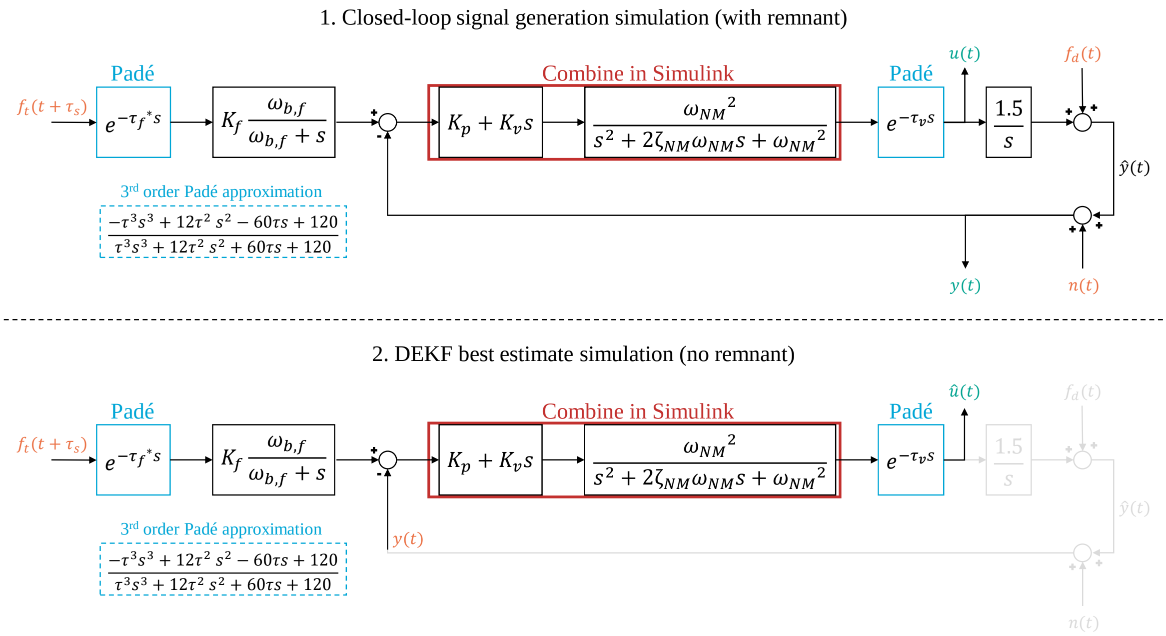

Figure 4.1: Schematic representation of the closed-loop and open-loop simulation.

$$\underline{\dot{x}} = \begin{bmatrix} 0 & 1 & 0 & 0 & 0 & 0 & 0 & 0 & 0 \\ 0 & 0 & 1 & 0 & 0 & 0 & 0 & 0 & 0 \\ 0 & 0 & 0 & 1 & 0 & 0 & 0 & 0 & 0 \\ 0 & 0 & 0 & 0 & 1 & 0 & 0 & 0 & 0 \\ -a_{2,0} & -a_{2,1} & -a_{2,2} & -a_{2,3} & -a_{2,4} & b_{1,0} & -b_{1,1} & b_{1,2} & -b_{1,3} \\ 0 & 0 & 0 & 0 & 0 & 0 & 1 & 0 & 0 \\ 0 & 0 & 0 & 0 & 0 & 0 & 0 & 1 & 0 \\ 0 & 0 & 0 & 0 & 0 & 0 & 0 & 0 & 1 \\ 0 & 0 & 0 & 0 & 0 & -a_{1,0} & -a_{1,1} & -a_{1,2} & -a_{1,3} \end{bmatrix} \underline{x} + \begin{bmatrix} 0 & 0 \\ 0 & 0 \\ 0 & 0 \\ 0 & 0 \\ 0 & -1 \\ 0 & 0 \\ 0 & 0 \\ 0 & 0 \\ 1 & 0 \end{bmatrix} \begin{bmatrix} f_t \\ y \end{bmatrix} \tag{2.19}$$

$$\hat{u} = \begin{bmatrix} b_{2,0} & b_{2,1} & b_{2,2} & -b_{2,3} & -b_{2,4} & 0 & 0 & 0 & 0 \end{bmatrix} \underline{x} + \begin{bmatrix} 0 & 0 \end{bmatrix} \begin{bmatrix} f_t \\ y \end{bmatrix}$$

$$a_{2,0} = \frac{120\omega_{NM}^2}{\tau_v^3} \qquad b_{2,0} = \frac{120K_p\omega_{NM}^2}{\tau_v^3}$$

$$a_{2,1} = \frac{60\tau_v\omega_{NM}^2 + 240\zeta_{NM}\omega_{NM}}{\tau_v^3} \qquad b_{2,1} = \frac{120K_v\omega_{NM}^2 - 60K_p\omega_{NM}^2\tau_v}{\tau_v^3}$$

$$a_{2,2} = \frac{12\omega_{NM}^2\tau_v^2 + 120\zeta_{NM}\omega_{NM}\tau_v + 120}{\tau_v^3} \qquad b_{2,2} = \frac{12K_p\omega_{NM}^2\tau_v^2 - 60K_v\omega_{NM}^2\tau_v}{\tau_v^3}$$

$$a_{2,3} = \frac{\omega_{NM}^2\tau_v^3 + 24\zeta_{NM}\omega_{NM}\tau_v^2 + 60\tau_v}{\tau_v^3} \qquad b_{2,3} = \frac{K_p\omega_{NM}^2\tau_v^3 - 12K_v\omega_{NM}^2\tau_v^2}{\tau_v^3}$$

$$a_{2,4} = \frac{2\omega_{NM}\zeta_{NM}\tau_v^3 + 12\tau_v}{\tau_v^3} \qquad b_{2,4} = K_v\omega_{NM}^2$$

$$a_{1,0} = \frac{120\omega_{b,f}}{(\tau_f^*)^3} \qquad b_{1,0} = \frac{120K_f\omega_{b,f}}{(\tau_f^*)^3}$$

$$a_{1,1} = \frac{60\omega_{b,f}\tau_f^* + 120}{(\tau_f^*)^3} \qquad b_{1,1} = \frac{60K_f\omega_{b,f}}{(\tau_f^*)^2}$$

$$a_{1,2} = \frac{12\omega_{b,f}(\tau_f^*)^2 + 60\tau_f^*}{(\tau_f^*)^3} \qquad b_{1,2} = \frac{12K_f\omega_{b,f}}{\tau_f^*}$$

$$a_{1,3} = \frac{\omega_{b,f}(\tau_f^*)^3 + 12(\tau_f^*)^2}{(\tau_f^*)^3} \qquad b_{1,3} = K_f\omega_{b,f}$$

In the figure and equation on the previous page, the relation between canonical states and parameters is showcased. Should all parameters be known, the canonical state progression $\underline{\dot{x}}$ and the remnant-free human tracking input $\hat{u}$ can be found with a simple solver. For this to work, all parameter values should be updated to their scheduled value at every time step. This is exactly what the open-loop simulation does. The measurable signals produced by the custom closed-loop and open-loop solver can be verified by comparing them to Simulink results. For the Simulink results, the realisation of the differential equation is not studied in this research. In Simulink, it is not tracked how many canonical states are to be solved for, or whether the realisation is minimal. The design of the control diagram is created in such a way that all transfer functions are exactly identical to the custom solver. For that, the compensatory and neuromuscular blocks are to be combined. In the time delay blocks, the Padé approximation option should be set to third order.

Verification Results

One environment is created in Simulink by integrating the control diagrams (Figure 4.1), the other is created in Matlab code and uses the custom minimal state-space representation. Human behaviour – and its variations – can be scheduled by defining HO parameter values for every time step. Combined with this scheduling, the closed-loop simulations can be run with data on the suspended target signal $f_t(t+\tau_s)$, the disturbance signal $f_d(t)$ and the remnant $n(t)$. This produces HO tracking input signals **including** remnant $u(t)$, and CE state progression signals $y(t)$. The signals $u(t)$ and $y(t)$ can be used to verify the custom minimal state-space system solver. Note that these signals have to be generated with the same update rate. This is selected to be 100 Hz, in line with the update rate of the HMI-Lab data collection. Two power spectral density (PSD) analyses were performed. Figure 4.2 and Figure 4.3 show the PSD of the tracking input $u(t)$ for both closed-loop simulations. In the analysis, a number is calculated representing the Pearson Correlation Coefficient (PCC) between the signals from both simulations. Figure 4.2 and Figure 4.3 show the PSD of the CE state $y(t)$, also accompanied by the PCC. Evident from both verification analyses, the simulations are behaving as they should, since the PSD plots nearly overlap and the PCC is near unity.

Remember that, in the open-loop simulation, the differential equation is exactly the same as the one fundamental to the DEKF. This is deemed important, to always be able to explain certain filtering behaviour. The open-loop simulations also use the scheduled HO parameter values for the definition of behaviour. The input for these simulations are the suspended target signal $f_t(t+\tau_s)$, and the CE state progression signals $y(t)$ (output of closed-loop). The single output produced by the open-loop simulation is the HO tracking input signal **excluding** remnant $\hat{u}(t)$. This HO tracking input of the closed-loop and the open-loop simulation can be compared as verification step. This can be done by performing both a closed-loop and an open-loop simulation with the custom differential equation. If the remnant is set to zero in the closed loop, the results should be exactly coinciding with the open-loop. Again, a PSD analysis was performed, this time comparing $u(t)$ with $\hat{u}(t)$, the closed-loop and open-loop signal, respectively. It can be seen in Figure 4.6 and Figure 4.7 that the signals nearly exactly coincide and that the PCC was again nearly 1. What this open-loop simulation will show, is the best signal reconstruction that the DEKF can theoretically reach. In the performance analysis, it would be interesting to see how the values for the canonical states and parameters compare for the DEKF estimation and the open-loop simulation.

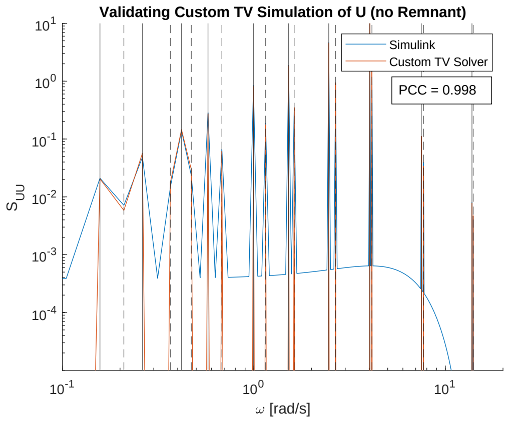

Figure 4.2: PSD plot comparing remnant-free $u(t)$ signals in custom simulation environment.

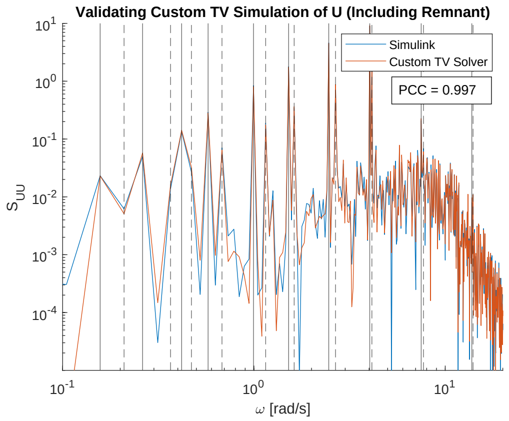

Figure 4.3: PSD plot comparing $u(t)$ signals of one remnant realisation in custom simulation environment.

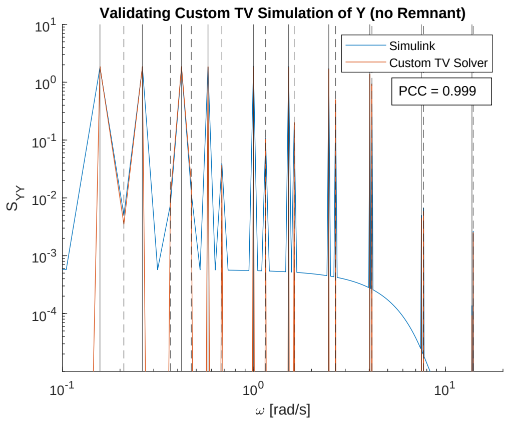

Figure 4.4: PSD plot comparing remnant-free $y(t)$ signals in custom simulation environment.

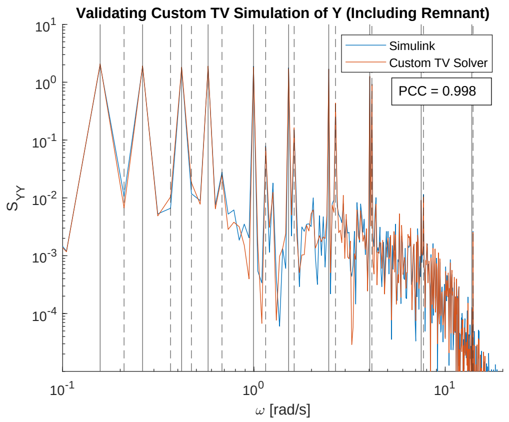

Figure 4.5: PSD plot comparing $y(t)$ signals of one remnant realisation in custom simulation environment.

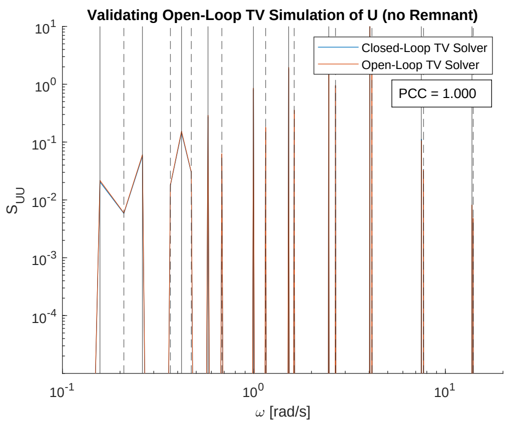

Figure 4.6: PSD plot comparing remnant-free $u(t)$ signals from 'ideal filter' simulation to 'original' simulation.

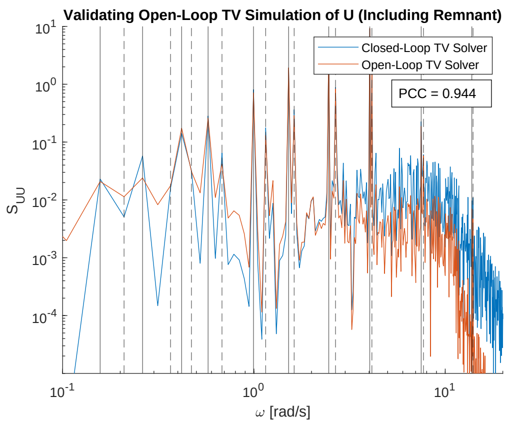

Figure 4.7: PSD plot comparing $u(t)$ signals of one remnant realisation from 'ideal filter' simulation to 'original' simulation.

4.3. Determining Expectations and Performance Indicators

At this point, a verified simulation environment has been established. This can be used to generate time-varying human-like behaviour by scheduling variation in the HO parameters, contributing to the assessment of the DEKF. The parameter of main interest is the apparent time delay τ_f^*, which can be directly translated to the look-ahead time τ_f, as defined in the preview model. Before letting the DEKF estimate the look-ahead time based on the previewed target $f_t(t+\tau_s)$ and the CE state $y(t)$, the parameter's effect on the tracking input u should be investigated. This way, knowledge can be obtained on what variations are likely to be captured by the Kalman Filter. This section describes the initial τ_f sensitivity expectations and the defined performance indicators for DEKF estimations.

4.3.1. Effect of Look-Ahead Time on HO Tracking Input

Using measurable signals f_t, u and y, the DEKF will in its definition make a weighted estimation of the nine canonical states $\underline{x}$ and the eight HO parameters. As described in Chapter 2, in the preview model's formulation, some parameters describe similar signal features, and there is always a non-linear remnant signal which cannot be accounted for. For this reason, it was decided to focus on the estimation of τ_f, and assume a fixed value for the other parameters. These assumptions are based on the measured parameter values in time-invariant scenarios (Appendix A). Before applying the DEKF for such a complex constrained estimation problem, the effect of the look-ahead time parameter should be studied. It is interesting to understand what difference it makes on HO behaviour when this parameter has a different value, and when it shows time-variance. Further down this section, results are shown for different simulations. Both the time traces and the power spectral density (PSD) of the tracking signal u are presented. In both time-domain and frequency-domain graphs, a similarity score between the two lines is presented to provide a quantitative value for comparison.

Simple Look-Ahead Time Variations

In real-life applications, the DEKF will never have knowledge of the actual HO parameter values. The filter can only observe changes in the measurable signals, and possibly attribute these changes to state and parameter variations. To gain insights in how look-ahead time variations reflect in the human behaviour, some simple scenarios have been designed. Next to all scenarios, a baseline simulation is presented showing behaviour with a constant HO strategy ($\tau_f = 0.35$). Without investigating its cause, HO look-ahead strategy can basically deviate from the baseline in two ways. The look-ahead time can deviate further away from the baseline, or faster around it. By using a sine variation of τ_f, four simple scenarios can be designed with a combination of small/large amplitude changes and low/high frequency changes. Small amplitude variations are defined as +/- 0.1 s compared to the baseline look-ahead time. Large amplitudes scenarios show +/- 0.35 s, representing the minimum and maximum values of τ_f that humans show in SI dynamics preview tasks. These variations can be found in the upper plots of Figure 4.8 until Figure 4.11.

Time-Domain Analyses

The middle plots of Figure 4.8 until Figure 4.11 show the time-domain traces of the human tracking input $u(t)$, as a reaction to the same specific FoFus. The baseline (black line) stays the same for all analyses. The scenario under investigation (blue line) shows what the effect is of HO look-ahead time variations on human behaviour. The first and last 30 seconds of the run are studied, mostly to enlighten the effect of higher frequency variations, while keeping the shared mean of the plot equal to the baseline. These time-domain values $u(t)$ are the signals that the DEKF needs to process. Knowledge on the similarity between the scenario and the baseline tracking inputs, can create expectations on the accuracy of the DEKF. This is important in terms of both variance and bias. For example, if the DEKF's estimates are constantly ranging between -20% and +20% of the actual value of τ_f, this can be easily explained if the human behaviour is very similar for all values. Similarity can be investigated by comparing time traces. However, care should be taken that visual perception of similarity can be misleading. For that reason the PCC is included for all time traces. Another detail to keep in mind is that time-domain analyses often lack to display fundamental signal properties. Therefore, the frequency-domain representation of the tracking input is studied as well.

Frequency-Domain Analyses

Often, algorithms tend to interpret measured data differently than humans in their analysis. The DEKF is a time-domain analysis tool, motivating to analyse signals in this same domain. Still, to ensure that DEKF behaviour can be best explained, the frequency-domain analysis is considered as well. Human behaviour is induced by a combination of target and disturbance FoFus. These FoFus are designed as a summation of sines with uniquely identifiable frequencies. Therefore, if analysed in a PSD, these input signals f_t and f_d only have power at their designed frequencies. If these FoFus are processed by the HO, this signal power is converted to tracking input, which can also be presented in a PSD. In this spectogram, the linearly processed signals and the remnant can be showcased with specific power again. How exactly these signals are processed by the HO depends on applied strategy, and thus look-ahead time. In the lower plots of Figure 4.8 until Figure 4.11, the PSDs of the same HO tracking input signals are shown. This way, it can be studied how specific parts of the FoFus are translated, and how look-ahead variations are influencing this translation. Again for these plots, a value is shown, trying to compare the PSD traces to each other numerically. However, note that the data points in a PSD do not represent a reading in the time domain. Although the same calculations as for the time-domain analysis are used, this does not represent the actual PCC. Both the time-domain and frequency-domain plots are shown on the next pages. Some additional descriptions on the findings can be found there.

Results

The parameter variations in Figure 4.8 and Figure 4.9 show a small and large amplitude, respectively, while both have a low frequency. In the small amplitude scenario, the look-ahead time varies significantly (roughly +/- 25%), but hardly any variation is shown in the output signal (PCC nearly 1). On the other hand, when the look-ahead time is varied further away from the baseline, significant behaviour changes are visible. As can be expected from a HO that anticipates more, a higher value of τ_f translates to earlier target responses and seemingly less excitation of the manipulator. For lower τ_f values, the opposite holds. Looking at the PCC between the two traces, the value dropped significantly, and this value becomes even lower if time-invariant scenarios are run with constant τ_f values at the sine extremes. These insights in amplitude variations can create expectations for the DEKF performance. Using the plots below, it is predicted that even the most thoroughly tuned DEKFs will have difficulty finding small look-ahead time changes. Simultaneously, constant HO strategy might still provide τ_f estimations with heavy noise characteristics.

From initial visual inspection, some expectations have been created regarding the human tracking behaviour, and thus the DEKF estimation performance. Although the estimation is performed in the time domain, it was decided to include frequency-domain analyses on the data as well. These results for low frequency variations are presented in the lower parts of Figure 4.8 and Figure 4.9. As explained, the PCC calculations have been performed in order to create a numerical comparison between the PSDs. For the small amplitude, low frequency scenario, the plots nearly overlap, and the similarity value is approximately 1. This supports the hypothesis that low amplitude look-ahead time variations will be hard to detect for the DEKF. On the other hand, Figure 4.9 shows that high amplitude variations have a significant effect on the HO tracking input. It can be seen in the PSD plots that, at the target frequencies (left spikes of duos), there is a lesser uniquely identifiable response. From a stochastic system analysis perspective, this means that there is some extra power at the frequencies surrounding the target FoFus, at the cost of the original signal power. In previous work on frequency-domain analysis of time-varying systems by John Lataire [50], it was proven that the additional power surrounding the key frequencies is caused by the parameter's time variations. Additionally, it was qualitatively shown that a higher amplitude or frequency of parameter variation comes with a larger affected bandwidth surrounding the key signal frequencies. The effect of amplitude changes is clearly visible comparing Figure 4.8 and Figure 4.9. Also, the numerical similarity value is significantly lower. This is in line with the time-domain expectations.

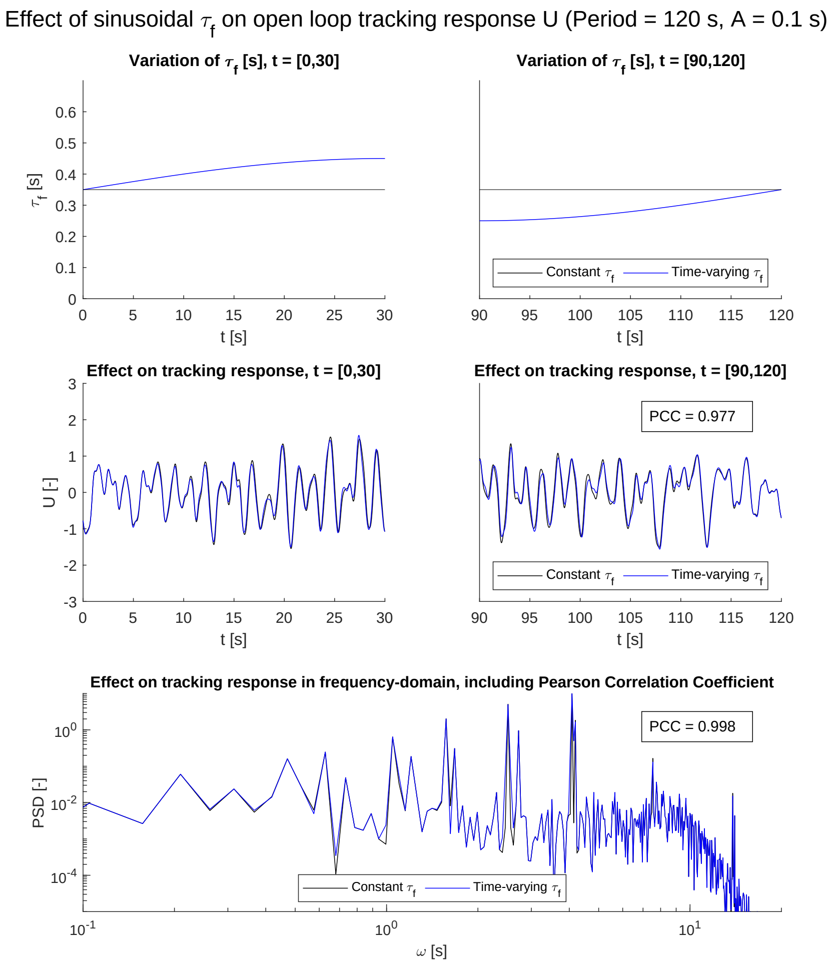

Figure 4.8: Sensitivity analysis for low frequency, small amplitude τ_f variations.

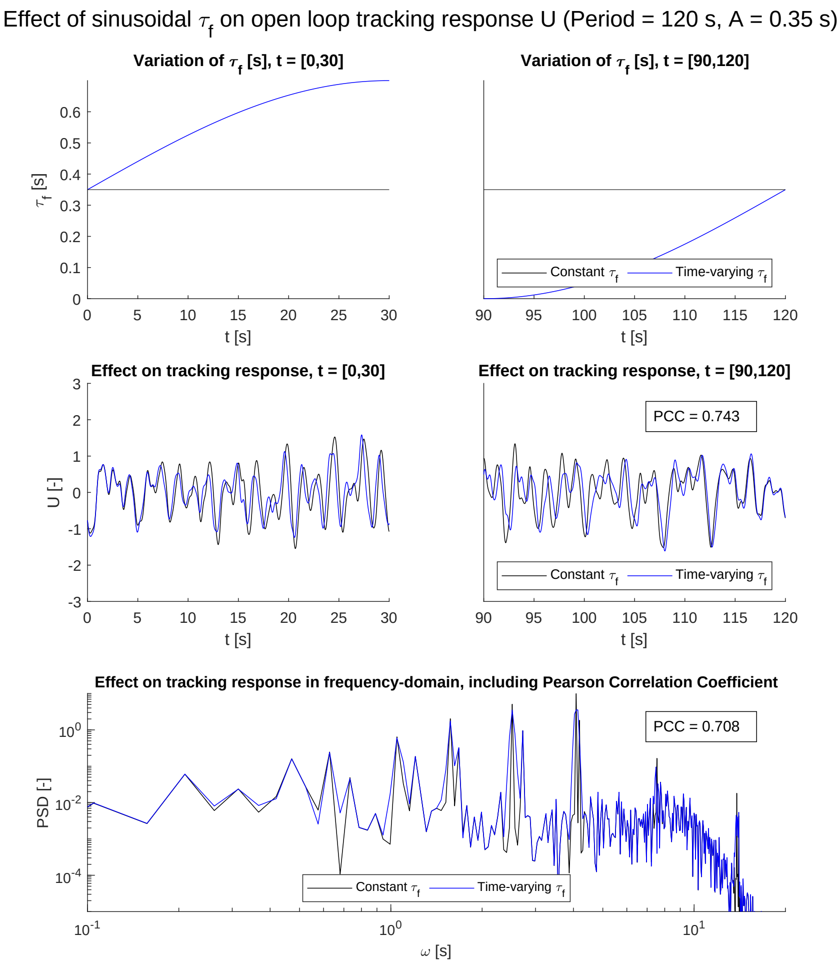

Figure 4.9: Sensitivity analysis for low frequency, large amplitude τ_f variations.

Figure 4.10 and Figure 4.11 also have different amplitudes for the τ_f variations, but now the frequency is much higher. The motivation for investigating this higher frequency, is that the behaviour changes might be more pronounced, since there are more abrupt parameter variations. Should specific differences between the low and high frequency cases be visible, this could later be used to explain certain readings of the DEKF. For the low amplitude case, again, little variation in the $u(t)$ signal (middle plots) is witnessed and the PCC is close to 1. This restates that significant variance is expected to remain for DEKFs, even though properly set up. With higher amplitudes, the scenario's behaviour seems to deviate much more from the baseline than in the low frequency example. However, from the plot, it is inconclusive whether these pronounced differences originate from the variation of the parameter, or from the moment in the tracking task that the parameter has a certain value. Still, the DEKF is expected to detect such pronounced changes and attribute this to variations in τ_f. The challenge will mostly be making the trade-off between being sensitive enough to cope with high frequency variations and being rigid enough to keep the estimation variance within boundaries.

Since the visual time-domain inspection is harder for the high frequency scenarios, the frequency-domain analyses are especially of importance here. In the lower plot of Figure 4.10, it can be found that the introduction of a higher frequency for low amplitude scenarios induces merely slight differences in the PSD plot. Compared to the low amplitude, low frequency case, the smearing effect of Lataire [50] could be slightly more visible in the lower frequencies. However, it should be noted that both variation frequencies of τ_f are relatively low. The most notable difference is at approximately 2 rad/s and 3 rad/s, where the time-varying parameter case seems to have a small spike at those response frequencies, whereas the constant scenario only shows remnant power. No direct explanation could be established, but this difference could possibly be attributed to the points in time where the look-ahead time parameter varies, which can be studied in future work. Nonetheless, the similarity value between the two PSDs is still nearly unity. Showcased in the lower plot of Figure 4.11, the large amplitude, high frequency variations of look-ahead time clearly have a significant effect on the tracking response. Although the baseline and time-varying scenario seem to mostly overlap at first sight, this is not the case. Much more frequencies are excited in the response than initially present in the target signal. From the plots it is visible that when a human is applying a highly variable preview strategy during an experiment, more high frequency signals can be expected in the response. It can be expected that the DEKF will detect that such significant variations occur, however unsure to what extent the estimations will follow the actual strategy. The similarity value in the PSD plots confirms the difference in PSDs. For comparison, one can look at Figure 4.9.

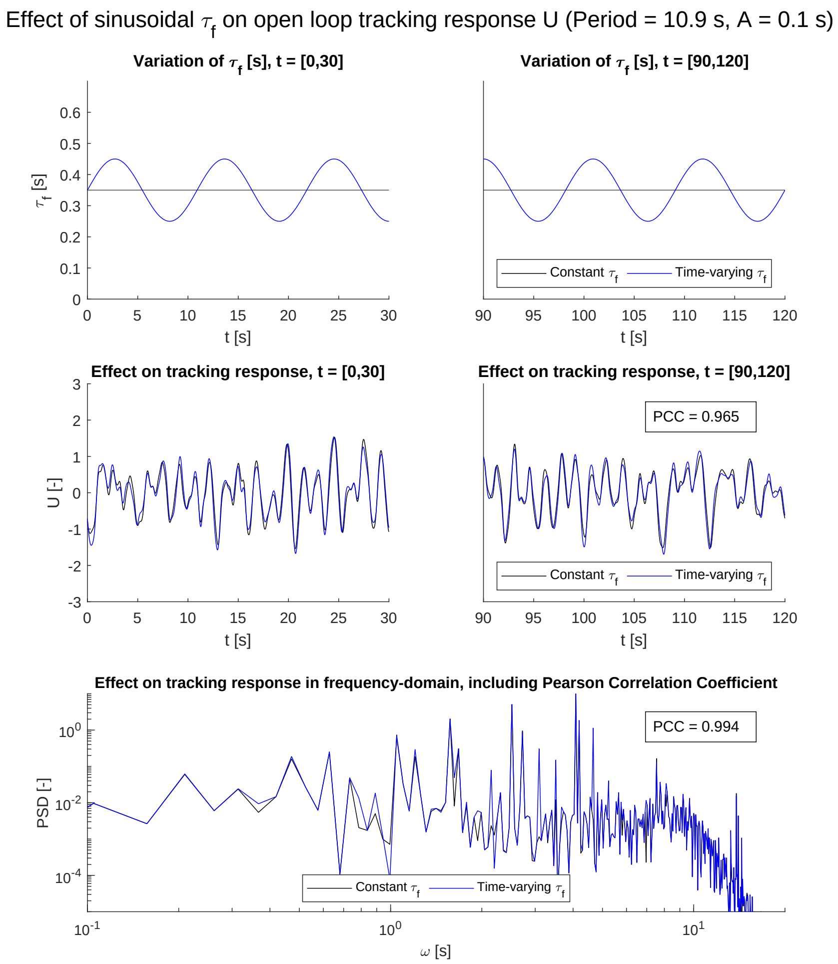

Figure 4.10: Sensitivity analysis for high frequency, small amplitude τ_f variations.

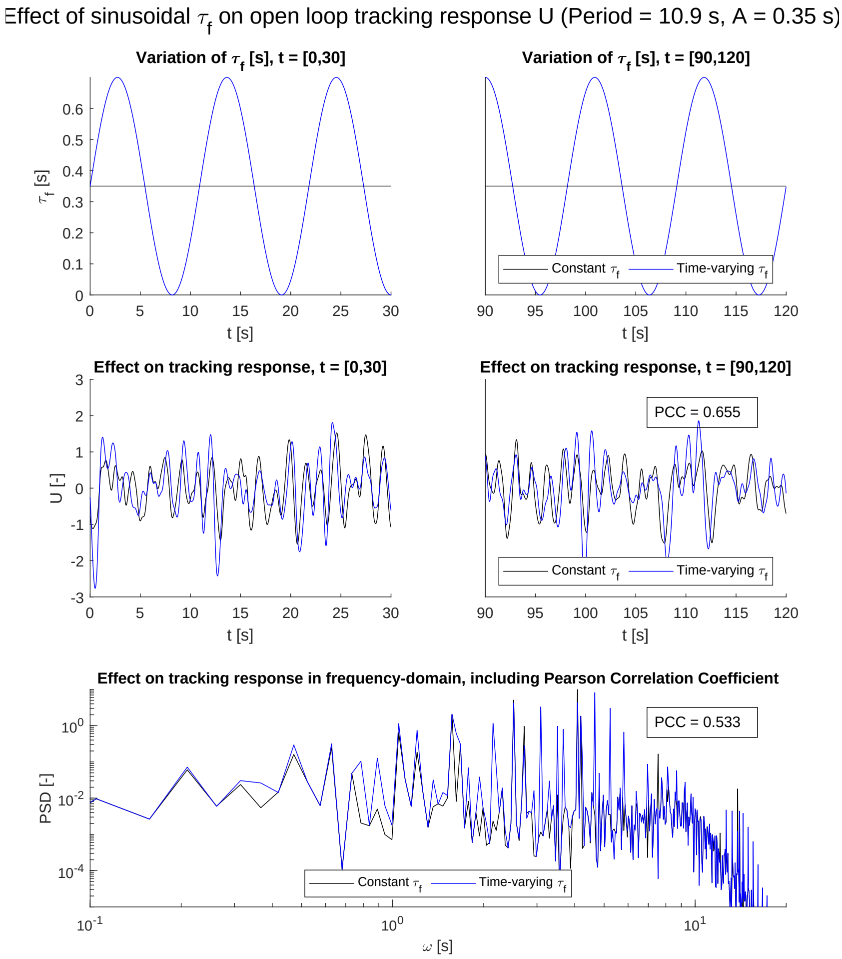

Figure 4.11: Sensitivity analysis for high frequency, large amplitude τ_f variations.

Looking at all plots in Figure 4.8 until Figure 4.11, it can be concluded that DEKF's estimation will mostly rely on the amplitude of the parameter changes, rather than the frequency. This works both ways, thus the filter can also estimate higher frequency variations within certain τ_f boundaries, although the behaviour is expected to be constant. Whether the DEKF will find the actual values during high frequency parameter variations depends on the speed at which it can make the required estimation steps. How DEKF estimation is assessed, can be found in the upcoming subsection on performance indicators.

4.3.2. Performance Indicators of DEKF Analyses

When the DEKF is estimating the HO parameters – or only τ_f, if constrained – much information can be gathered regarding its performance. Before elaborating on the filter settings (Section 4.4), it is described how to assess this performance. First, it is possible to investigate the estimated HO parameter values themselves, and compare them to the scheduling of the closed-loop simulation. Simultaneously, one could study the estimation of the canonical states, and compare these to the open-loop DEKF best estimate simulation. However, these canonical states have no direct meaning in the physical world, making it more interesting to look into the estimation error. These parameters and states only virtually exist in the modeled environment. For that reason, it is also interesting to look at the physically existing tracking input u, and compare the DEKF estimations to both the simulations. Lastly, since the DEKF should react to time-varying signals, the state and parameter covariance matrices can be researched in combination with the tracking error. Below all signals of interest and the accompanying performance indicators are elaborated upon. Although no conclusions will be drawn on performance here, some actual estimation runs are used in this section to illustrate the performance indicators. Investigating the complete signal time traces makes it difficult to compare large numbers of simulations. Therefore, from these time traces, higher level performance indicators should be abstracted. Below, the signal time traces are shown for both sigmoid and sine time-variance. Besides showing the signals in the time domain, it is elaborated upon how the higher level performance information can be abstracted.

HO Parameters

The main purpose of the DEKF is estimating the HO strategy parameters, focusing on look-ahead time τ_f. Performance can be expressed in terms of how the estimated parameter values compare to the initial simulated values. Figure 4.12 and Figure 4.13 show examples of the time traces for sigmoidal steps and sine variations, respectively. The dotted line represents the simulated human strategy in the scenario, and the red lines are what the DEKF estimates based on the measurable data. Nine runs with different remnant seeds and FoFu realisations are combined to an averaged estimation, shown with the bold red line. Looking at these plots, conclusions can be drawn regarding estimation performance. However, due to the large number of scenarios that are to be investigated, and in order to compare all these runs quantitatively, single data points should be extracted from the plots. The sigmoid step variations (Figure 4.12) presents a change from one scenario to another, both time-invariant. Therefore, the time it takes to reach a time-invariant DEKF state is sought after. Conversely, in the sine variation scenarios (Figure 4.13), there is not a converged strategy, but it is constantly changing with a specific amplitude and frequency. In the DEKF response, it seems as if the algorithm starts a periodic response, with the same frequency as the simulated variations. It can be investigated over which frequency range this holds. If a sine is fitted to the averaged DEKF estimations, it can be compared to the simulations. Here, one can investigate the gain and phase shift between the simulations and DEKF estimations as a measure of performance. Lastly, regardless of the variation type, the steady state bias and variance of the estimations compared to the simulations are a performance indication as well. The performance is in this case expressed in terms of HO strategy parameters. However, already explained in the previous section, the parameters might show limited sensitivity towards the actual behaviour. For that reason, also performance analyses regarding the HO tracking input behaviour are included.

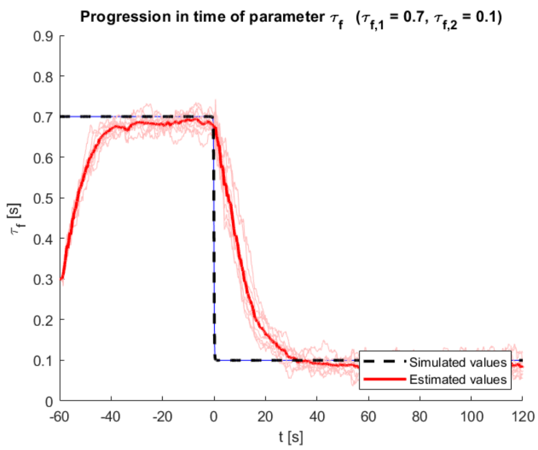

Figure 4.12: Example of τ_f estimation for sigmoid step.

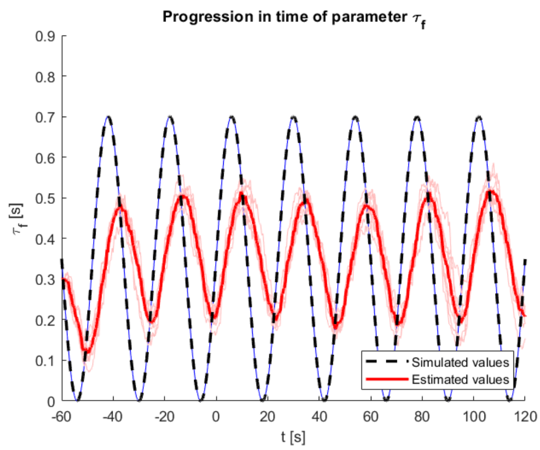

Figure 4.13: Example of τ_f estimation for sine variation.

HO Tracking Input U

The DEKF's estimated values for τ_f can be included in a re-simulation of the open-loop control system. This will result in new data for the HO tracking input $u(t)$ and CE state progression $y(t)$. The results are expected to be comparable to the initial open-loop simulations (no remnant), that used scheduled look-ahead time variations. Note that the values of the re-simulation have only virtual meaning, but they do provide performance insights that include the parameter sensitivity. Figure 4.14 shows 40 seconds of the tracking behaviour $u(t)$ for all the 9 individual runs of Figure 4.12. The plots' central value is 0, where the sigmoid step variation occurs. The blue line represents the open-loop simulation, and the red line the re-simulation using the DEKF's estimated look-ahead time values. It is clearly visible that the lines initially overlap well, then deviate more around the sigmoid step, and finally start to show similar behaviour again. These visual inspections are a verification step, but have no significant contribution to the performance analysis of the DEKF yet.

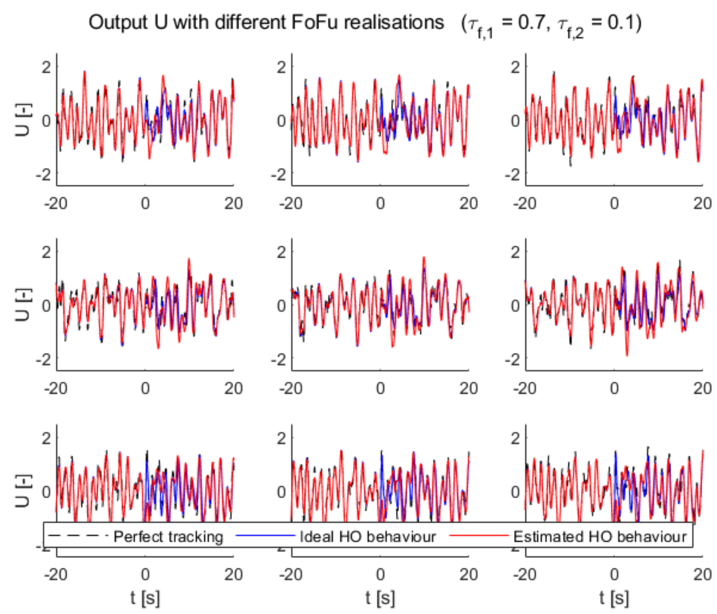

Figure 4.14: Example of the tracking input traces for all scenario realisations.

Just visual inspection lacks the possibility to average the results of different realisations of the same scenario. Furthermore, it is not possible to quantitatively describe the performance of the DEKF re-simulation. For that reason, a numerical measure for similarity between the open-loop simulation and the DEKF re-simulation has to be described, which is repeatable for different realisations. A remaining important requirement is that the performance indicator can be updated at every time step. In previous work [19], the *variance accounted for* (VAF) was selected as similarity value. Equation (4.3) shows how this value can be calculated. VAF is expressed as a percentage, where 100% effectively means complete similarity. The lower the percentage, the lower the similarity, where negative values are possible as well. This calculation is often used to find one single value for similarity between two complete traces. However, the calculation can also be *windowed*, meaning that a value is calculated for a selected time range in the past relative to the current time step. This calculation occurs at every time step.

$$VAF = \left(1 - \frac{\sum_{k=1}^{N_{meas}} |u(k) - \hat{u}(k)|^2}{\sum_{k=1}^{N_{meas}} u^2(k)}\right) \cdot 100\% \tag{4.3}$$

From the selected time window size onward, the windowed VAF can be calculated at every time step. This is a quantitative value for performance, with the possibility to average results of individual runs. Figure 4.15 shows the VAF plot corresponding to the $u(t)$ traces of Figure 4.14. The dotted line corresponds with the actual tracking input $u(t)$, the blue line represents the averaged simulated open-loop response $\hat{u}(t)$ (no remnant), and the red line lines up with the averaged DEKF estimation re-simulation. Due to the open-loop nature, the VAF of the re-simulation can only become as good as the blue line. Around $t = 0$ s, the VAF clearly dips to below 10%, which is expected since the sigmoid step of τ_f occurs there. The value recovers towards the open-loop simulation's VAF, meaning that the estimation of τ_f is able to reconstruct HO behaviour without remnant again. Since it is still desired to retrieve a single performance indicator from these 9 runs, a new definition of convergence time is defined. Convergence can be defined relative to the perfect tracking (dotted line, closed-loop). However, it is preferred to find a description that neglects the effects of remnant in the conclusion. For that reason, convergence is determined relative to the *best possible* signal reconstruction (blue line, open-loop). The point from which the estimation VAF (red) is greater 95% of the open-loop simulation VAF (blue) is defined as the *REL95 convergence time*. This performance indicator can be used in the further analysis steps. As can be seen in Figure 4.16, the VAF data is not all too insightful for the analysis of sine parameter variations. Note that it is still wise to collect such data in order to verify the estimation results at later stage. At this point, during the simulations, performance can be analysed in terms of parameter estimation precision and in terms of sensitivity on the actual behaviour. Both performance indicators are defined after a complete run of the DEKF algorithm. Should unexpected behaviour occur, performance knowledge of intermediate DEKF steps is to be collected as well.

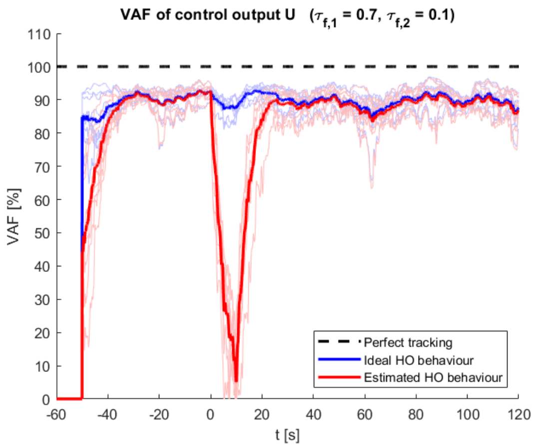

Figure 4.15: Example of VAF plot for all sigmoid steps.

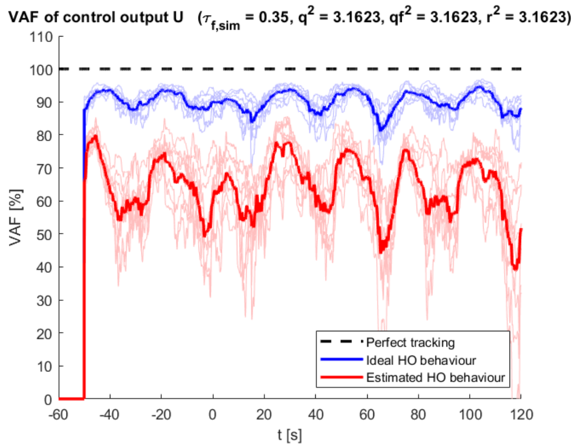

Figure 4.16: Example of VAF plot for all sine variations.

DEKF Parameter/State Covariance Matrix and Estimation Error

At this point, the output of the DEKF can be analysed and some performance indicators are established. Should unexpected performance occur, or should an optimisation of the DEKF be desired, one must also investigate the dynamics of the filter itself. The DEKF algorithm entails several steps where various values and matrices are updated. For every time step, the filter performs a weighted estimation of the canonical states as well as the HO strategy parameters. For general applications where only the state updates are to be found, the convergence of the DEKF can be found in the state covariance matrix P. This is a matrix containing the variances of the states on its diagonal. If all variances reach a constant value, the filter should be operating at its optimum. In this optimum, the weighted inclusion of measurements versus predictions remains constant.

For this research, the P matrix needs to be approached slightly differently. The DEKF includes two separately running filters, thus there are both a state covariance matrix P_s and a parameter covariance matrix P_p. In a time-invariant scenario, both matrices should approach a constant value to showcase filter convergence. The lower the variance on the prediction, the more the DEKF will rely on its value in the weighted average. If the variance increases, it should trust its predictions less. Looking at these matrices, filter convergence can be determined, even before it is visible in the parameter estimations or the HO tracking behaviour. Note that in this further research – and in actual control applications – parameters are of time-varying nature. In the simulated environment, emphasis is on sigmoid steps and sine variations. When states or parameters are expected to vary, it is desirable that the DEKF can deviate from its predictions, after which it tries to converge to a new optimum. To facilitate this, P matrix values for the standard deviation of the predictions should scale with the recorded estimation error. The actual state or parameter error can never be known to the DEKF. For that reason, a measurable value representative for these errors should be included in the definition for at least one of the covariance matrices. The matrix P_s includes both the variance of the HO tracking input $u(t)$ and of the CE state $y(t)$ for scaling its values. Concluding, for time-invariant estimations and sigmoid variations, the main performance indicator is the time it takes for the P matrices to recover to a constant value. For time-varying sine scenarios, the focus is on the sensitivity of the DEKF to state estimation errors. The covariance matrix performance indicators are graphically further explained for both sigmoid step variations (Figure 4.17, Figure 4.18) and sine variations (Figure 4.19, Figure 4.20).

The upper plots of Figure 4.17 and Figure 4.19 show the P matrix values corresponding to the standard deviation of the DEKF's τ_f prediction. In the same figures, the lower plots represent the absolute estimation error for τ_f. In Figure 4.18 and Figure 4.20, one can find similar plots, now for the nine canonical states. The dotted green line represents the point in time where REL95 convergence was established after parameter variations. Clearly visible in the sigmoid plots is that at $t = 0$ s, the variation occurs. The standard deviation values of the P_s matrix converge to a new optimum, much faster than the REL95 convergence indicates. In the sine variation case, it can be seen that the state covariance matrix values are updated based on the estimation error. The values of all these plots can be incorporated as extra verification steps of the DEKF. Note that the focus is mostly on the parameter estimation and the sensitivity towards the actual human behaviour. The covariance matrix data is used to ensure decent functionality of the algorithm. Looking at Figure 4.17 until Figure 4.20, it would be desirable to find some form of reaction of the two P matrices to time variations in τ_f. If the estimations are incorrect or too slowly adapting HO parameter vary, the P matrices can be investigated to find whether the filter reacts according to changes in individual states and parameters. The sensitivity of the DEKF to parameter and state variations is defined in the definition of the Q matrices, which is elaborated upon in Section 4.4.

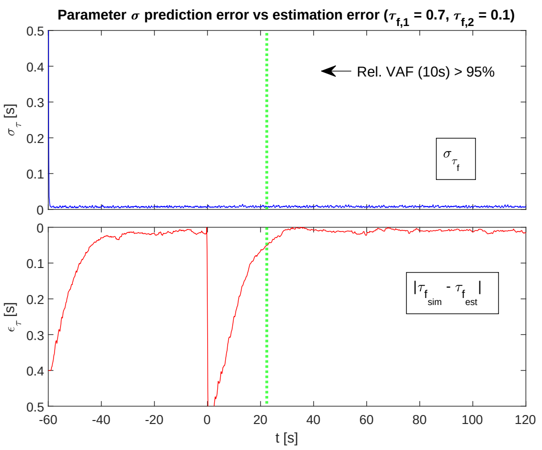

Figure 4.17: Example of DEKF parameter sensitivity plot (sigmoid).

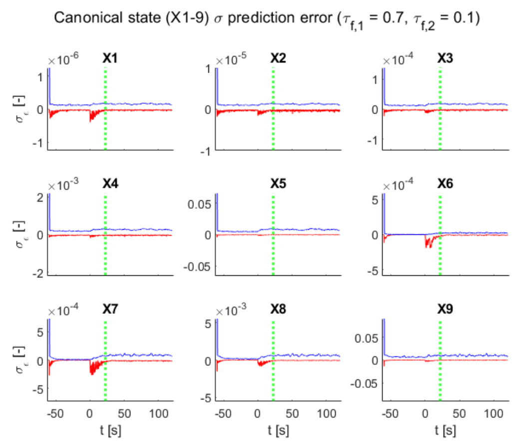

Figure 4.18: Example of DEKF state sensitivity plot (sigmoid).

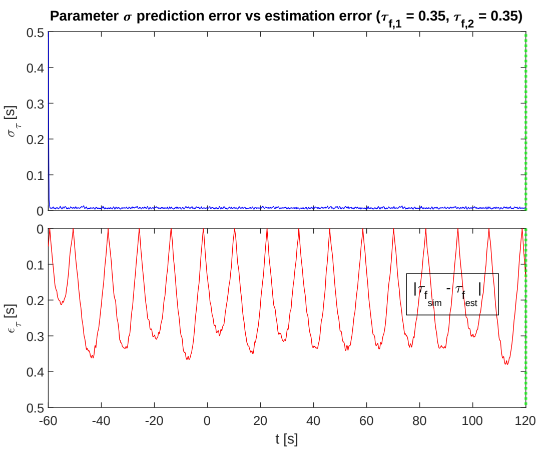

Figure 4.19: Example of DEKF parameter sensitivity plot (sine).

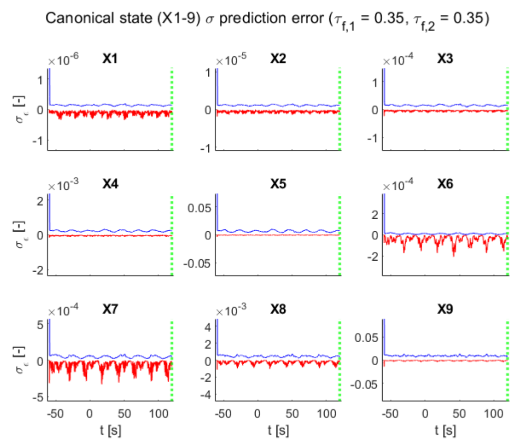

Figure 4.20: Example of DEKF state sensitivity plot (sine).

4.4. Setting up DEKF for Preliminary Results

All types of performance indications have been elaborated upon in the previous section. In the scoping section, the high dimensionality of the DEKF estimation process has been outlined. This sections serves the purpose of finding the best initial settings for the DEKF to perform preliminary analyses. In order to achieve that, first, the focus points for the set-up are elaborated, after which the results are presented. From these results the best preliminary settings can be retrieved.

4.4.1. Fixed DEKF Settings

Before focusing on the variable settings, the fixed settings of the DEKF are elaborated upon. As was determined in the development of the simulation environment, the apparent delay τ_f^* and the neuromuscular delay τ_v are modeled as a third order Padé approximation. The reason for using exactly the same definitions for the behaviour simulation and the state-parameter estimation is that every anomaly in the signals can be detected, rather than only on behavioural or parameter level. The estimation of the apparent delay – and thus look-ahead time τ_f – is dependent on the choice for suspension time τ_s. This shift of reference makes sure that the DEKF never has to estimate a negative delay. A value of $\tau_s = 0.9$ s is selected for all SI dynamics scenarios. Since solely τ_f will be estimated in this research, all other parameters will be fixed at a specific value. For the preliminary research scenarios, these fixed parameter values are shown in Table 4.1. At later stage, these parameters can be assigned other values for different scenarios. For example, when data from HMI experiments are analysed, it can be desirable to feed the DEKF with parameter values that have been determined in frequency-domain LTI calculations. Should at some point in future research all parameters be free to vary during DEKF estimations, they should be kept within physically feasible limits. An example of these physical limitation is presented in Table 4.2.

Table 4.1: Fixed parameter values during DEKF estimation in preliminary research.

Parameter	Value	Unit
K_f	1	-
$\omega_b f$	13	rad/s
τ_f	**Varies**	s
K_p	1.3	-
K_v	0	-
ζ_{nms}	0.2	-
ω_{nms}	10.5	rad/s
τ_v	0.25	s

Table 4.2: Suggested physically feasible limits for DEKF.

Parameter	Lower limit	Upper limit	Unit
K_f	0.01	2.5	-
$\omega_b f$	5	18	rad/s
τ_f	0.01	τ_s− 0.01	s
K_p	0.01	2.5	-
K_v	0.01	2.5	-
ζ_{nms}	0.1	0.5	-
ω_{nms}	8	13	rad/s
τ_v	0.1	0.5	s

In the DEKF, the P matrices for both the parameters and the states are initialised arbitrarily. In the first phase of the estimation run, the Q matrix and the R value are constant, which is dependent on some sensitivity parameters selected by the designer. These sensitivity factors are defined as q^2, q_f^2 and r^2, which can be used to change the DEKF's sensitivity to variance of measurable signals. In Table 4.3, the initialisation of P, Q and R is summarised. The parameter N_{retro} describes how many time steps are included in the variance calculation of the signals e, f_t and u. Up until N_{retro}, the Q matrix and R value are constant, after which they will become a function of the changing signal variances. In Equation (4.4) until Equation (4.6), the descriptions are shown for Q and R during the rest of the DEKF estimation run.

Table 4.3: Initialisation of DEKF values P, Q and R.

DEKF Value	Definition of initialisation
$P_{p,0}$	1
$P_{s,0}$	$5 \cdot \mathbf{I}$
$Q_{p,0}$	0.06
$Q_{s,0}(\dot{x}_5)$	$q^2\sigma^2_{e(1:N_{retro})}$
$Q_{s,0}(\dot{x}_9)$	$q_f^2\sigma^2_{f_t(1:N_{retro})}$
R_0	$r^2\sigma^2_{u(1:N_{retro})}$

$$Q_{s,k}(\dot{x}_5) = q^2\sigma^2_{e(k-N_{retro}:k)} \tag{4.4}$$

$$Q_{s,k}(\dot{x}_9) = q_f^2\sigma^2_{f_t(k-N_{retro}:k)} \tag{4.5}$$

$$R_k = r^2\sigma^2_{u(k-N_{retro}:k)} \tag{4.6}$$

In the equations, N_{retro} represents the number of steps of the past that are considered for the variance calculations. By default, this is fixed at 500 data points (5 seconds) to the past. The degree to which the DEKF variables $Q_{s,k}$ and R should react to changes in behaviour is still to be determined. The optimal settings for the DEKF for q^2, q_f^2 and r^2 are elaborated upon in the next part of this section.

4.4.2. Convergence Time and Bias in Time-Invariant Scenarios

As many engineering problems, there exists no single best setting for the DEKF algorithm. For example, in scenarios with high variability of the parameters, it is desired to have a filter that is sensitive to these changes. On the other hand, when scenarios are rather static, a more rigid filter is preferred to reduce the variance of the estimations. Simultaneously, robustness is striven for, to ensure acceptable solutions for all scenarios to be encountered. Testing all the DEKF's initialisation settings in all types of scenarios (both TI and TV) is computationally heavy, and outside the scope of this research. For that reason, during the tuning, a scenario selection is made that can account for both TI and TV runs. The underlying assumption in these scenarios is that the initial guess for the states and parameters is unchanged. In initial analyses, an arbitrarily high value for the canonical states, and the value of 0.3 s for τ_f were determined to be good starting points. It was also determined that there was no significant difference in DEKF performance moving the starting point through the domain of physically possible τ_f values. The most important aspect of the scenario was the size of the step up or down. For that reason, a simple range of scenarios could be designed. These scenarios for the look-ahead time scheduling are all time-invariant, with three step sizes the DEKF has to make relative to its initialisation. A small, medium, and large step both upward and downward were investigated. This sums to a total of six research scenarios, where every scenario is run 9 times (3 remnant seeds, 3 FoFu realisations). These scenarios are investigated to find the optimal settings for the preliminary research.

As ultimate goal, the DEKF runs in parallel with the measurements. In this case, the measurement trace cannot be analysed beforehand, and thus initialisation should be designed for as much scenarios as possible. In the selection of best settings, it is important that the filter does not diverge under any circumstances. Furthermore, it is required that the filter converges in a decent time frame, so that it keeps up with the human adaptation. Also, the calculations should be close enough to the actual parameter so that the estimated human behaviour is representative for reality. All above motivates for finding an optimum for the DEKF's convergence speed and its accuracy. As explained before, these features oppose each other, and a trade-off is to be made. In the analysis, the speed characteristic is expressed in terms of REL95 convergence time (see Section 4.3) and estimation bias. A constraining requirement is the robustness of the filter, making it fit for many different situations.

4.4.3. Optimal DEKF Sensitivity Settings for Q and R

The values for q^2, q_f^2 and r^2 in combination with the measurable signal variances are presented in Equation (4.4) until Equation (4.6). They represent the reactivity of the DEKF's Q matrix and R value to changes in the parameter values. The intention of tuning these variables is to find a starting point for the further time-varying DEKF analyses. For this, just the order of magnitude already suffices. Due to the virtual nature of the research, fully optimising the DEKF serves no direct purpose for the experimental phase. Understanding the effects of these sensitivity parameters on the DEKF performance is most insightful. This ensures that the filter can be tuned according to specific needs in future research. All three squared values are therefore varied over the range $\{0.01, 0.1, 1, 10, 100\}$, and for all six scenarios both the REL95 convergence time and the parameter estimation bias was investigated.

REL95 Convergence Time

In Figure 4.21 until Figure 4.23, the heatmaps show the REL95 convergence time for different sensitivity variables in a single scenario. Every individual plot represents a specific setting for the R sensitivity. The Q sensitivities are presented on the horizontal and vertical axes of the plots. The plots for $r^2 = 0.01$ and $r^2 = 100$ are excluded from this report, because too many combinations proved divergent or overly rigid, respectively. The scenario under investigation is a large step upward from the look-ahead time initialisation ($\tau_{f,0} = 0.3$ s, $\tau_f = 0.7$ s). This was the most constraining scenario, and the selected settings that can converge well in this scenario were also effective in the other scenarios. The values in the heatmaps present how long it takes for the DEKF re-simulation's VAF to reach 95% of the open-loop simulation's VAF, and sustain this until the final data point. A black bracket means that the filter's re-simulation never reached the 95% threshold. Values close to 120 s imply that the VAF reaches 95% at times, but this cannot be sustained.

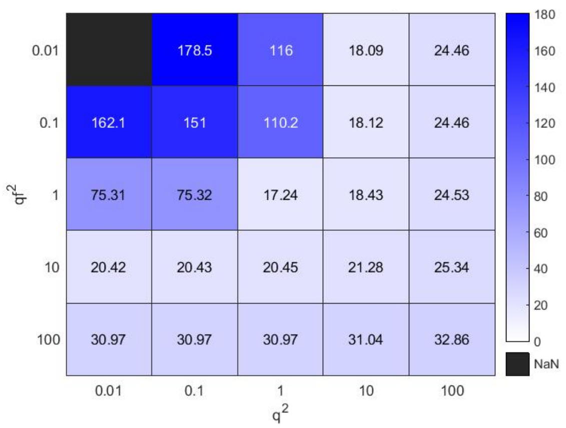

Figure 4.21: Convergence as function of q^2 and q_f^2 ($r^2 = 0.1$).

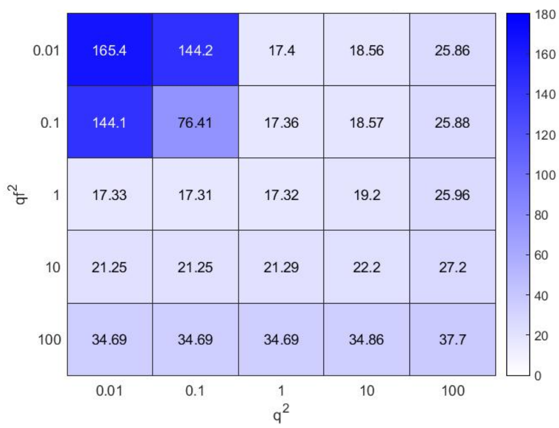

Figure 4.22: Convergence as function of q^2 and q_f^2 ($r^2 = 1$).

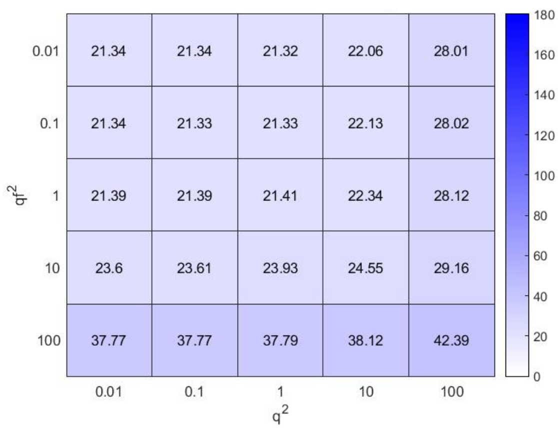

Figure 4.23: Convergence as function of q^2 and q_f^2 ($r^2 = 10$).

With the plots on REL95 convergence time at hand, one can find the best initial order of magnitude for the sensitivity variables. The lowest possible value for REL95 convergence can be found in Figure 4.21, corresponding to DEKF settings $r^2 = 0.1$, $q^2 = 1$ and $q_f^2 = 1$. However, these settings prove to be on the fringes of stability in the q^2 and q_f^2 domain. It can be seen that lower values for these variables result in much higher convergence time, hinting to never actually sustaining REL95. The second-best – and more stable – solutions can be found if the the values for r^2 are increased. It was concluded that both robust and fast performance can be guaranteed if all sensitivity values are in the range $\{1, 10\}$. One slightly more granular analysis was performed, selecting $\sqrt{10} \approx 3.16$ for all variables as decent optimum for the preliminary analysis.

Estimation Bias

Since it is a trade-off, convergence speed can come at the cost of accuracy and consistency. As a verification step, the estimation bias after convergence should also be investigated in all the analyses of the set-up. Figure 4.24 until Figure 4.26 show the offset of the mean of the estimation after REL95 convergence, compared to the simulated value of τ_f. The axes of the figures overlap exactly with the convergence time heatmaps. Again, a black bucket indicates a run that never reached REL95. Note that the 95% threshold is arbitrarily determined, and that convergence can continue after reaching it. This results in the introduction of some bias in every scenario from a theoretical perspective already. Estimating values higher than the initialisation value always show some negative bias at their optimum. For lower values, positive bias can be expected. In Section 4.3, some expectations regarding the precision of the estimation were already determined. Due to the sensitivity of the HO parameter τ_f towards behaviour, the DEKF might encounter difficulty in detecting small changes. Still, averaged over many runs, it is desirable to reach a low value for estimation bias.

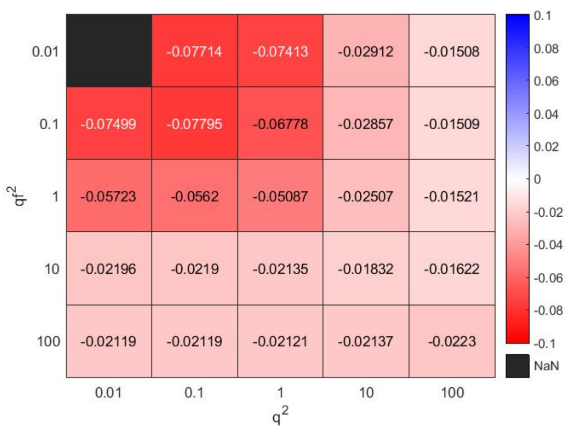

Figure 4.24: Bias as function of q^2 and q_f^2 ($r^2 = 0.1$).

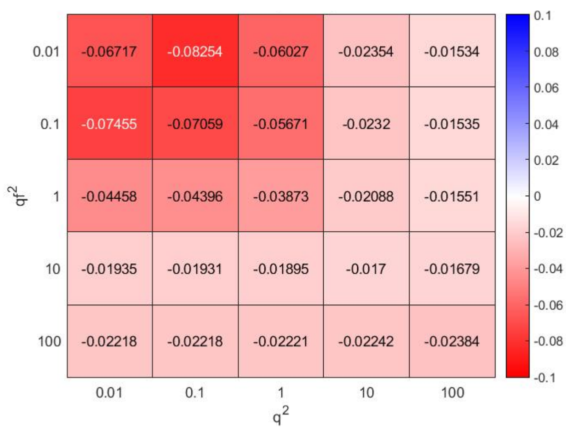

Figure 4.25: Bias as function of q^2 and q_f^2 ($r^2 = 1$).

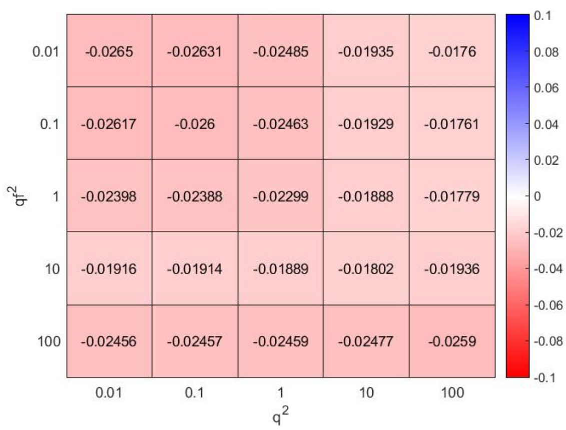

Figure 4.26: Bias as function of q^2 and q_f^2 ($r^2 = 10$).

Besides boosting the performance, the ambition is to create a set-up that shows consistency in terms of speed and accuracy. In the bias plots, one can verify whether the selected range of $\{1, 10\}$ for all three sensitivity variables supports this ambition. Looking at the bias found for $r^2 = 1$, $q^2 = 1$ and $q_f^2 = 1$ (Figure 4.25), one can see a rather large difference with its direct neighbors. This finding suggests that a robuster choice is slightly increasing the r^2 value. After the more granular analysis, the value of $\sqrt{10}$ for all three sensitivity variables proved to be an adequate trade-off between convergence and accuracy. After these set-up analyses, these design settings are trusted to provide stable preliminary results. Now that the DEKF has been initialised, the first results on time-varying estimation can be acquired.

4.5. Analysing DEKF Performance in Time-Varying Scenarios

As final part of the preliminary research, the DEKF is implemented for the state and parameter estimation in scenarios with time-varying operating strategies. After the set-up in Section 4.4, the DEKF is expected to provide converging solutions in a reasonable time frame. Ultimately, the algorithm should be tested in an experimental environment with actual human operators, or in a simulation environment with human-like, and stochastic variation. Because it is difficult to predict HO strategy parameter variations in these cases, it is preferred to investigate a scoped time variation in this phase of the research. The parameter if primary interest is look-ahead time τ_f. The time-varying scenarios are designed so that only τ_f shows variation. All other HO strategy parameters are fixed at the value they would have based on a full preview experimental scenario (Appendix A). These variations of look-ahead time are scheduled in generalised scenarios, in order to ensure quantitative analysis of the results. The goal of this preliminary performance analysis is to create insights in the theoretical best possible performance of the algorithm. Should the algorithm be understood in this environment, more complexity can be added in the simulation. After that, it can possibly be implemented for actual human experiment data. Two generalised functions for variation are further elaborated upon: sigmoid steps and (multi-)sines. The experiment descriptions and the accompanying results of both variation types can be found in this section.

4.5.1. Sigmoid Step Variation

In real-life tracking tasks, there exist many factors influencing the HO look-ahead time strategy of the operator. For example, a tracking task obstruction or heavy weather can drastically decrease the available preview. If the HO is forced to focus on the task closer ahead, this means that the look-ahead time is decreased in terms of strategy. Besides external constraints, a human can also showcase varying look-ahead time due to internal situations, e.g. distraction or fatigue. Such strategy changes can occur gradually, or rather abruptly, and the steps can have different sizes. The gradual steps can be modeled as a range of smaller abrupt steps. In all cases, it is interesting to find whether the DEKF can detect the sigmoid steps in τ_f and converge to an accurate estimation of both the initial and terminal value.

The goal of analysing DEKF performance in sigmoid scenarios is finding whether all changes in the physically feasible range can be detected by the DEKF. Furthermore, it can provide knowledge on the convergence time for all possible sigmoid variations. A nearly instant step of 1 s provides best insights in the convergence time performance indicators. For single integrator tracking tasks, the HO look-ahead time parameter is generally expected to range between 0.0 s and 0.6 s (Appendix A). To also show the performance in the vicinity of these expected limits, 0.7 s is selected as upper boundary for the preliminary research. The effect of sigmoid step size on the DEKF REL95 convergence time is studied. This motivates for introducing all possible step sizes in the feasible range. Furthermore, the influence of the initial value, the terminal value and the step direction (increased or decreased τ_f) is to be studied. To facilitate these requirements, a balanced scenario selection is introduced. These scenarios include 5 possible initial values ({0.0, 0.15, 0.35, 0.55, 0.7} s) and 15 possible terminal values ({0.0:0.05:0.7} s). All combinations of the value progressions are included as a scenario, except the cases where the values are equal. Comparable to Section 4.4, 3 remnant seeds and 3 FoFo realisations are combined to 9 runs per specific scenario. This increases the validity of the simulation results. This sums to a total of 630 complete runs for an analysis. These analyses were performed for 5 sigmoid function designs with different steepness. It was found that the most insightful results came from simulations were it took 1 second to vary τ_f from the initial to the terminal value. With all DEKF estimations for the individual scenario runs, it is desired to find how long it takes for the re-simulation's VAF to recover to REL95 convergence after the step change. Additionally, it should be visible whether differences exist between starting points and step directions. All these results should be taken into consideration when creating hypotheses for the human-like simulations and HO experiments.

Results

For sigmoid step variations, the preliminary key insight should be how much time it takes for the algorithm to recover to a new sufficiently accurate equilibrium set of parameters. Figure 4.27 shows how long it takes for the DEKF's re-simulation to reach the 95% VAF similarity threshold, compared to the open-loop simulation. The *step time* describes the time passed between the initial an terminal τ_f value in the simulations. On the horizontal axis, one can find the absolute step size of the sigmoid function for τ_f. The vertical axis represents the time to re-converge the DEKF estimations, based on the arbitrary REL95 rule. The coloured circles are the averaged datapoints of the 9 runs for a specific scenario. The bold black line shows the mean REL95 convergence time for scenarios with identical absolute step size. The dotted and dashed line represent the means for only the steps down and up, respectively.

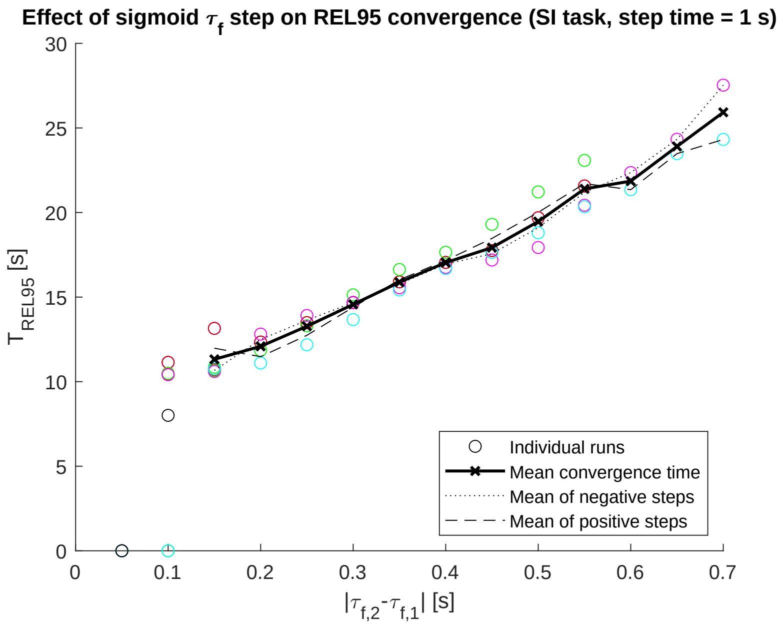

Figure 4.27: The effect of sigmoid step size in τ_f on the time it takes for the DEKF to reach REL95 convergence.

Clearly visible in Figure 4.27, the sigmoid step size of τ_f should be between 0.05 s and 0.1 s to trigger the need for re-convergence. Evidently, when a lower threshold for convergence (e.g. >90%) is selected, this could influence the conclusions on convergence time. Still, useful results regarding DEKF performance can be retrieved from this plot. Most importantly, for all introduced sigmoid steps, the DEKF managed to accurately estimate τ_f at some point. With these re-converged estimates, the DEKF re-simulations show at least 95% similarity with the open-loop best estimate simulation. Then, within the feasible range for τ_f, there seems to exist a linear relation between the step size, and the time it takes to re-converge. For large variations in look-ahead time (e.g. 0.6 s), the DEKF can be expected to take approximately 20 seconds to provide parameter estimations that create re-simulation with REL95 convergence. Two final important insights are that the DEKF seems to be able to equally well estimate positive and negative sigmoid steps, and that specific initial and terminal points show no significant differences. This means that only the step size is expected to influence the results.

4.5.2. (Multi-)Sine Variation

Re-visiting the real-life examples, operators can encounter situations that trigger a periodical variation of look-ahead time. For example, in urban areas, every time an operator drives past a crossing, one can expect the focus of preview information to become closer to the car. If such driving scenarios are regularly repeated – some roads have many crossings, nearly equally spaced from each other – the strategy might change periodically with that. Furthermore, purely from a HO perspective, just as for the sigmoid case, the look-ahead time parameter could also show rhythmic variations intrinsically. For these reasons, further research into the DEKF performance is executed, now focusing on sine variations of τ_f.

Since the constantly changing values for τ_f impede the DEKF from converging, the goal of the sine variation analysis is to investigate which patterns in parameter estimation can be identified for specific scenarios. If such a pattern exists, it is interesting to find the influence of the scheduled τ_f amplitude and frequency on the DEKF performance. The experiments for the sine variations are meant to complement the sigmoid analysis in the DEKF validation. Therefore, the same look-ahead time range of $\{0.0, 0.7\}$ is used. This time, the performance indicators cannot be expressed in convergence time. Still, it is insightful to know the VAF similarity between the open-loop simulation and the DEKF re-simulation. In the complete analysis of sine scenarios, the VAF of both open-loop simulation and DEKF re-simulated can be compared for different amplitudes and frequencies. For this investigation, the relative VAF (DEKF re-simulation divided by open-loop simulation) is collected for every time step. Note that it should be ensured that the estimations show periodic progression for this method to work. An arbitrary point where this is guaranteed is after 60 seconds of estimation. The mean value of these relative VAF points provides a similarity score with the open-loop best estimate. These scores can be presented in a heat map or surface plot, as function of parameter variation amplitude and frequency. The studied frequencies are expressed in *base numbers*, which represent how many complete periods fit in the complete measurement time of 120 s. The range for base numbers is $\{0.06, 0.15, 0.3, 0.65, 1, 1.5, 2, 3, 5, 7, 11, 17\}$, and for amplitudes, it is $\{0.1, 0.2, 0.35\}$ s. If all combinations are repeated 9 times to account for remnant an FoFu variations, this adds up to 324 complete runs of 180 seconds (60 s run-in time, 120 s measurements). The problem can also be addressed from a parameter estimation perspective. Since the input frequency for look-ahead time variation is a sine, it can be expected that the DEKF τ_f estimation response is a sine as well. Initial research proved that this expectation holds for the analysis range that is used. After averaging the 9 estimation runs for a specific scenario, a sine curve can be fitted to the data between $t = 0$ s and $t = 120$ s. Figure 4.28 shows what such a sine fitting looks like for an arbitrarily chosen scenario trio with equal frequency.

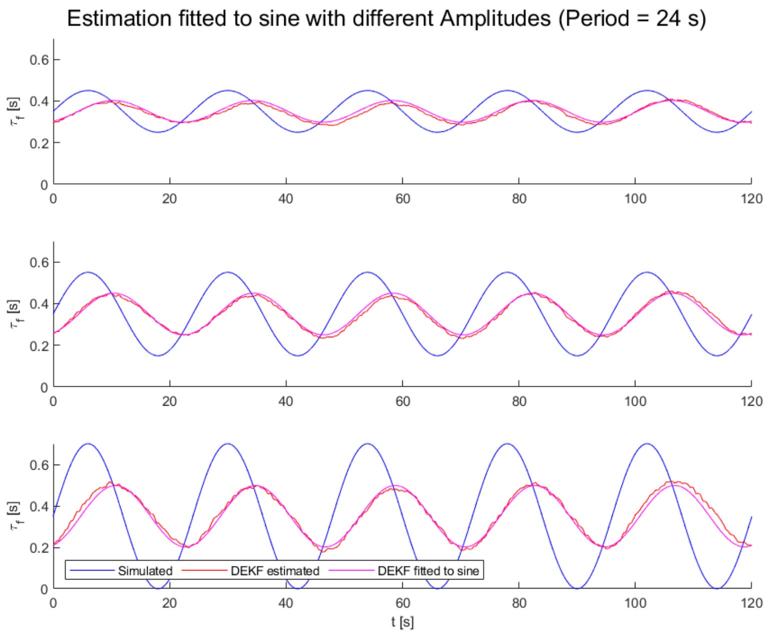

Figure 4.28: Illustration of sine curve regression on averaged DEKF estimation data for τ_f.

The figure clearly shows that for a range of amplitude-frequency combinations, the DEKF's τ_f estimation looks like a frequency response with a constant gain and phase shift. First of all, similarity between the two traces could be studied using a PCC calculation. Furthermore, a plot can be constructed, which captures the gain and delay between the originally scheduled parameter trace and the DEKF estimated trace. Performing this regression and analyses for all amplitude-frequency combination can show fundamental insights in estimation performance. It is interesting to see within what range the estimation is nearly identical to the original. Furthermore, it can be investigated at what frequency the performance starts to deteriorate, and how steep this degradation is. This knowledge, in combination with the sigmoid analysis forms the basis for further research into more sophisticated simulations and HMI experiments.

Results

For sine time variations of τ_f in SI tasks, the most important results should be showing how the DEKF algorithm performs in the studied amplitude-frequency domain. It is interesting to see whether there exists a domain where the REL95 criterion is sustained, and to find where this arbitrary definition of performance is not met anymore. The relative VAF performance as function of amplitude and frequency is shown in Figure 4.29. For this analysis, the mean value for τ_f was set at 0.35 s. Various frequencies (horizontal axis) and amplitudes (vertical axis) were combined, and the relative VAF between the DEKF re-simulation and open-loop simulation was documented. The value is presented as a fraction, combined with an associated color code.

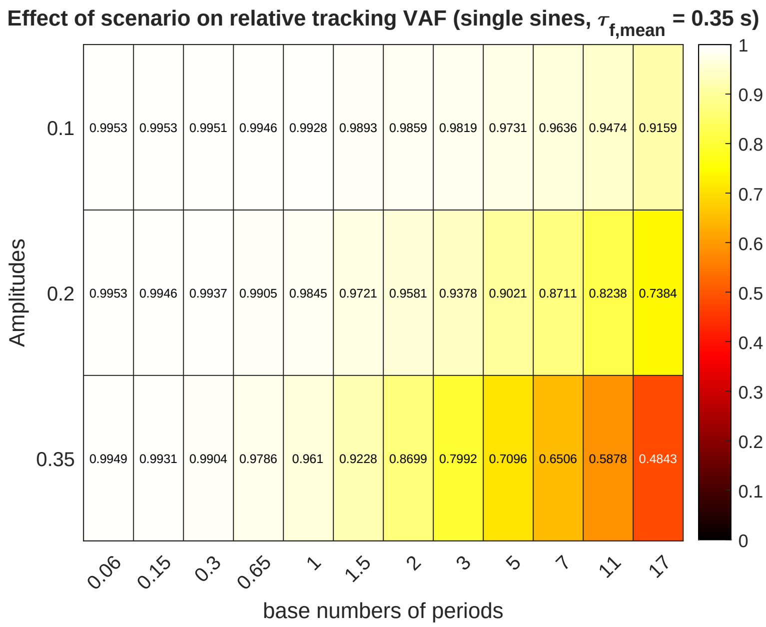

Figure 4.29: Heatmap of relative tracking VAF as function of τ_f scheduling frequency and amplitude.

As can be seen in Figure 4.29, increasing either τ_f amplitude or frequency both negatively affect DEKF VAF performance. In line with expectations, the amplitude of the variation is significantly more influential than the frequency. Evidently, this is due to the more pronounced behaviour changes due to larger differences in τ_f. Also visible in the heatmap, is that the DEKF in its current design is tailored to relatively low frequency changes. In practical applications, should the human be periodically changing its strategy with higher amplitude and frequency, the DEKF is expected to perform poorly. Investigating the VAF results in the domain, there seems to exist a pattern between the scheduled variation and the estimated variation.

As more in-depth research, it is interesting to find at which point the estimation performance starts to drop, and whether there exists an analytical relation between amplitude-frequency and performance. For this further investigation, the results are analysed on a parameter estimation level, using the sine regression on the averaged DEKF output as explained earlier in this section. While exploring the possibility for the sine regressions, it was discovered that this step is only possible in the low frequency domain. After a specific threshold frequency, the averaged DEKF estimation curve stopped showing characteristics comparable to the schedules values. Although potentially still a periodic signal, no direct linear frequency response could be retrieved. Figure 4.30 showcases the PCC, the gain and the delay between the scheduled and estimated values for τ_f. Only the frequency domain where the sine regressions holds is included. On the horizontal axis, the frequency of the scheduled look-ahead time sine variations can be found can be found on a logarithmic scale. The vertical axes represent the the PCC, gain (logarithmic), and delay between the scheduled values and estimated values. The red line corresponds to 0.1 s amplitude variations of τ_f, the green and blue line show the 0.2 s and 0.35 s results, respectively. The data points correspond to the amplitude-frequency combinations presented in Figure 4.29.

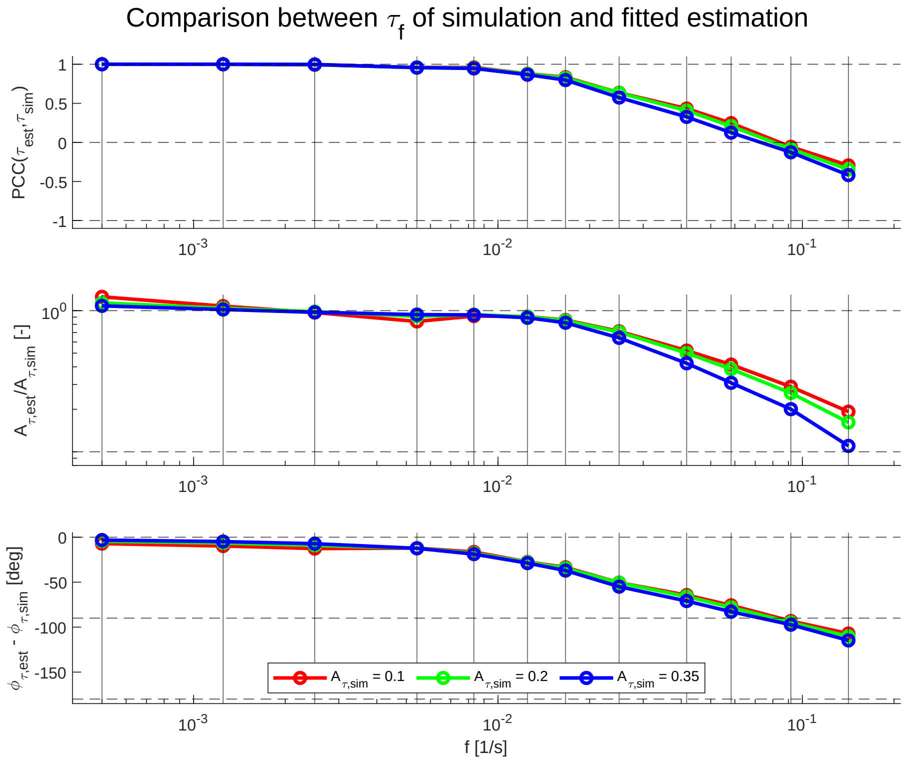

Figure 4.30: Frequency response plot between the scheduled variations and DEKF estimations of τ_f.

The results presented in Figure 4.30 support the suggestion that there exists a relation between amplitude-frequency and parameter estimation performance. These results are unique to the DEKF settings that were fixed in Section 4.4. Very important for the interpretation of the results, is that they are based on a look-ahead time parameter level comparison. The actual sensitivity to the corresponding HO behaviour is occluded in the plots. For example, the small amplitude variations in τ_f are expected to have little influence on HO tracking input (Section 4.3). Therefore, for these smaller perturbations, the DEKF might not be able to reconstruct the sine patterns in more elaborate simulations or HMI experiments. Still, the parameter level analysis provides useful insights for the final research phase.

In the PCC plot (upper sub-plot), one can see that, for the lower frequencies, the DEKF estimated τ_f trace shows a correlation of nearly unity with the scheduled trace of the simulation. In the researched domain, the PCC progression is approximately equal for the three amplitudes. At $f = 0.01$ Hz, the estimation begins to show less correlation, after which the correlation increases again, now in inversed form. Should the analyses be allowed to go beyond the highest frequency in this plot, the negative correlation is expected to increase further. Besides this correlation, it should also be investigated what the frequency response looks like.

The plot regarding the response gain (middle sub-plot) shows that the estimation's gain with respect to the original simulation stays nearly unity until $f = 0.015$ Hz. For the gain plots, the difference between the different τ_f variation amplitudes is more pronounced. The estimation's response gain drops faster for the higher amplitude variations in the simulations. Nonetheless, the progression of the gain with respect to variation frequency is similar for all amplitudes. Remember that in these plots, nothing can be immediately distinguished regarding HO behaviour. For the high amplitude case (0.35 s τ_f), at the end of the analysis domain, only 10% of amplitude is left in the response. This is 0.035 s, meaning that it consistently under- or over-estimates the value for look-ahead time with approximately 0.3 s. This would be significantly visible in HO behaviour, and thus make the τ_f estimation insufficient. For this same frequency, the gain for the low amplitude case (0.1 s τ_f), 20% of the scheduled amplitude is sustained in the response. This corresponds to the DEKF being consistently off by less than 0.1 s. In terms of behaviour, this is far less significant than the high amplitude scenarios. One can re-visit Section 4.3 for more elaborate explanation of the sensitivity of HO behaviour. The little peaks that exceed unity at the lowest frequencies are estimation errors caused by the merely small part of the scheduled period observable to the DEKF. The measurement time frame counts 120 s, whereas the investigated frequency's simulation should span 2000 s to span one complete period. The actual response gain of the DEKF estimation trace is expected to be unity, should the measurement duration be extended.

The response delay plot (lower sub-plot) portrays that the DEKF can keep up with the lower frequency variations, which is as expected. Similar to the PCC plot, the curve is nearly identical for all scheduled amplitudes. The phase delay, and thus correlated delay time, seems to increase rather slowly until $f = 0.01$ Hz. For higher frequencies, the drop in phase becomes steeper, which is sustained toward the upper fringe of the domain. The plot suggests that for higher frequencies, the estimation will run completely in counter-phase with the originally scheduled trace. However, this cannot be confirmed yet, as non-linear effect might play a role for higher frequencies.

4.6. Reflection on Results

The main goal of current DEKF studies is to find a time-varying tool that can estimate the HO strategy based on the measurable signals in the control loop. In this study, the preview strategy is parameterised following the theory of Van der El's preview model [14]. With this preliminary research, it is intended to make a first step in a validation study of the DEKF as a time-varying identification tool, and to propose final analyses. A simulation-verification environment has been created, capable of comparing all DEKF estimated states and parameters with an open-loop simulation. For the estimation of τ_f in simulated environments, performance indicators have been established, both in terms of behaviour as purely the parameter values. Based on these performance indicators, a DEKF has been set up which is expected to perform relatively well in following research. During this set-up, knowledge was gained on the effects of DEKF sensitivity and initialisation on the performance. The preliminary DEKF was implemented in analyses where only τ_f was scheduled to vary, and only τ_f was free for the algorithm to estimate. Both for sigmoid steps and for sines, the DEKF response for simulated τ_f schedules was recorded. This provided significant insights in the expected performance of the DEKF within specific research domains. The minimum time required for filter convergence, and the dynamic response to specific periodic behaviour changes create the basis for further analyses. This is important for the understanding of filter limitations, when the algorithm is used for human tracking data.

Some assumptions and scoping decisions should be carefully considered in the interpretation of the results. The most important scoping decision made is the limitation to single integrator dynamics research. The double integrator dynamics have proven to be fundamentally different [21] [19], and require a similar analysis before conclusions can be drawn. It is expected that more fundamental research is required in the parameterisation and the definition of the remnant, before the DEKF can become effective for double integrator studies. Second, the parameters were scheduled such that only τ_f varied, and the estimations were restricted to solely the estimation of τ_f. This effectively means that, if the behaviour is changed due to the parameter change (depends on sensitivity), the algorithm is expected to attribute this change correctly to τ_f. It is therefore important to introduce a more complex simulation and tuning phase, where the challenge for the DEKF is comparable to real-world applications, before the algorithm can be implemented for HMI experiment data. An additional note on the preliminary results, is that the invariant parameters of the simulations did not coincide with the fixed parameter predictions of the DEKF. The first corresponded to a time-invariant scenario with $\tau_p = 2.0$ s, and the latter to a scenario with $\tau_p \approx 0.3$ s. This anomaly was not intentional and discovered at later stage, and fortunately, the effect on the results is manageable. Lastly, some care has to be taken for the interpretation of the DEKF's sine variation response. For the presented frequencies, it was possible to regress a sine curve based on the averaged estimated values for τ_f. Due to this regressions, it was possible to find the gain and delay, compared to the originally scheduled τ_f variation. The analysis deliberately stopped at a frequency base number of 17, since this was the highest primal number that would induce an estimation trace on which a sine could be fitted. The higher the frequencies, the more the estimations move away from sine-like traces. Looking at the plots, it might seem as if the linear relation would have progressed further for higher frequencies. This is not the case, and it might even be that the actual estimation response is of non-linear nature. Still, within this low frequency domain, the DEKF seems to be quite predictable in its output. This should be used to the researcher's advantage. If the DEKF's τ_f estimation shows low frequency sine-like progression, it will most likely represent a slightly different value in the preview model look-ahead time definition. This frequency response plot might become useful for the investigation of the actual look-ahead time values when only the DEKF estimation is observable. This is a suggestion for future research. In the process toward implementing the DEKF for HO tracking task data with time-varying preview, follow-up steps to these preliminary results are proposed in Chapter 5.

5

Proposed Final Analyses

During the preliminary research phase, Vertregt's Dual Extended Kalman Filter [19] algorithm has been iterated. One of the research focus points was to create a robust estimator. Another area of focus was to examine its performance for both time-invariant and time-varying human operator behaviour. The analyses up until this point were performed with highly simplified scenarios. The most important assumptions were that the algorithm was limited to the estimation of look-ahead time τ_f, and that only the look-ahead time varied during the simulation with simple scheduled strategy variance. Constraining the filter to τ_f estimation is substantiated with the knowledge that this parameter is most variable with display preview, and shows most sensitivity to the behaviour. Discovering a time-varying identification tool that can accurately describe just this parameter during HO tracking tasks would already be adding value. However, the isolated and simplified scheduled look-ahead time variance of the preliminary analyses do not directly translate to HMI experiments. For that reason, the further investigation focuses on preparing the algorithm for simulations where all HO strategy parameters vary, and for HMI experiments that have highly stochastic human features. If the DEKF is well-understood in simulated scenarios, it can be implemented for estimation runs on HO data. Since human strategy – and thus behaviour – is fundamentally different for single integrator and double integrator preview tracking tasks, it is decided to proceed with only the first dynamics in the final research phase. In this chapter, the re-iteration of the DEKF is described in Section 5.1, using simulations where all strategy parameters are varying. Especially important for the validation of estimations in real-life applications, in Section 5.2, a description can be found of how the DEKF will be implemented for existing time-invariant HMI experiment data. Then, in Section 5.3, a new experiment is described for single integrator tracking tasks with time-varying preview. In this same section, it is discussed how the algorithm will be analysed, and what is expected of the results for time-varying HMI experiment data. To conclude, Section 5.4 discusses what the contribution of the findings will be to the larger scope of time-varying identification methods for preview tracking tasks.

5.1. Simulations for Final Analyses

Until this point, only the look-ahead time parameter τ_f has been varied in the scheduled simulations. All other parameters, such as the compensatory response parameters to internal error e^* and the lumped response time delay τ_v were assumed to be invariant. Now that the DEKF performance for these isolated τ_f variations has been studied, there are insights in its theoretical best performance. Before implementing the estimation algorithm for HMI experiment data traces, it needs to be studied whether the look-ahead time can still be accurately retrieved when the DEKF is exposed to variations of all HO strategy parameters. Including all strategy parameters' variations is not directly translated into HO output $u(t)$ realism. Consequently, this simulation phase will not guarantee adequate performance for HMI experiment data. Still, it is an important step before testing the algorithm with data from real humans performing the preview tracking task. In this section, the fundamental updates of the simulations are presented, after which suggestions are given for a re-tuning process of the DEKF.

5.1.1. Simulating the HO Parameter Variations

Including All Strategy Parameters – Expected Variation Based on Time-Invariant Experiments

After initial analyses of HO strategy parameter sensitivities to the signal output, the look-ahead time τ_f proved to be most variable and influential. During this first step in the preliminary research, the benchmark settings for the HO strategy parameters' sensitivities were based on the time-invariant experiments of Van der El [21] (Appendix A). The benchmark scenario entailed that all HO strategy parameters were assigned the mean value measured for an experiment with 2.0 s of display preview time. This amount of preview is far beyond the critical preview time value for human operators in single integrator tracking tasks. From this baseline, every parameter was varied individually over its entire physical range for the single integrator preview time experiments, with τ_p ranging from 0.0 s to 2.0 s. In real-life, all HO strategy parameters are expected to vary simultaneously due to display preview time variations. Although not yet studied in time-varying experiments, the range of time-invariant experiments of Van der El show a trend for the parameters moving from high values of preview time to pursuit tracking tasks. All these strategy parameters have effect on the HO output, most of them likely to a lesser extent than the look-ahead time. The ambition to estimate τ_f with HMI experiment data motivates to include the knowledge from Van der El [21] in the time-varying simulations. Including more parameter variations is not intended to represent actual human behaviour, since that has not been studied yet. The analyses are added to prepare the algorithm better for real-life scenarios, where all parameters will most likely vary when the display is varied.

Since there are 8 parameters that influence behaviour, varying them altogether might create a HO output signal trace that differs significantly from the preliminary research, where solely τ_f was varied. Figure 5.1 schematically shows what this more interdependent variation of parameters looks like. All parameters are assumed to change linearly with τ_f. In further simulations, it is assumed that no non-linearity exists in the parameter dynamics, and that a specific value for τ_f is always combined with specific values for the other parameters. The upper and lower limits of the parameters are determined by the values presented in Van der El's research [21] (Appendix A) for $\tau_p = 2.0$ s and $\tau_p = 0.0$ s. Figure 5.1 schematically shows the key differences in the parameter traces between the preliminary (black, dashed) and the final (blue) simulations.

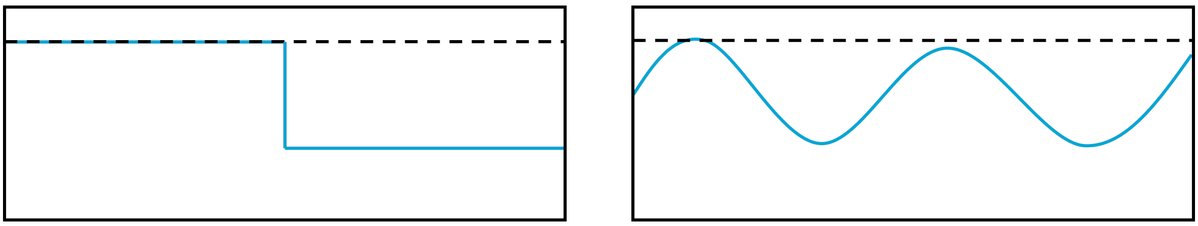

Figure 5.1: Schematic representation of new parameter variations (blue) compared to preliminary schedules (dashed).

In Figure 5.1, an arbitrary parameter time trace is presented for both a sigmoid step variation (left) and a sine variation (right). For the interpretation of the figure, it is not relevant what the corresponding step or sine variation of τ_f is. The dotted line shows the parameter value that was measured by Van der El [21] for a preview time $\tau_p = 2.0$ s. Except the look-ahead time, all parameters have been assumed to have this constant value during the simulation. The blue line represents the parameter's progression as function of τ_f variation. Again, this is not intended to reflect reality, since the actual traces are yet to be determined. The goal of adding these parameter variations stays to test whether the DEKF can still attribute fairly accurate values to τ_f, even if its direct influence is slightly occluded by other parameters.

Remarks on Final Simulations

The goal of this extended simulation research remains fairly equal to the preliminary phase. It is still investigated how well the DEKF can identify the look-ahead time parameter τ_f while it is varied over the course of the measurements. However, an important difference is that the future simulations primarily focus on complementing the time-varying HMI experiment analyses. As defined in Chapter 3, in the final EXP research phase, it is important to discover how the DEKF would behave using time-varying HMI experiment data. Time-invariant HMI data can be used to assess influence of some DEKF settings (initialisation, variance sensitivity, fixed parameters). The time-varying behaviour in the experiments is expected to be different from the time-varying simulations that have been investigated thus far. In order to match the SIM research phase to the EXP phase, more parameters are varied, while the scenarios overlap with the experiments performed in HMI-Lab. More scenario settings could be studied to find differences in the theoretically possible solutions between simulations where only τ_f varies, and where all other parameters vary as well. With the knowledge available, it is not yet possible to analyse the DEKF while it simultaneously estimates all strategy parameters. It is desired to first analyse look-ahead time estimation from start to end – preliminary simulations to time-varying HMI experiments – and validate the DEKF's performance for that application. Therefore, all parameters except τ_f are estimated at the same fixed values as in the preliminary research. These are the values found at τ_p = 2.0 s in Van der El's research on preview time sensitivity of the parameters [21] (Appendix A). Also note that the simulated variations are a based on a simple linear extrapolation between a parameter's highest an lowest mean value. The HMI experiments supporting these limits were time-invariant preview display tracking tasks. Both the general non-linearity of the parameters, and the possible additional non-linearity introduced by time-varying tasks are occluded. This should be kept in mind while creating expectations. Furthermore, remember that stochastic features like fatigue, learning and general variability are excluded from the simulations.

5.1.2. Preparing DEKF for Complex Simulations and HMI Experiments

In the preliminary research, the DEKF was set up such that it would ensure relatively stable and consistent estimations for τ_f. Motivated by the complexity of the time-varying simulation and estimation runs, finding a perfectly tuned algorithm is not the research goal. However, it is important that the filter can showcase stable responses in the highly complex cybernetics environment. Furthermore, as much knowledge as possible should be gained about expected behaviour and points for improvement. Actual human strategy parameter variation can never be known. Still, the filter should be prepared as well as possible to create sensible results for HMI experiments. The performance insights in the preliminary phase were based on isolated τ_f variations. The more complex simulations inspire for a new tuning process, this time performed slightly differently. Important experience is gained about the analysis of the algorithm in the first analyses. This is relevant for the design of the further analyses processes. Three key notions for improvement are included below, being an increased number of realisations for selected scenarios, the focus on estimation robustness and the knowledge-based optimisation of the DEKF settings.

Less Scenarios, More Realisations

As can be seen in Chapter 4 and Appendix B, a large number of different scenarios is investigated in the preliminary research phase. The main reason for this was that little knowledge existed on how dependent the performance of the DEKF was of certain features in the parameter traces. An important knowledge gap at that point was whether there existed performance asymmetry between estimation of high and low values of τ_f. Also it was not known yet whether performance asymmetry was present between upward and downward variations. Lastly, the influence of DEKF paramter estimation initialisation was yet to be determined. To not be surprised at later stage, the algorithm has been stress-tested with a wide range of scenarios. However, this does not directly mean that all these scenarios have to be re-investigated in the final phase. Clearly visible in the preliminary results, the DEKF response is mostly sensitive to the size of the variation. Other characteristics like the tau_f variation's visited values and the speed with which it varies are far less influential. Conversely, something that might deserve more attention in this phase, is the verification of the results for a specific scenario. In the preliminary research, all possible combinations of 3 remnant seeds and 3 FoFu realisations were studied for one scenario. To draw statistically more sound conclusions, this range of seeds and realisations should be increased per scenario. Note that if both the remnant seeds and FoFu realisations are increased, this will increase the number of simulations quadratically. These insights can be used to switch the focus from the scenarios to the realisations per scenario in upcoming research. While making a selection of the scenarios, they should be brought in line with the time-varying HMI experiment. This way, the analyses can complement each other in the formation of conclusions.

Focus on Stability and Accuracy, Rather Than Speed

For the preliminary tuning, emphasis was assigned to the convergence time of the algorithm. This was defined as the point where the DEKF re-simulation's VAF reached 95% of the open-loop simulation's VAF. An order of magnitude of relatively quick convergence and relatively accurate estimation was selected as best starting point. Within the domain that was determined most promising, the convergence time varied only by approximately 10%. Additionally, this was convergence time for a highly simplified scenario, and should not be directly copied for the more complex investigations. Another focus point in the preliminary analysis, was the constraint that the entire selected domain and its direct neighbours should be showing stable results. Abrupt changes in convergence time and estimation bias where labeled unstable and therefore to be avoided. For the final research, the arbitrary convergence time performance indicator is dropped, to focus more on the estimation accuracy and the sensitivity towards HO behaviour. A performance indicator that describes the re-simulation's similarity with the open-loop simulation is still used. This time, the VAF relative to open-loop VAF is collected and stored fore every point in time, rather than that the convergence time is abstracted. This can be used for both sigmoid and sine variations, and the applicability is not decreased due to the noise in the parameter variations. This performance indicator, in combination with the increased number of realisations, can facilitate finding a new stable base setting for the filter.

Knowledge-Based Tuning, Rather than Monte Carlo

The DEKF is expected to require re-tuning before performing sufficiently stable and accurate estimations. In the preliminary research, knowledge is gained on decent algorithm settings for the simplified scenarios. The investigated settings domain for the final analyses can be scoped to significantly more selective values. The new optimisation domain for q^2, q_f^2 and r^2 will be limited to $[0.1, 10]$. In the preliminary research, the studied range for each sensitivity variable was $\{0.01, 0.1, 1, 10, 100\}$. All combinations were visited, summing up to a Monte Carlo analysis of 125 unique settings, which were exposed to 6 different scenarios that all had 9 realisations. As explained in this section, resources are aimed at more validity per scenario, both in terms of remnant seeds and FoFu realisations. This will quadratically increase computational expense. The preliminary tuning process using solely Monte Carlo analyses is revised. For the re-tuning, the first step will be a Monte Carlo analysis of performance in the sensitivity variable range $\{0.1, 1, 10\}$. This sums up to 27 unique settings. After this order of magnitude study, the most promising octant is selected. Within this octant, the further optimsation will be performed with linear scale. Every octant can be subdivided in 8 sub-octants by adding 18 data points (unique settings) which are the mid-way points of all edges. Investigating these unique settings enables to find a the tuning to become significantly more granular. If required, this downscoping of the optimum domain can repeated several times, while still being less computationally expensive than the preliminary Monte Carlo tuning. Should the terminal optimum lie at the outer fringes of the initially selected domain, a new smaller optimisation has to be performed with this optimum as centre point. However, the optimal values are not expected at the fringes based on the preliminary research.

5.2. Time-Invariant HMI Experiments

In the final simulation phase, the primary scenarios involve time-varying HO strategy parameters. Logically following after such simulations, are time-varying HMI experiments where task variables vary in order to induce the variation of strategy parameters. The largest difference in the case of experimental data usage is that no certainty exists of the parameters at every given point in time. This means that the time-varying identification tool cannot yet be validated in time-varying HMI experiments, since no data on adequate performance exists. It is thus difficult to discover whether the DEKF is a suitable candidate for the combined state and parameter estimation during time-varying preview tracking tasks. In previous research, a range of experiments has been performed where the preview model parameters have been estimated and validated already [14]. These experiments were of time-invariant nature, and should thus be concluded with time-invariant values for the HO strategy parameters. Before letting the DEKF algorithm estimate time-varying values that cannot be directly validated, these previous experiments can be used to the advantage of the further research. This section elaborates on which time-invariant HMI experiment data is proposed to be used, and how the estimation results can be compared with the time-invariant analyses.

Experimental Data

Over the course of last decades, many HMI experiments have been performed with single integrator controlled element dynamics and time-invariant preview in the display. Data has to be selected that best serve the purpose of the final research: finding out how a DEKF performs in identifying look-ahead time. For this to be possible, time-invariant experiment data of the same HO with different amounts of look-ahead time should be available. An analysis referred to regularly in this report (Appendix A [21]) investigates the effects of display preview time τ_p on all preview model parameters [**empty citation**]. The look-ahead time τ_f is a strategy parameter that relates directly to the amount of preview available. As confirmed in the paper, in the data, different values for τ_f from several unique HOs are available. The experiment data entails 8 different conditions for the amount of available preview time τ_p, ranged $\{0.0, 0.25, 0.5, 0.75, 1.0, 1.33, 1.66, 2.00\}$ s. The

8 different conditions require an integer multiple participants for the data validation, since the influence of condition order can then be mitigated using a Latin square HO scheduling. Per participant, each condition was collected for 5 different realisations. After the acquisition of data, the differences between the conditions were studied using linear time-invariant (LTI) identification methods. The results of this LTI identifications correspond to the time-invariant values of strategy parameters that are presented in the plot in Appendix A. The experimental data from this research is suited to be implemented in the time-invariant research of the DEKF. Should more data traces be desired, many other experiments presented in the compilation of Van der El's preview model research [14] can be added to the time-invariant DEKF validation.

Expectations for DEKF Time-Invariant Experiment Results

In the preceding research by Vertregt [19], the same experiment data set was used to study the DEKF's performance for time-invariant scenarios. In Vertregt's work, the research focus was mostly on the design and the construction of the DEKF algorithm, and on the proof that it is a promising time-varying identification tool. In its time-invariant single integrator performance analysis, the strategy parameters K_f, τ_f and K_p were simultaneously estimated. For the individual experiment conditions, the filter was initialised with knowledge from the LTI results as presented in [21]. The suspension time values were dependent on the amount of display preview time presented in the experiment. This was to keep the anticipation close enough to the actual look-ahead time in its lower range for accurate application of Padé approximations. For the higher range values of look-ahead time, the anticipation should be far enough from its estimation to prevent negative delays. Furthermore, Vertregt initialised all parameters with the values retrieved from the LTI analyses. From the initialisation onward, all parameters, except the neuromuscular ω_{NM}, ζ_{NM} and τ_v, were free for the estimation. For most investigated preview model parameters from the single integrator experiments, the average of all DEKF estimations overlapped fairly well with the average of all LTI identifications. This suggested the DEKF to be a promising candidate as time-varying identification tool. In that research, it was unfortunately more difficult to draw conclusions with regard to the applicability of the DEKF for estimation of individual parameters, such as τ_f. This was because some parameter estimations' average was far off from the LTI analysis, and because the spread of the individual estimations sometimes spanned the entire possible domain.

In the final analyses proposed in this research, focus will be primarily on estimating τ_f, while no scenario-specific knowledge is used in the initialisation. The intention is to have a robust algorithm, that can give convergent results for every arbitrarily provided scenario. It could well be that the results are far apart from the LTI results, but it is never the intention of these analyses to make them perfectly overlap. In the DEKF definition, all parameters except look-ahead time will be fixed at values that are closest to the truth for any arbitrary scenario. For example, τ_v is expected to slightly vary from 0.2 s to 0.3 s when τ_p is altered from 2.0 s to 0.0 s. In this case, the value is fixed at 0.25 s, completely independent from the scenario. These means of the limits are based on the figures from Appendix A. Furthermore, the suspension time is fixed at 0.9 s for every scenario and the initial guess of the look-ahead time is always 0.35 s. Before analysing the estimations for the time-invariant preview tracking tasks, some expectations can already be set for the τ_f. It is not proven that there is a direct analytical relation between HO look-ahead time and display preview time. However, some theory and experimentally proven features can be used in the further analyses. First, based on the theory, the look-ahead time can never exceed the preview time, since then signal information is used that is not visible. Second, Van der El's experiments show that, over an entire scenario run, HOs normally use all available preview time until a critical value. It is interesting to study whether the DEKF estimations support these findings when solely τ_f is allowed to vary. Should the look-ahead time estimations still be highly variable for time-invariant scenarios, it could be investigated what the root cause is. The most important question to ask is whether it is caused at the operator's end or at the algorithm's end. Until now, the DEKF's capability of estimating the parameters has been highlighted. Just like in the simulation phase, it might be interesting to put the parameter estimation in perspective with the HO performance of the actual tracking task. Here it would be very interesting to know whether there is a relation between HO accuracy and specific DEKF parameter estimations.

5.3. HMI Experiments With Time-Varying Display Preview Time

With time-invariant experiment data, using the LTI identification as reference, it can be examined whether the DEKF finds the correct values for τ_f, and what the main origins for estimation errors could be. The time-varying HMI experiments cannot serve as a direct validation tool, since there exist no valid records yet of the preview model parameters as functions of these variations. Additionally, the experiments should not serve as a validation of the results created in the final simulation phase. The parameter scheduling is knowledge-based, but it is not proven to be representative of actual human behaviour. Still, the time-varying experiment analysis is a key step in the description of the DEKF performance. It shows what the DEKF makes of the time-varying behaviour induced by a time-varying display. It provides insights in to what extent the algorithm attributes the changing behaviour to τ_f. It can be showcased whether the algorithm's performance is systematic for all participants, or rather arbitrary. Furthermore, it will be illuminated how well the estimation tool can adhere to the physical limitations of τ_f, imposed by τ_p. This section describes for the time-varying HMI experiments the proposed experimental set-up, the variations in the display and the expectations for the results.

Experimental Set-Up

The time-varying HMI experiments should be complementary to preview tracking task research performed in TU Delft's HMI-Lab. The creation of and fundamental discoveries regarding the preview model have been published in work by Van der El [14]. The creation of the DEKF for preview tracking task application is documented by Vertregt [19]. These studies use the HMI-Lab simulator, which is operated in the DUECA environment that runs with C++ coding. For the experiment, a servo-controlled electro-hydraulic side-stick is used to generate the HO control inputs, only allowing for roll-axis rotation. An experimental preview display tracking task is presented on the screen, and the only task variable that can change is the display preview time. It collects the measurements with a frequency of 100 Hz. For complete description of hardware, the thesis on human preview processing by Van der El [14] can be consulted.

Time Variations of Display in HMI Experiment

In the simulation phase, large numbers of scenarios can be generated due to the computational power at hand. Additionally, many scenarios can be compared since the designer is always in control of the parameter scheduling. Differences between the simulations can be subtle, since the HO is programmed to behave exactly the same for different realisations in terms of strategy. Conversely, for HMI experiments, resources are limited, using unique hardware for extensive amounts of time. Also, while conducting these experiments, humans show vastly different behaviour per individual, and the individuals show intrinsic variability. Optimal use of resources is essential, and confounding factors are to be mitigated. For this to be true, the time-varying scenarios have to be selected serving a specific purpose. Furthermore, it is important that every experiment is correctly presented to a human participant, in order to make the results as reliable as possible.

Some findings from the preliminary results can be used in the scenario design for the time-varying HMI experiments. First, in the sigmoid step analyses, it was found that step size is the key of variation, and that other factors such as initial and terminal points are less important. This insight can be supported with two experiments, where the first makes a small step in display preview time, and the other a large step. The goal is to examine what the DEKF registers as a result of display-induced behaviour changes. It should be researched whether the estimated look-ahead time varies and whether the DEKF finds a new equilibrium state-parameter combination. Second, combining theoretical τ_f sensitivity results with sine variation analyses, the preliminary research shows that for large amplitude τ_f variations, the DEKF is not able to adequately recreate the original tracking behaviour. To examine these findings, again two experiments are required. Both experiments implement a large amplitude sine variation of display preview, one with a relatively low frequency, the other with a high frequency. Here, the goal is to find out whether this periodic variation of τ_p will result in a periodic estimation of τ_f. Should he response be periodic, it is interesting whether a sine signal could be regressed and how this relates to the originally scheduled display variation. The higher frequency experiment serves specifically to find whether the parameter estimation shows gain and delay compared to the lower frequency. Also, it might show that the time-varying identification algorithm indeed is not capable of estimation values that provide a re-simulation comparable to the original human behaviour. Last, an important experiment to perform is implementing a time-invariant display preview time, fixed at the highest τ_p values found in the sigmoid and sine experiments. In the preliminary phase, the higher τ_p values are expected to be in the range of 0.75 s, and the lower values in the range of 0.25 s. The lower values are deliberately not reduced to the vicinity of 0.0 s, because in that range, pursuit tracking is induced. The pursuit tracking strategy proves to be a difficult one to estimate parameters for, since it shows significant similarity with compensatory tracking. In the compensatory case, many parameters regarding preview do not exist. The large sigmoid step would be defined from 0.75 s to 0.25 s τ_p, and the large amplitude is described by 0.25 s around a mean value of 0.5 s τ_p. The low-frequency sine variation would span exactly one run of 120 s. In the high-frequency case, the sine period is in the range of 10 s, which proved to be the highest frequency to which the DEKF could respond with a sine-like τ_f estimation. The time-invariant scenario would show the operator a constant τ_p of 0.75 s. The small sigmoid step could be a decrease in display preview time in the range of 0.25 s. The exact values for the time-invariant, sigmoid step and sine scenarios are still to be tested, and could be altered at later stage. In Table 5.1, a summary of the five proposed HMI experiments is presented.

Table 5.1: Five proposed HMI experiments with time-varying display preview time

Scenario	Display Preview Time τ_p
SCN1: Time-Invariant	$\tau_p = 0.75$ s
SCN2: Small Sigmoid Step	$\tau_{p,1} = 0.75$ s, $\tau_{p,2} = 0.5$ s
SCN3: Large Sigmoid Step	$\tau_{p,1} = 0.75$ s, $\tau_{p,2} = 0.25$ s
SCN4: Low Frequency Sine	$\tau_{p,mean} = 0.5$ s, $A_{\tau_p} = 0.25$ s, $T_{\tau_p} = 120$ s
SCN5: High Frequency Sine	$\tau_{p,mean} = 0.5$ s, $A_{\tau_p} = 0.25$ s, $T_{\tau_p} = 120/17$ s

Data from the five scenarios mentioned in Table 5.1 should be carefully collected with HMI experiments. Per participant, from briefing to debriefing, such HMI experiment sessions can easily take hours to complete. When humans participate in the experiment, they are required to perform all scenarios several times to increase the confidence of their response to certain input signals. This many complete runs can induce some secondary human behaviour that might influence the performance significantly. For example, human participants are expected to be sharper and more motivated in the beginning of the experiment compared to the final scenarios. Conversely, human adaptability and learning might provide that the operator becomes more skilled at the task over the course of the experiment. Evidently, the order in which the scenarios are recorded needs to be designed in such a way that these secondary behaviour changes are not systematically present in the data. Five scenarios requires at least five participants to mitigate this confounding factor in the research. In Table 5.2 and Table 5.3, two examples are shown in what order the scenarios can be presented to the individual participants. Such a square matrix describing a unique order of scenarios for every participant is called a *Latin Square*. There are often many options for a 5x5 Latin Square. More participants in the experiment increase the confidence in results. Note that if the number of participants is increased, it should always be at least by an integer multiple of the number of scenarios. A trade-off between increased confidence and experiment time motivaates to invite 10 participants for the data acquisition.

Table 5.2: Example of Latin Square

Participant	Scenario Order				
1	1	2	3	4	5
2	2	3	5	1	4
3	3	5	4	2	1
4	4	1	2	5	3
5	5	4	1	3	2

Table 5.3: Similar Latin Square, reversed example

Participant	Scenario Order				
1	5	4	3	2	1
2	4	3	1	5	2
3	3	1	2	4	5
4	2	5	4	1	3
5	1	2	5	3	4

For a single participant, the complete experiment is expected to progress as follows. A briefing document is sent in advance, and handed out at the beginning of the session. An oral briefing is given to refresh the task objectives and what the participant can expect in terms of tracking tasks and breaks. Every scenario is introduced once to familiarise with the set-up. Then, every scenario should be performed as many times as required to obtain around 5 usable data traces for the DEKF. It is predicted that this will take around 7 runs per scenario on average. For every usable trace, a different realisation of the forcing function should be seeded, to ensure that the signal appears pseudo-random (see Chapter 2. This all accumulates to a total number of 40 tracking runs of 128 seconds per participant. For this, around 90 to 100 minutes of active measuring time can be expected, meaning that the entire experiment is expected to take slightly more than 2 hours. After the data collection for the 10 participants, it is possible to use the DEKF algorithm for time-varying parameter estimation in preview tracking tasks with time-varying display preview time.

Expectations for DEKF Time-Varying Experiment Results

The most difficult aspect in the estimation analysis for time-varying experiment data, is that no validation values exist for the look-ahead time parameter τ_f. Thus, for every estimation point, it should be noted that the value of τ_f is the best model representation of the measurable signals that the constrained and limited DEKF can give. Therefore, should the DEKF's τ_f estimations show variation, it cannot be directly concluded that the look-ahead time indeed varies. As said before, no direct analytical relation is proven between time-varying values of τ_p and τ_f. Nonetheless, it is theoretically set that τ_f can never surpass τ_p, and based on experiments, humans tend to use as much preview as possible until a critical point. This means that, in case of display preview time variations, at some point the look-ahead time will vary along in response. What this response exactly looks like is yet to be determined. It is interesting to investigate how changes in the display relate to changes in the DEKF's τ_f estimations.

For the large sigmoid step variations in τ_p (SCN3), it is expected that the τ_f values at the initial and terminal display settings will be estimated fairly accurately. The preliminary research showed that large steps induce sufficiently large behaviour variations for the DEKF to attribute this to the look-ahead time parameter. The theoretical convergence time of the DEKF for large steps in look-ahead time is in the range of 20 seconds. In practice, this time is expected to be even higher. This means that higher frequency strategy variations due to the sudden changes in the display (duration of 1 s) cannot be recorded by the algorithm. Should the human adaptation be significantly slower than the convergence performance of the algorithm, this is expected to be visible in the τ_f estimations. Since many parameters are constrained in the estimation, the DEKF is expected to adhere fairly well to the physical limits of τ_f, imposed by τ_p. The smaller sigmoid step variations (SCN2) are expected to be harder to detect for the algorithm. This is due to the expected intrinsic variability of human strategy, regardless of display variations. When all data traces of the 10 participants are estimated, and the result is averaged, it is expected that τ_f will show a clear small drop as response to the changing display. However, on individual runs, it might well be that the variability of strategy around $\tau_f = 0.7$ s is the size of the variation in τ_p. Furthermore, even if the operator's strategy is relatively constant, due to the sensitivity to the behaviour, the DEKF is expected to attribute values to τ_f with a variability of +/- 0.1 s. This makes it difficult for the estimation algorithm to keep track of smaller step sizes. In terms of behaviour, this does not necessarily mean that the filter is flawed, but it could also mean that small steps are not that important to be directly recorded.

The low frequency sine variations of preview time (SCN4) vary between $\tau_p = 0.7$ s and $\tau_p = 0.2$ s and have a period of 120 s (i.e. base number 1). In the preliminary analyses, when this frequency was implemented for the τ_f variations, it proved to be easily tracked by the DEKF for all sine amplitudes. On behaviour level, the relative VAF of the DEKF re-simulation stayed on average well above 95% of the open-loop simulation VAF. On parameter estimation level, the response gain was nearly unity and only a slight phase delay existed between the scheduling and the estimation. Should τ_f be relatively directly related to τ_p, the τ_f estimation traces – averaged over the 10 participants – is expected to be showing nearly similar variation as the display. Here, it is interesting to monitor whether unexpected changes in strategy are attributed by the algorithm. Such changes can find their origin either in the human adaptation or in the DEKF performance. For the higher frequency τ_p sine variations (SCN5), the algorithm is expected to perform poorly. Due to the unknown human adaptation, the intrinsic variability and the filter sensitivity, the filter might not even show a periodic estimation response. The trace of the averaged τ_f estimation is expected to be close to the mean value of τ_p. The variance of all individual traces is most likely to span the entire τ_p domain, and no specific relation is expected to be found between the preview time scheduling and the look-ahead time estimation. This would be a proof that the DEKF is not suited yet for higher frequency variations.

5.4. Intended Research Contribution

Combining Van der El's preview model theory [14] with Popovici's fundamental DEKF implementation for compensatory tracking [17], Vertregt has established a time-varying identification algorithm for preview tracking tasks [19]. In the preliminary research phase, a sensitivity analysis was performed for all preview model parameters on the HO behaviour. This proved that τ_f is undoubtedly most influential in terms of behaviour, and simultaneously most variable as function of τ_p. After that, it was studied how this algorithm can be tested in a simulation environment where all states and parameters are estimated simultaneously. As next step, understanding has been created on the initialisation and settings of the DEKF in single integrator dynamics tasks. This created a robust algorithm, capable of estimating τ_f in all expected time-invariant scenarios in shortest possible time frame. The last preliminary analyses evaluated the performance of this stable DEKF in isolated τ_f variations, for both sigmoid steps and (multi-)sines. For the isolated τ_f variation simulations, the DEKF proved to show consistent responses.

In real-life, it is not possible to verify the actual definition of human strategy. However, the preview model parameters serve as a tool to describe certain features of behaviour. The final research phase intends to investigate whether the DEKF could still identify changes in τ_f, based on behaviour of actual human operators. For these operators, it can be expected that more strategy features than look-ahead time are constantly varying, which all influence the tracking behaviour. Without exact knowledge of the parameter traces, a more complex simulation description should generate behaviour, for which all parameters have showed variation as a response to varying display preview time. These parameter variation schedules are based on the time-invariant display preview study by Van der El [21]. Constraining all other parameters in the estimation to a fixed value, it is desirable that the DEKF still finds relatively accurate values for τ_f. Also, re-simulations of HO behaviour with the DEKF's estimated parameters should coincide fairly well with the open-loop simulations. After re-tuning in more complex simulated environments, the DEKF look-ahead time estimation can be validated using time-invariant single integrator dynamics HMI experiments. Should the mean of individual DEKF estimations be close to or closely related to the linear time-invariant identification, the algorithm proves to be a time-varying alternative to the time-invariant identification techniques. Evidently, the main advantage of a time-varying identification tool, is that it should be capable of capturing time-varying values of HO look-ahead time. To collect tracking data where humans are forced to vary their look-ahead strategy, HMI experiments with time-varying display preview time τ_p can be conducted. Using a time-invariant τ_p scenario as baseline experiment, this can be compared with the time-varying experiments. It would be adding significant value to cybernetics research, if the DEKF can trace back a systematic response – expressed in τ_f – to specific changes in τ_p. Besides the focus on controlled element single integrator dynamics, no scenario-specific knowledge is seeded in the filter. If the DEKF is capable of consistent and fairly accurate estimations of τ_f, this would be the first proof-of-concept for a future DEKF algorithm that can run online with the tracking task, regardless of tuning.

Besides the induced behaviour changes due to the display, it should be studied in future research what variation remains for the DEKF estimation in individual scenarios, and what the root-cause of these variations is. It could both be caused by strategy variations of humans, and by definitions of the preview model parameters and the DEKF algorithm. Should the upcoming single integrator dynamics analyses indeed prove that the DEKF can make consistent and explainable estimations of τ_f, a next step would be to start a similar research for double integrator dynamics. Clearly visible in Appendix A, significantly more parameter variation is to be expected based on time-invariant analyses. Especially the parameters describing preview processing (τ_f,K_f,$\omega_{b,f}$) are more sensitive to variations in τ_p. These human adaptations to display preview time, combined with the low-pass filtered white noise signal of the remnant, create a less observable control system. For future double integrator research, fundamental algorithm changes with regard to remnant modeling could be studied, as well as a sensitivity analysis per parameter under investigation. Another next step, both for single integrator and double integrator dynamics, is research into the necessity and possibility of constraining less HO strategy parameters. An ideal algorithm would be designed comparable to Popovici's DEKF [17], capable of relatively accurately estimating all parameters of interest. This precision is not expected to be found with the current DEKF definition, due to the complex environment definition, and the interchangeable features of the parameters. If consistent parameter estimations are found for different experiment participants, this would already be a large contribution to cybernetics research. If a certain response can be related to specific behavioural scenarios, it means that the scenario is identifiable. Another research could be focused on making the parameter-specific features in the behaviour more pronounced. From a model perspective, the parameters should be uniquely distinguishable. However, in the current set-up, the look-ahead time τ_f (estimated as apparent delay τ_f^*) has comparable effect on the behaviour as the reaction time delay τ_v. To better find parameter characteristics in the behaviour, the individual signals in the tracking task could be updated. It can be investigated what values should be chosen for e.g. the FoFus, the tracking input gains and the display size, to create clearly distinguishable parameters. With all these future studies and applications in mind, the proposed final analyses of this DEKF will bring cybernetics research one step closer to finding a competitive time-varying identification tool in preview tracking tasks.

Bibliography

[1] S. Barendswaard. "Modelling Individual Driver Trajectories to Personalise Haptic Shared Steering Control in Curves". In: (2021). DOI: 10.4233/UUID:7292E35D-D45A-4AD1-9663-AE2B5C5A9F16. URL: https://repository.tudelft.nl/islandora/object/uuid%7B%5C%%7D3A7292e35d-d45a-4ad1-9663-ae2b5c5a9f16.

[2] F. Flemisch et al. "Towards a dynamic balance between humans and automation: Authority, ability, responsibility and control in shared and cooperative control situations". In: *Cognition, Technology and Work* 14.1 (Mar. 2012), pp. 3–18. ISSN: 14355558. DOI: https://doi.org/10.1007/s10111-011-0191-6. URL: https://link.springer.com/article/10.1007/s10111-011-0191-6.

[3] J. Rasmussen. "Skills, Rules, and Knowledge; Signals, Signs, and Symbols, and Other Distinctions in Human Performance Models". In: *IEEE Transactions on Systems, Man and Cybernetics* SMC-13.3 (1983), pp. 257–266. ISSN: 21682909. DOI: 10.1109/TSMC.1983.6313160.

[4] B. Strauch. "Ironies of Automation: Still Unresolved after All These Years". In: *IEEE Transactions on Human-Machine Systems* 48.5 (Oct. 2018), pp. 419–433. ISSN: 21682291. DOI: 10.1109/THMS.2017.2732506.

[5] R. Parasuraman, T. B. Sheridan, and C. D. Wickens. "A model for types and levels of human interaction with automation". In: *IEEE Transactions on Systems, Man, and Cybernetics Part A:Systems and Humans.* 30.3 (2000), pp. 286–297. ISSN: 10834427. DOI: 10.1109/3468.844354.

[6] L. Li et al. "Cognitive cars: A new frontier for ADAS research". In: *IEEE Transactions on Intelligent Transportation Systems* 13.1 (Mar. 2012), pp. 395–407. ISSN: 15249050. DOI: 10.1109/TITS.2011.2159493.

[7] D. A. Abbink, M. Mulder, and E. R. Boer. "Haptic shared control: Smoothly shifting control authority?" In: *Cognition, Technology and Work* 14.1 (Mar. 2012), pp. 19–28. ISSN: 14355558. DOI: 10.1007/S10111-011-0192-5/FIGURES/1. URL: https://link.springer.com/article/10.1007/s10111-011-0192-5.

[8] Z. Xu et al. "What drives people to accept automated vehicles? Findings from a field experiment". In: *Transportation Research Part C: Emerging Technologies* 95 (Oct. 2018), pp. 320–334. ISSN: 0968-090X. DOI: 10.1016/J.TRC.2018.07.024.

[9] D. A. Mindell. *Our robots, ourselves : robotics and the myths of autonomy.* 2015, p. 260. ISBN: 9780525426974.

[10] J.-F. B. A. Shariff and I. Rahwa. "Psychological roadblocks to the adoption ofself-driving vehicles. Nature, Human Behaviour". In: *Nature* 10 (2017), pp. 694–696. ISSN: 0968-090X. DOI: 10.1016/J.TRC.2018.07.024.

[11] W. Scholtens et al. "A New Haptic Shared Controller Reducing Steering Conflicts". In: *Proceedings - 2018 IEEE International Conference on Systems, Man, and Cybernetics, SMC 2018.* Institute of Electrical and Electronics Engineers Inc., Jan. 2019, pp. 2705–2710. ISBN: 9781538666500. DOI: 10.1109/SMC.2018.00462.

[12] M. Mulder et al. "Manual Control Cybernetics: State-of-the-Art and Current Trends". In: *IEEE Transactions on Human-Machine Systems* 48.5 (2018), pp. 468–485. ISSN: 21682291. DOI: 10.1109/THMS.2017.2761342.

[13] L. R. Young. "On Adaptive Manual Control". In: *Ergonomics* 12.4 (July 1969), pp. 635–674. ISSN: 13665847. DOI: 10.1080/00140136908931083.

[14] K. van der El et al. "Effects of Preview on Human Control Behavior in Tracking Tasks With Various Controlled Elements". In: *IEEE Transactions on Cybernetics* 48.4 (Apr. 2018), pp. 1242–1252. ISSN: 21682267. DOI: 10.1109/TCYB.2017.2686335. URL: https://doi.org/10.1109/TCYB.2017.2686335.

[15] K. Van Der El et al. "An empirical human controller model for preview tracking tasks". In: *IEEE Transactions on Cybernetics* 46.11 (2016), pp. 2609–2621. ISSN: 21682275. DOI: 10.1109/TCYB.2015.2482984.

[16] W. Plaetinck et al. "Online Identification of Pilot Adaptation to Sudden Degradations in Vehicle Stability". In: *IFAC-PapersOnLine* 51.34 (Jan. 2019), pp. 347–352. ISSN: 2405-8963. DOI: 10.1016/J.IFACOL.2019.01.020.

[17] A. Popovici, P. Zaal, and D. M. Pool. "Dual Extended Kalman Filter for the Identification of Time-Varying Human Manual Control Behavior". In: *Proceedings of the AIAA Modeling and Simulation Tech- nologies Conference, Denver (CO)* (2017). DOI: 10.2514/6.2017-3666.

[18] D. McRuer and H. Jex. "A Review of Quasi-Linear Pilot Models". In: *IEEE Transactions on Human Factors in Electronics* HFE-8.3 (1967), pp. 231–249.

[19] C. Vertregt. "Estimation of Time-Varying Human Manual Control Behaviour in Preview Tracking Tasks using a Dual Extended Kalman Filter". MSc Thesis Delft University of Technology. 2020.

[20] E. Rezunenko et al. "Relating Human Gaze and Manual Control Behavior in Preview Tracking Tasks with Spatial Occlusion". In: *Proceedings - 2018 IEEE International Conference on Systems, Man, and Cybernetics, SMC 2018*. Institute of Electrical and Electronics Engineers Inc., July 2018, pp. 3440–3445. ISBN: 9781538666500. DOI: 10.1109/SMC.2018.00583. URL: https://doi.org/10.1109/SMC.2018.00583.

[21] K. Van Der El et al. "Effects of preview time in manual tracking tasks". In: *IEEE Transactions on Human-Machine Systems* 48.5 (Oct. 2018), pp. 486–495. ISSN: 21682291. DOI: 10.1109/THMS.2018.2834871. URL: https://doi.org/10.1109/THMS.2018.2834871.

[22] H. A. Van Grootheest et al. "Identification of time-varying manual-control adaptations with recursive ARX models". In: *Proceedings of the AIAA Modeling and Simulation Technologies Conference, Kissimee*. AIAA-2018- 0118. American Institute of Aeronautics and Astronautics Inc, AIAA, 2018. ISBN: 9781624105289. DOI: 10.2514/6.2018-0118. URL: https://doi.org/10.2514/6.2018-0118.

[23] J. Rojer et al. "UKF-based Identification of Time-Varying Manual Control Behaviour". In: *Proceedings of the 14th IFAC Symposium on Analysis Design and Evaluation ofHuman Machine Systems Tallinn, Estonia*. Vol. 52. 19. Elsevier B.V., Jan. 2019, pp. 109–114. DOI: 10.1016/j.ifacol.2019.12.120.

[24] K. van der El. *How Humans Use Preview Information in Manual Control*. 2018. ISBN: 978-94-6186-967-8. DOI: 10.4233/uuid:cda9dd80-0a51-436e-9c70-ea174505692a. URL: http://repository.tudelft.nl/.

[25] K. Van Der El, D. M. Pool, and M. Mulder. "Analysis of Human Remnant in Pursuit and Preview Tracking Tasks". In: *Proceedings of the 14th IFAC Symposium on Analysis Design and Evaluation ofHuman Machine Systems Tallinn, Estonia*. Vol. 52. 19. Elsevier B.V., Jan. 2019, pp. 145–150. DOI: 10.1016/j.ifacol.2019.12.165.

[26] K. Van Der El et al. "Effects of Target Trajectory Bandwidth on Manual Control Behavior in Pursuit and Preview Tracking". In: *IEEE Transactions on Human-Machine Systems* 50.1 (Feb. 2020), pp. 68–78. ISSN: 21682305. DOI: 10.1109/THMS.2019.2947577.

[27] M. Mulder. "Cybernetics of tunnel-in-the-sky displays". In: (1999), p. 418. DOI: 10.4233/uuid:627f30e0-0a70-43f5-b4c8-043c36dda641. URL: https://www.researchgate.net/publication/35016939%7B%5C_%7DCybernetics%7B%5C_%7Dof%7B%5C_%7DTunnel-in-the-Sky%7B%5C_%7DDisplays.

[28] M. Land and J. Horwood. "How Speed Affects the Way Visual Information Is Used in Steering". In: *Vision in Vehicles - VI* (1998), pp. 43–50. URL: https://trid.trb.org/view/492266.

[29] R. W. Allen and J. F. O'hanlon. "Effects of Roadway Delineation and Visibility Conditions on Driver Steering Performance". In: *Transportation Research Record* 739 (1979), pp. 5–8. URL: https://www.semanticscholar.org/paper/EFFECTS-OF-ROADWAY-DELINEATION-AND-VISIBILITY-ON-Allen-O%7B%5C%%7D27hanlon/eb0484614672f1b84c2db3a5f70e46e075cff8b4.

[30] P. M. Zaal. "Manual control adaptation to changing vehicle dynamics in roll-pitch control tasks". In: *Journal of Guidance, Control, and Dynamics* 39.5 (May 2016), pp. 1046–1058. ISSN: 15333884. DOI: 10.2514/1.G001592. URL: https://arc.aiaa.org/doi/10.2514/1.G001592.

[31] M. F. Land and D. N. Lee. "Where we look when we steer". In: *Nature 1994 369:6483* 369.6483 (1994), pp. 742–744. ISSN: 1476-4687. DOI: 10.1038/369742a0. URL: https://www.nature.com/articles/369742a0.

[32] H. J. Damveld et al. “Design of Forcing Functions for the Identification of Human Control Behavior”. In: *https://doi.org/10.2514/1.47730* 33.4 (May 2012), pp. 1064–1081. ISSN: 15333884. DOI: 10.2514/1.47730. URL: https://arc.aiaa.org/doi/abs/10.2514/1.47730.

[33] T. Yamashita. “Effects of sine wave combinations on the development of precognitive mode in pursuit tracking”. In: *The Quarterly journal of experimental psychology. A, Human experimental psychology* 42.4 (Nov. 1990), pp. 791–810. ISSN: 0272-4987. DOI: 10.1080/14640749008401250. URL: https://pubmed.ncbi.nlm.nih.gov/2287762/.

[34] D. McRuer. “Human dynamics in man-machine systems”. In: *Automatica* 16.3 (May 1980), pp. 237–253. ISSN: 0005-1098. DOI: 10.1016/0005-1098(80)90034-5.

[35] R. A. Hess and A. Modjtahedzadeh. “Preview control model of driver steering behavior”. In: *Proceedings of the IEEE International Conference on Systems, Man and Cybernetics* 2 (1989), pp. 504–509. ISSN: 08843627. DOI: 10.1109/ICSMC.1989.71347.

[36] G. J. Silva, A. Datta, and S. P. Bhattacharyya. “Controller design via pade approximation can lead to instability”. In: *Proceedings ofthe 40th IEEE Conference on Decision and Control (Cat. No. 01CH37228)*. Vol. 5. 2001, pp. 4733–4737. DOI: 10.1109/CDC.2001.980953.

[37] E. R. Boer and R. V. Kenyon. “Estimation of Time-Varying Delay Time in Nonstationary Linear Systems: An Approach to Monitor Human Operator Adaptation in Manual Tracking Tasks”. In: *Systems and Humans* 28.1 (1998), pp. 89–99.

[38] R. F. Duarte et al. “Experimental Scheduling Functions for Global LPV Human Controller Modeling”. In: 50.1 (July 2017), pp. 15853–15858. ISSN: 24058963. DOI: 10.1016/J.IFACOL.2017.08.2329. URL: www.sciencedirect.com.

[39] J. Steen et al. “A review of visual driver models for system identification purposes”. In: *Conference Proceedings - IEEE International Conference on Systems, Man and Cybernetics*. 2011, pp. 2093–2100. ISBN: 9781457706523. DOI: 10.1109/ICSMC.2011.6083981.

[40] C. You, J. Lu, and P. Tsiotras. “Nonlinear Driver Parameter Estimation and Driver Steering Behavior Analysis for ADAS Using Field Test Data”. In: *IEEE Transactions on Human-Machine Systems* 47.5 (Oct. 2017), pp. 686–699. ISSN: 21682291. DOI: 10.1109/THMS.2017.2727547.

[41] X. Li and R. Kennel. “General Formulation of Kalman-Filter-Based Online Parameter Identification Methods for VSI-Fed PMSM”. In: *IEEE Transactions on Industrial Electronics* 68.4 (Apr. 2021), pp. 2856–2864. ISSN: 15579948. DOI: 10.1109/TIE.2020.2977568.

[42] P. M. Zaal and B. T. Sweet. “Estimation of time-varying pilot model parameters”. In: *AIAA Modeling and Simulation Technologies Conference 2011* (2011). DOI: 10.2514/6.2011-6474.

[43] T. A. Wenzel et al. “Dual extended Kalman filter for vehicle state and parameter estimation”. In: *Vehicle System Dynamics* 44.2 (Feb. 2006), pp. 153–171. ISSN: 0042-3114. DOI: 10.1080/00423110500385949. URL: http://www.tandfonline.com/doi/abs/10.1080/00423110500385949.

[44] G. Walder and C. Campestrini. “Adaptive State and Parameter Estimation of Lithium-Ion Batteries Based on a Dual Linear Kalman Filter”. In: *The Second International Conference on Technological Advances in Electrical, Electronics and Computer Engineering (TAEECE2014)*. 2014, pp. 16–24. ISBN: 9780989130547.

[45] R. E. Kalman. “A New Approach to Linear Filtering and Prediction Problems”. In: *Journal of Basic Engineering* 82 (1 Mar. 1960), pp. 35–45. ISSN: 0021-9223. DOI: 10.1115/1.3662552.

[46] J. R. Schiess and V. R. Roland. *Kalman filter estimation of human pilot-model parameters*. Washington, D.C. : National Aeronautics and Space Administration ; 1975. URL: https://books.google.nl/books?id=wVF3vwEACAAJ.

[47] D. P. C.C. de Visser. *AE4320 System Identification of Aerospace Vehicles: Lecture 3, Kalman Filtering*. TU Delft. Feb. 2020.

[48] D. J. Simon. “Kalman Filtering With State Constraints: A Survey of Linear and Nonlinear Algorithms”. In: *IET Control Theory & Applications* 4.8 (2010), pp. 1303–1318. URL: https://engagedscholarship.csuohio.edu/enece%7B%5C_%7Dfacpub.

[49] W. H. Levison, S. Baron, and D. L. Kleinman. “A Model for Human Controller Remnant”. In: *IEEE Transactions on Man-Machine Systems* 10.4 (1969), pp. 101–108. ISSN: 21682860. DOI: 10.1109/TMMS.1969.299906.

[50] J. Lataire and R. Pintelon. “Frequency Domain Identification of Linear, Deterministically Time-Varying Systems”. In: *IFAC Proceedings Volumes* 41.2 (2008), pp. 11474–11479. ISSN: 14746670. DOI: 10.3182/20080706-5-KR-1001.01944.

A
Time-Invariant HO Parameter Adaptation to Different Preview Times

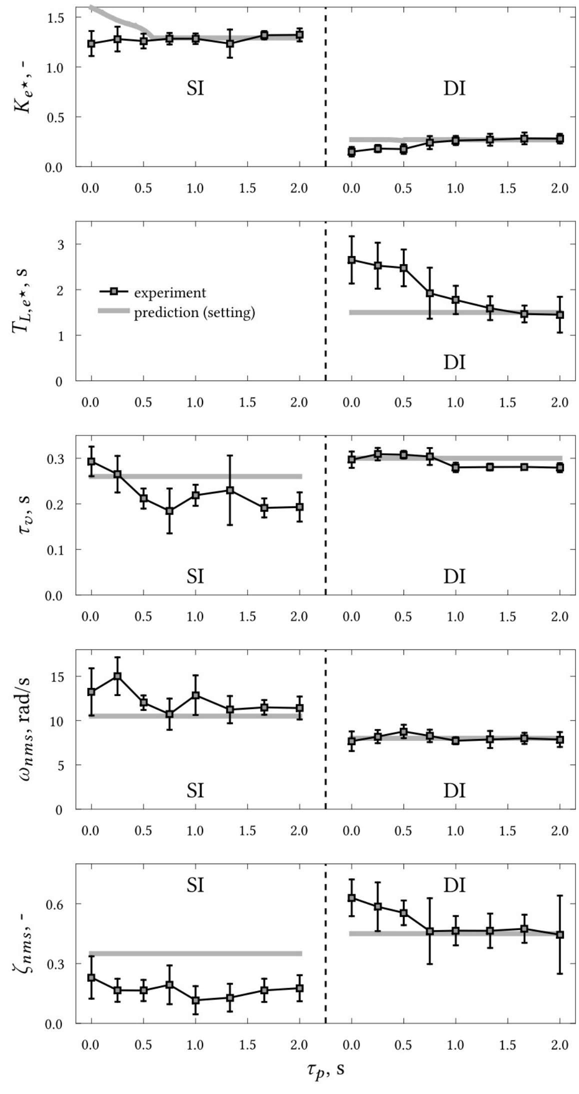

Figure A.1: Effect of preview time on HO equalization and physical limitation parameters [21].

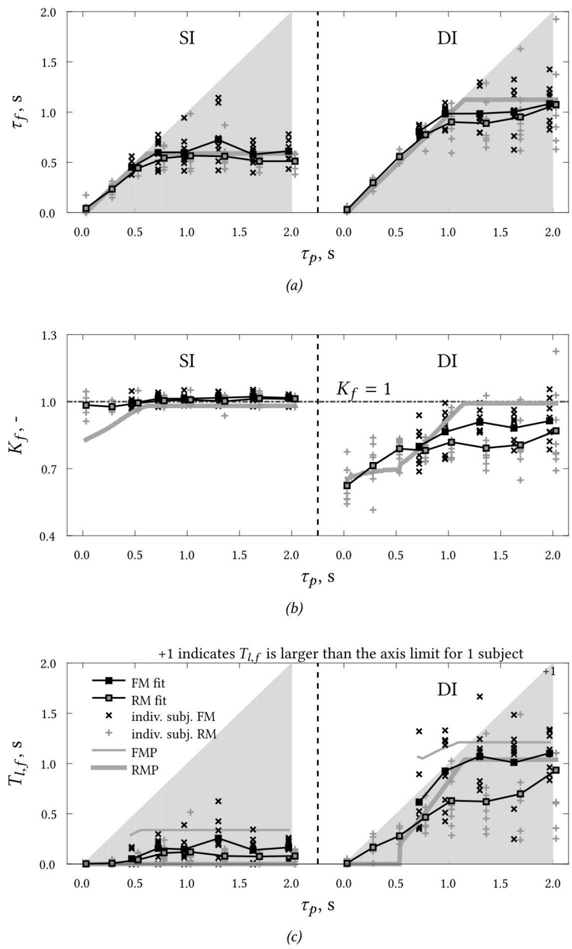

Figure A.2: Effect of preview time on far-viewpoint target processing parameters [21].

B
Results Multi-Sine Analyses

Besides the sine variations described in the preliminary Results section, some preliminary analyses have been performed on multi-sine variations of τ_f and the accompanying DEKF performance. Comparable figures have been collected for individual runs, and a comparable VAF analysis has been performed to find the tracking performance as a function of sine amplitude and frequency. In this appendix, some examples of the individual runs are presented, as well as the outcome of the VAF study. It is not further placed in the context of the preliminary results, other than that some expectations can be created with respect to estimation performance.

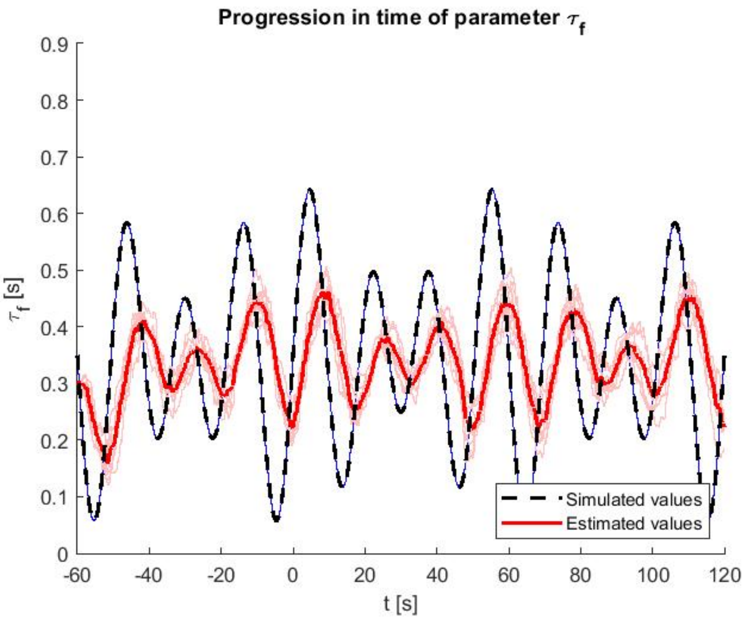

Figure B.1: Example of τ_f estimation for multi-sine variation..

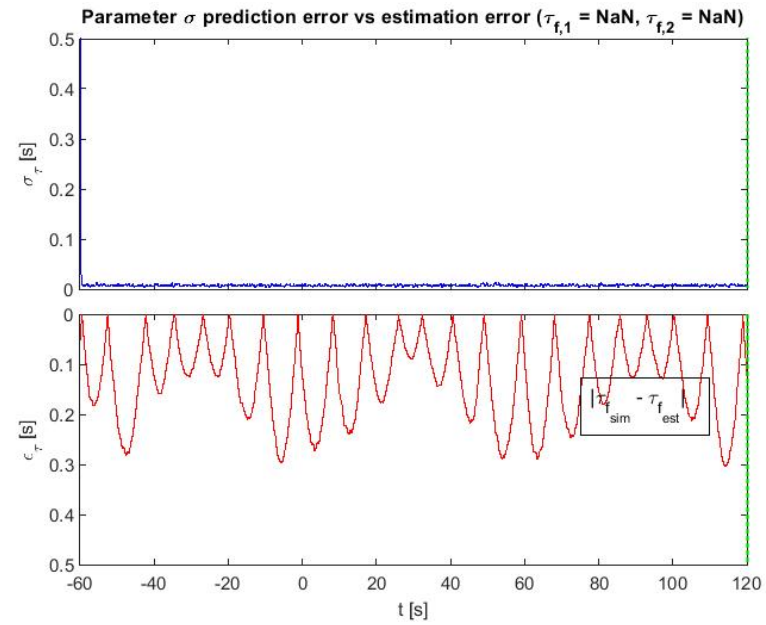

Figure B.2: Example of DEKF parameter sensitivity plot (multi-sine).

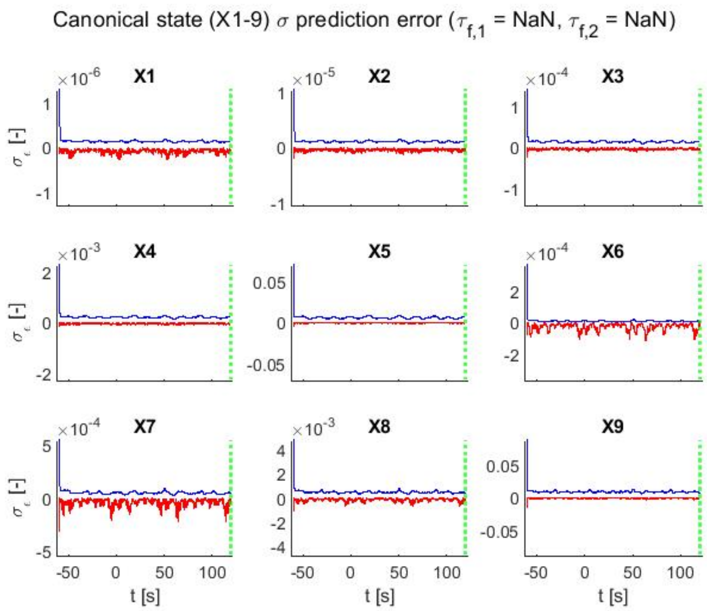

Figure B.3: Example of DEKF state sensitivity plot (multi-sine).

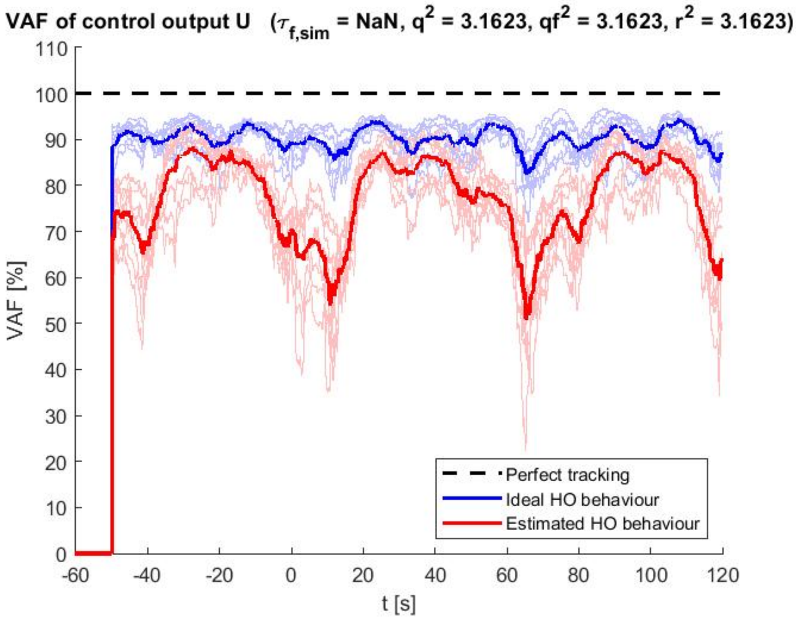

Figure B.4: Example of VAF plot for all multi-sine variations.

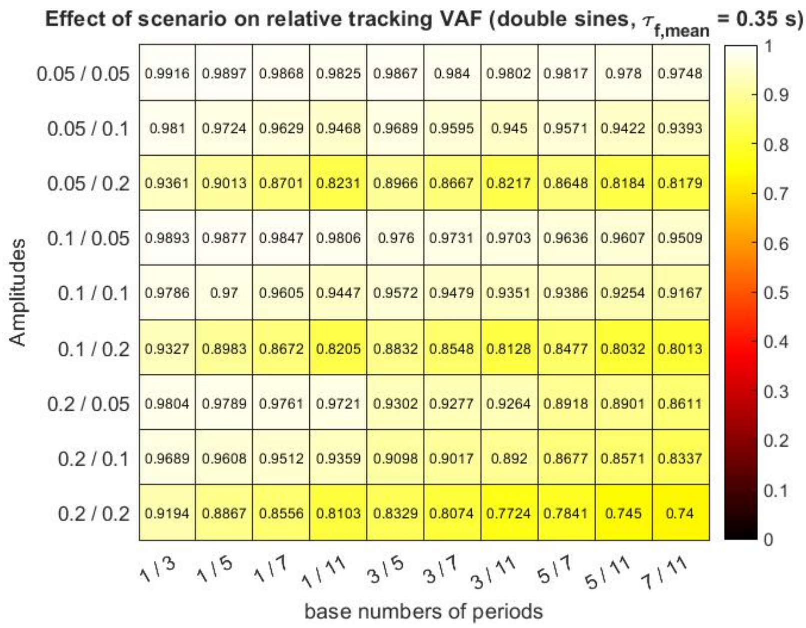

Figure B.5: Heatmap of relative tracking VAF as function of τ_f scheduling frequency and amplitude (multi-sine).